

ADA018729

AFRPL TR-75-16

HYDRAZINE ENGINE PLUME CONTAMINATION MAPPING
Final Report

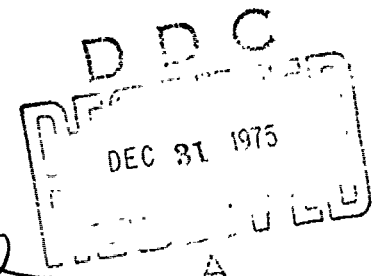
JET PROPULSION LABORATORY
4800 OAK GROVE DRIVE
PASADENA, CALIFORNIA 91103

AUTHOR: J. E. CHIRIVELLA

O C T O B E R 1 9 7 5

APPROVED FOR PUBLIC RELEASE
DISTRIBUTION UNLIMITED

AIR FORCE ROCKET PROPULSION LABORATORY
DIRECTOR OF SCIENCE AND TECHNOLOGY
AIR FORCE SYSTEMS COMMAND
EDWARDS, CALIFORNIA 93523



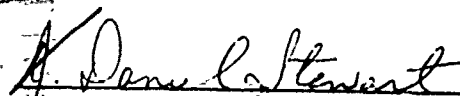
FOREWORD

This report was submitted by the Jet Propulsion Laboratory, 4800 Oak Grove Drive, Pasadena, California 91103 under Project Order 5730-74-2, Job Order No. 573009 BJ, with the Air Force Rocket Propulsion Laboratory, Edwards, CA 93523.

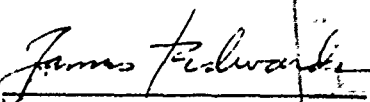
This report presents the results of one phase of research carried out at the Jet Propulsion Laboratory, California Institute of Technology, for the Air Force Rocket Propulsion Laboratory by agreement with the National Aeronautics and Space Administration (Contract NAS7-100).

This report has been reviewed by the Information Office/DOZ and is releasable to the National Technical Information Service (NTIS). At NTIS it will be available to the general public, including foreign nations. The report has been reviewed and is approved for publications.


IVAN WITBRACHT, Lt., USAF
Project Engineer


DANIEL STEWART, GS-14, Chief
Plume Group

FOR THE COMMANDER:


Deputy Chief, Technology Division

 NOTICES

When U.S. Government drawings, specifications, or other data are used for any purpose than a definitely related government procurement operation, the Government thereby incurs no responsibility nor any obligation whatsoever, and the fact that the Government may have formulated, furnished, or in any way supplied the said drawings, specifications or other data, is not to be regarded by implication or otherwise, or in any manner licensing the holder or any other person or corporation, or conveying any rights or permission to manufacture, use or sell any patented invention that may in any way be related thereto.

UNCLASSIFIED

SECURITY CLASSIFICATION OF THIS PAGE (When Data Entered)

119 REPORT DOCUMENTATION PAGE		READ INSTRUCTIONS BEFORE COMPLETING FORM
1. REPORT NUMBER (18) AFRPL-TR-75-16	2. GOVT ACCESSION NO.	3. RECIPIENT'S CATALOG NUMBER
4. TITLE (and Subtitle) (6) HYDRAZINE ENGINE PLUME CONTAMINATION MAPPING	5. TYPE OF REPORT & PERIOD COVERED (9) Final rept.	
7. AUTHOR(s) (10) J. E. Chirivella	6. PERFORMING ORG. REPORT NUMBER	
9. PERFORMING ORGANIZATION NAME AND ADDRESS Jet Propulsion Laboratory 4800 Oak Grove Drive, Pasadena 91103	8. CONTRACT OR GRANT NUMBER(s) (16) AF-5730-74-2 (17) 5730-74	
11. CONTROLLING OFFICE NAME AND ADDRESS Air Force Rocket Propulsion Laboratory/DYSP Edwards, California 93523	10. PROGRAM ELEMENT, PROJECT, TASK AREA & WORK UNIT NUMBERS (15) NAS7-100 -JON-573009	
14. MONITORING AGENCY NAME & ADDRESS (if different from Controlling Office)	12. REPORT DATE (11) Oct 1975	
	13. NUMBER OF PAGES 116 (12112 p.)	
	15. SECURITY CLASS. (of this report) UNCLASSIFIED	
	15a. DECLASSIFICATION/DOWNGRADING SCHEDULE N/A	
16. DISTRIBUTION STATEMENT (of this Report) APPROVED FOR PUBLIC RELEASE; DISTRIBUTION UNLIMITED		
17. DISTRIBUTION STATEMENT (of the abstract entered in Block 20, if different from Report)		
18. SUPPLEMENTARY NOTES		
19. KEY WORDS (Continue on reverse side if necessary and identify by block number) Plume contamination Quartz Crystal Microbalances Plume Mapping		
20. ABSTRACT (Continue on reverse side if necessary and identify by block number) Instrumentation for the measurement of plume exhaust specie deposition rates were developed and demonstrated. The instruments, two sets of quartz crystal microbalances, were designed for low temperature operation in the back flow and variable temperature operation in the core flow regions of an exhaust plume. These quartz crystal microbalances performed nominally, and measurements of exhaust specie deposition rates for 8400 number of pulses for a 0.1-lb monopropellant thruster are reported.		

DD FORM 1 JAN 73 1473

EDITION OF 1 NOV 65 IS OBSOLETE

UNCLASSIFIED

SECURITY CLASSIFICATION OF THIS PAGE (When Data Entered)

191150- DN

UNCLASSIFIED

SECURITY CLASSIFICATION OF THIS PAGE(When Data Entered)

- I. Introduction
- II. Experimental Vacuum Facility
- III. Propulsion System
- IV. Instrumentation
 - A. QCM Principles
 - B. Temp compensation
 - C. QCM unit design
 - 1. Low temp
 - 2. Variable temp
- V. General Arrangement of Experiment
 - A. Data acquisition
 - 1. DC signals
 - 2. AC signals
 - B. Far field mapping
 - C. Plume Contaminant mapping
 - D. Logging of operations (summarize and use appendix)
 - E. Discussion of results
- VI. Procedures
- VII. Results
- VIII. Conclusions and Recommendations.

UNCLASSIFIED

SECURITY CLASSIFICATION OF THIS PAGE(When Data Entered)

TABLE OF CONTENTS

I.	INTRODUCTION	1
II.	EXPERIMENTAL VACUUM FACILITY	3
III.	PROPULSION SYSTEM	6
IV.	INSTRUMENTATION	8
	A. QCM Working Principles	9
	B. Temperature Compensation	10
	C. QCM Unit Design	11
	1. Low Temperature QCMs	12
	2. Variable Temperature QCMs	13
V.	GENERAL ARRANGEMENT OF THE EXPERIMENT	14
	A. Propulsion Systems	14
	B. QCM Systems	15
	C. Data Acquisition System	16
	1. DC Signals	16
	2. AC Signals	16
VI.	PROCEDURES	16
VII.	RESULTS	17
	A. Far-Field Plume Mapping Test	17
	B. Plume Contaminant Mapping Results	20
	C. Discussion of Results	22
VIII.	CONCLUSIONS AND RECOMMENDATIONS	26
	REFERENCES	89
	GLOSSARY	91
	APPENDIX A	A-1
	APPENDIX B	B-1

LIST OF ILLUSTRATIONS

<u>Figure</u>	<u>Title</u>	<u>Page</u>
1	MOLSINK Vacuum Chamber and Auxiliary Equipment	28
2	Molecular Sink (MOLSINK) Ultrahigh-Vacuum Chamber	29
3	Rocket Plume in MOLSINK Chamber	30
4	General Arrangement of the Different Systems at the MOLSINK (Not to Scale)	30
5	TRW-FLTSATCOM 0.44 N (0.1 lbf) Hydrazine Rocket Engine	31
6a	Schematic Diagram of Propulsion Subsystem Inside the MOLSINK	32
6b	Thermal Control System for Propellant Lines	33
7	Propulsion System Schematic Diagram	34
8	Quartz Crystal Electrodes and Demonstration of the Thickness Vibration Mode	35
9	Doublet QCM	35
10a	Low Temperature Quartz Crystal Microbalance	36
10b	Other Perspective of a Low Temperature QCM	37
11a	Quartz Crystal Doublet with Two Independent Electrodes (Side 1)	38
11b	Quartz Crystal Doublet with Common Electrode (Side 2)	38
12	Schematic Diagram of the Circuitry Used for the Low- Temperature QCM Units	39
13	Schematic Diagram of a Variable Temperature QCM Unit	40
14a	A View of a QCM Unit with the Teflon Collimator Removed	41
14b	A View of a QCM Unit as it is Installed for Operation	41
15	Perspective of Installation of the Thruster in the MOLSINK Chamber	42

LIST OF ILLUSTRATIONS (contd)

<u>Figure</u>	<u>Title</u>	<u>Page</u>
16a	Systems Arrangement at MOLSINK Top Door (Viewed from Outside the Chamber)	43
16b	Propellant Feed Module	44
17a	QCM Orientation and Positions in MOLSINK Chamber	45
17b	QCM Orientation and Positions in MOLSINK Chamber.	46
18	View of Top of the Chamber, Low Temperature QCMs and Thruster (Looking Upward)	47
19	Low Temperature QCM Mounted on MOLSINK Walls	48
20	View of the 5 QCMs Used for Contamination Mapping and Their Location in the MOLSINK Chamber. (From a point near the engine).	49
21	Frequency Shift of a Low Temperature QCM versus Time	50
22	Solid Angle Subtended by the QCM Active Surface	51
23a	Mass Flux Measurements (Nitrogen)	52
23b	Mass Flux Measurements (Nitrogen)	53
23c	Mass Flux Measurements (Nitrogen)	54
23d	Mass Flux Measurements (Nitrogen)	55
24a	Frequency and Temperature Readings for Crystal A, May 15, 1974	56
24b	Frequency and Temperature Readings for Crystal B, May 15, 1974	56
24c	Frequency and Temperature Readings for Crystal C, May 15, 1974	57
24d	Frequency and Temperature Readings for Crystal D, May 15, 1974	57
24e	Frequency and Temperature Readings for Crystal E, May 15, 1974	58

LIST OF ILLUSTRATIONS (contd)

<u>Figure</u>	<u>Title</u>	<u>Page</u>
25a	Frequency and Temperature Readings for Crystal A, May 16, 1974	58
25b	Frequency and Temperature Readings for Crystal B, May 16, 1974	59
25c	Frequency and Temperature Readings for Crystal C, May 16, 1974	59
25d	Frequency and Temperature Readings for Crystal D, May 16, 1974	60
25e	Frequency and Temperature Readings for Crystal E, May 16, 1974	60
26a	Frequency and Temperature Readings for Crystal A, May 17, 1974	61
26b	Frequency and Temperature Readings for Crystal B, May 17, 1974	61
26c	Frequency and Temperature Readings for Crystal C, May 17, 1974	62
26d	Frequency and Temperature Readings for Crystal D, May 17, 1974	62
26e	Frequency and Temperature Readings for Crystal E, May 17, 1974	63
27a	Frequency and Temperature Readings for Crystal A, May 18, 1974	63
27b	Frequency and Temperature Readings for Crystal B, May 18, 1974	64
27c	Frequency and Temperature Readings for Crystal C, May 18, 1974	64
27d	Frequency and Temperature Readings for Crystal D, May 18, 1974	65
27e	Frequency and Temperature Readings for Crystal E, May 18, 1974	65

LIST OF ILLUSTRATIONS (contd)

<u>Figure</u>	<u>Title</u>	<u>Page</u>
28a	Frequency and Temperature Readings for Crystal A, May 19, 1974	66
28b	Frequency and Temperature Readings for Crystal B, May 19, 1974	66
28c	Frequency and Temperature Readings for Crystal C, May 19, 1974	67
28d	Frequency and Temperature Readings for Crystal D, May 19, 1974	67
28e	Frequency and Temperature Readings for Crystal E, May 19, 1974	68
29a	Frequency and Temperature Readings for Crystal A, May 20, 1974	68
29b	Frequency and Temperature Readings for Crystal B, May 20, 1974	69
29c	Frequency and Temperature Readings for Crystal C, May 20, 1974	69
29d	Frequency and Temperature Readings for Crystal D, May 20, 1974	70
29e	Frequency and Temperature Readings for Crystal E, May 20, 1974	70
30a	Frequency and Temperature Readings for Crystal A, May 21, 1974	71
30b	Frequency and Temperature Readings for Crystal B, May 21, 1974	71
30c	Frequency and Temperature Readings for Crystal C, May 21, 1974	72
30d	Frequency and Temperature Readings for Crystal D, May 21, 1974	72
30e	Frequency and Temperature Readings for Crystal E, May 21, 1974	73
31a	Frequency and Temperature Readings for Crystal A, May 22, 1974	73

LIST OF ILLUSTRATIONS (contd)

<u>Figure</u>	<u>Title</u>	<u>Page</u>
31b	Frequency and Temperature Readings for Crystal B, May 22, 1974	74
31c	Frequency and Temperature Readings for Crystal C, May 22, 1974	74
31d	Frequency and Temperature Readings for Crystal D, May 22, 1974	75
31e	Frequency and Temperature Readings for Crystal E, May 22, 1974	75
32a	Frequency and Temperature Readings for Crystal A, May 23, 1974	76
32b	Frequency and Temperature Readings for Crystal B, May 23, 1974	76
32c	Frequency and Temperature Readings for Crystal C, May 23, 1974	77
32d	Frequency and Temperature Readings for Crystal D, May 23, 1974	77
32e	Frequency and Temperature Readings for Crystal E, May 23, 1974	78
33a	Frequency and Temperature Readings for Crystal A, May 24, 1974	78
33b	Frequency and Temperature Readings for Crystal B, May 24, 1974	79
33c	Frequency and Temperature Readings for Crystal C, May 24, 1974	79
33d	Frequency and Temperature Readings for Crystal D, May 24, 1974	80
33e	Frequency and Temperature Readings for Crystal E, May 24, 1974	80
34a	Frequency and Temperature Readings for Crystal A, May 25, 1974	81
34b	Frequency and Temperature Readings for Crystal B, May 25, 1974	81

LIST OF ILLUSTRATIONS (contd)

<u>Figure</u>	<u>Title</u>	<u>Page</u>
34c	Frequency and Temperature Readings for Crystal C, May 25, 1974	82
34d	Frequency and Temperature Readings for Crystal D, May 25, 1974	82
34e	Frequency and Temperature Readings for Crystal E, May 25, 1974	83
35a	Frequency and Temperature Readings for Crystal A, May 26, 1974	83
35b	Frequency and Temperature Readings for Crystal B, May 26, 1974	84
35c	Frequency and Temperature Readings for Crystal C, May 26, 1974	84
35d	Frequency and Temperature Readings for Crystal D, May 26, 1974	85
35e	Frequency and Temperature Readings for Crystal E, May 26, 1974	85
36a	Frequency and Temperature Readings for Crystal A, May 27, 1974	86
36b	Frequency and Temperature Readings for Crystal B, May 27, 1974	86
36c	Frequency and Temperature Readings for Crystal C, May 27, 1974	87
36d	Frequency and Temperature Readings for Crystal D, May 27, 1974	87
36e	Frequency and Temperature Readings for Crystal E, May 27, 1974	88

I. INTRODUCTION

When a rocket or thruster exhausts in space, there is a potential of contamination of sensitive surfaces by direct mass deposit and secondary effects. The prediction of contamination and its effects, although possible, is very complex and difficult. The development of the capability to provide basic experimental data and to verify the advanced, computerized models used in the analysis is a required major step in the studies of those processes leading to the prediction of contamination as well as its effects on the properties of spacecraft surfaces.

The presence of contaminants in the rocket exhaust is highly dependent on the type of engine. Monopropellant engine exhausts are, in general, much cleaner than those of bipropellants, and in this sense, one should be cautious on how to define contamination, detect its presence and measure its deposition rates.

When a monopropellant hydrazine engine is fired in vacuum, nitrogen, hydrogen and ammonia are the main exhaust components. The concentration of these gases depends on the percentage decomposition of the ammonia, which is regulated in turn by the desired specific impulse. The interaction of hydrogen and nitrogen with sensitive surfaces never constitutes a hazard if the impinging forces and heating rates are kept low. Ammonia has a very low vaporization rate at temperatures slightly below 80°K, but it is suspected of adhering to surfaces at temperatures higher than 80°K when in the presence of solar UV (due possibly to polymerization of ammonia by photon participation). Although it is possible to have contamination by the mechanism described above, its investigation will not be covered in this report and hereafter, when we refer to contaminants in hydrazine engines, we will refer to those species, other than H_2 , N_2 , or NH_3 , appearing as traces in the rocket plume. Even if the contaminant levels in the exhaust are very low, they may become a problem for long-life missions which use these types of engines for Attitude Propulsion Systems (APS).

The nature of the contaminants is not known, but different speculations can be made based on the understanding of the physical phenomenon present in the decomposition of hydrazine. Because of the chemical process used in the preparation of hydrazine, contents of water and aniline up to a total of 1% are presently accepted. When the hydrazine flows through the catalytic bed, the aniline probably becomes a hydrocarbon and the water may remain water or become ammonium hydrates. One would expect that the engine duty cycle would have small effect on the spatial distribution of this kind of contaminant, since its presence in the exhaust is only weakly coupled to the dynamic processes occurring at the catalytic bed.

Another source of contaminants could be the catalyst itself. Because of the strong shear forces, small particulates can be torn from the catalyst pellets. This effect seems to be small, in a new engine, and can be reduced considerably by a careful preparation of the catalyst.

A very important aspect of contamination has to do with the investigation of how much unreacted hydrazine appears in the exhaust. This concern is due to the continuous findings of traces of hydrazine in chemical analysis of exhaust gases. This would be caused, probably, by the short residence time of hydrazine in the catalyst, mostly at the start of a pulse in high vacuum. The relative amount of hydrazine in the exhaust would then be dependent upon the engine duty cycle, particularly, upon the width of the on-time pulse.

Finally, a word of caution should be added to emphasize the remarkable coupling between the rocket exhaust flow field and the performance of the vacuum chamber when a vacuum simulator is used as the environment wherein contamination measurements are performed. A small amount of recirculation in the chamber will distort the distribution of contaminants. This is particularly true for studies of hydrazine engines in which the traces of contaminants are very small. That is the reason why cryogenic chambers with very high pumping rates are used, and in particular, if hydrogen has to be cryopumped, simulators with walls at 10°K or less are necessary.

The present report describes a series of tests that have been conducted to quantify the contamination potential of a small hydrazine engine. A TRW FLTSATCOM 0.44N (0.1 lb_f) hydrazine engine was used for these purposes and operated by firing it vertically downward in an ultra-high vacuum chamber (MOLSINK). The thruster was fired in a pulsing mode. Pulse widths as short as 10 msec and off-times from 50 msec to 60 sec were investigated. Quartz crystal microbalances were used as detectors. Five of the QCMs were mounted below the engine to measure contamination from the exhaust products mentioned above. The QCMs were operated at temperatures from 223°K to 323°K. Another set of seven QCMs were positioned on the side wall of the chamber and run at 10°K to provide a mapping of the plume far field for large turning angles, with nitrogen flowing through the thruster.

The plume mapping portion of the experiment showed as found in earlier work (14) that significant mass fluxes are encountered in regions on the plume belt that are beyond the theoretical Prandtl-Meyer expansion angle. This finding is extremely important for those concerned with flight instrumentation that uses cryostats and cryogenics because of the potential cryotrapping of thruster exhaust molecules.

The contamination portion of the experiment did not show any significant deposits when the crystals were operated at 255°K, but all crystals showed some deposits when operated at 228°K. The amount of deposits varied from a few molecular layers to as much as 50, depending on the number of firings, and they could be critical for some sensitive flight instruments if exposed to these deposits in a long mission.

II. EXPERIMENTAL VACUUM FACILITY

For a proper evaluation of the experiment and a deeper insight into the results, a general understanding of the Molsink facility and its working principles is necessary. One of the major problems associated with the study of rocket nozzle plume far fields and contaminant distributions, is that sensitivity of the measurements to recirculation effects causes strong

distortion of space simulation. Since the measurements that this work is concerned with dealt with far field plume mapping and contaminant deposition rates, the Molsink facility was selected as it is an ultra-high vacuum chamber capable of cryopumping injected gases at a very high rate. This facility consists of a vacuum chamber and associated cryogenic and vacuum systems (see Figure 1). The vacuum chamber encloses two other chambers: the inner liner and the molecular trap. The inner liner is filled with liquid nitrogen that acts as a massive heat sink (see Figure 2). The molecular trap, the innermost chamber, is a sphere approximately 3m (10 ft.) in diameter, maintained at a temperature between 10 and 15°K with gaseous helium. The aluminum moltrap walls are wedge-shaped resembling an anechoic chamber, with a total surface area of 186 m² (2000 ft²). Liquid nitrogen is supplied to the inner liner from a central tank and vented to the atmosphere. The moltrap is cooled by a manifold of tubes within which gaseous helium circulates at approximately 7°K. The helium is kept at this very low temperature by a refrigerator located adjacent to the chamber. The chamber walls are also coated with titanium, which acts as a "getter" material to trap helium and hydrogen that are not cryopumped by the 10°K surfaces. The amount of helium and hydrogen that can be pumped is greatly increased by coating the walls with a frost of gas that has a relatively high melting point. Under this condition, the frost cryosorbs helium and hydrogen at a very high rate. Carbon dioxide has been used routinely for such purposes in Molsink operations. Generally speaking, only a molecular layer of hydrogen is cryosorbed by a frost layer and therefore, a continuous bleeding of carbon dioxide is necessary if hydrogen is being injected periodically into the vacuum chamber.

The behavior of a rocket plume in the Molsink can be described by comparing the flow field in space and inside the chamber (see Figure 3). The rocket exhaust expands freely in space and its far field can be considered as radial, the gas molecules sinking thus to infinity. If a hypothetical perfect sink surface would enclose that plume, the flow field enclosed by such surface would be identical to one experienced in space. This is the working principle of the Molsink chamber. However, since the walls of the chamber are not perfect sinks, a small molecular reflection occurs. This

reflection results in a recirculation that could degrade the space simulation if the reflection coefficient were allowed to grow. The molecular trapping is very effective for gases other than hydrogen and helium. For these two gases, the cryosorption rate is highly dependent on the wall temperature, and therefore any process that will affect the wall temperature will result in a variation of the chamber background pressure once the hydrogen has been injected into the chamber. During MOLSINK testing operations, a cryogenic environment exists inside the chamber. To operate the hardware inside the chamber, thermal control is necessary for items such as propellant lines and valves that are sensitive to freezing. These warm surfaces are protected from radiation cooling losses by appropriate shielding, while the heat conduction losses remain negligible if good insulation and low pressure are maintained in the chamber. If for some reason the hydrogen sorption onto the wall is diminished, any additional hydrogen injected into the chamber will reduce the vacuum, resulting in an increase in heat conduction losses. This causes an additional warming of the walls which results in more hydrogen desorption. This phenomenon has an exponential growth and results in the rapid desorption of hydrogen from the walls occurring within a matter of seconds; it will be referred to hereafter as the "avalanche effect".

The MOLSINK chamber has two doors. The upper door is used as a feed-through for the propulsion system lines and thermal control elements. The door makes a relatively small aperture in the moltrap surface. The bottom door temperature can rise as high as 200°K, and there was concern that when the exhaust plume impinges on this door some material could be scattered back and degrade the space simulation. To eliminate this problem, a copper cone was located above the door and cooled with liquid nitrogen or liquid helium as desired. With this technique, one can control the bottom door temperature, and maintain the deposited frost as a very thin film by collecting the excess in a "cold bucket" around the rim of the cone (see Figure 4). More information about the facility can be found in References (1), (2) and (3).

III. PROPULSION SYSTEM

A TRW 0.44N (0.1 lb) thruster-valve assembly was made available by AFRPL for this experiment. The TRW Flightweight Thruster FLTSATCOM 0.44N (0.1 lb) has the characteristics listed in Table 1. The nominal temperatures of the thermally controlled components of the propulsion system are listed in Table 2. The valve is a dual soft (Teflon) seat, dual coil solenoid valve using AF-E-411 seat material. Two manufacturers, Parker and Allen, produce this propellant valve.

The thruster was fabricated for TRW in November 1973 and prior to this experiment was subjected to the following tests during the TRW IR&D programs:

1. Acceptance Test
2. Delta 1900 Launch Vibration Test
3. Cold Start Test (<10000 pulses, 7200 cold starts at 277.4°K (40°F))
4. Baseline Performance

Therefore, at the time of the MO'SINK tests, the thruster had gone about 10,000 pulses. The valve, on the other hand, had accumulated 350,000 pulses, although its functioning proved to be satisfactory. A view of the thruster valve assembly is shown in Figure 5 and more information on the unit can be found in Reference 4.

A propulsion module, control box, valve driver and timing device were fabricated at JPL for this particular experiment. At the time of the test, however, they were not available yet and other JPL material was used to operate the propulsion systems. The AFRPL propulsion module, its control box and valve driver are presented in a separate document which describes follow on effort, and that will be published in the near future.

The JPL propellant feed module was available from past experiments (see Ref. 5). The module was located at the top of the MOLSINK chamber near the upper door, and the operations were commanded by remote control from

Table 1. Characteristics of TRW FLTSATCOM 0.44 - N (0.1 lb_f) Thruster

Steady State Inlet Pressure, N/m ² (psia)	9.646 x 10 ⁵ (140.0)
Steady State Thrust Level, N (lb _f)	0.44 (0.1)
Steady State Chamber Pressure, N/m ² (psia)	6.06 x 10 ⁵ (88.0)
Catalyst	Shell 405, 25-30 mesh
Nozzle Expansion Area Ratio	60:1
Throat Diameter, cm (in.)	0.076 (0.030)
Injector Type	Head Space Injector
Steady State I _{sp} , N-S/Kg (lb _f -s/lb _m)	2548.0 (260.0)

Table 2. Nominal Temperatures of Thermally Controlled Components

System	Temperature (°C)
Fuel Lines	20 - 30
Filter	20 - 30
Solenoid Valve	20 - 30
Catalyst Bed	200
QCMs	Variable (-50° C to 50° C)

the lower floor of the facility, after the propellant tank was pressurized. A Techtronics waveform generator and pulse generator were used to operate the thruster valve.

The engine and the valve were instrumented with several thermocouples and a coiled coaxial electrical heater. With this arrangement, thermal control of the engine catalyst bed could be maintained, while temperature readings of the throat, catalyst bed and other locations of interest on the thruster/valve assembly could be obtained. The volume of the pressure tap in the nozzle inlet was eliminated by positioning an appropriate needle in its interior, and the performance of the engine was judged by observing the temperature reached at certain standard duty cycles previously checked in other tests. A schematic diagram of the propulsion subsystems that were

located inside the chamber is shown in Figure 6a. The fuel is introduced through valve VF3, filling both lines with hydrazine from the solenoid valve to valve VN1. The line containing VN1 is used as a gaseous nitrogen purge. Both the fuel and purge line are packaged together and share the same thermal environment. This environment is controlled by a series of thermocouples distributed along the fuel lines and attached to them. Thermocouple cabling and fuel lines are encapsulated in an aluminum tube. The thermocouples control several low outgassing Kapton film heaters (manufactured by Electrofilm, Inc.) wrapped around the aluminum tube. The fuel lines are, in this manner, thermally controlled by radiation. The same type of heaters, as well as additional spot heaters, were used to thermally control the thruster valve assembly described earlier (see Figure 6b).

A schematic diagram of the propellant feed module, fuel and purge lines and hydrazine valving system is given in Figure 7.

The CO₂ injection system consisted of a nozzle-plenum assembly located near the top of the chamber. The flow of CO₂ was controlled by a solenoid valve operated by a relay which in turn was energized by a pulse generator synchronized by the Techtronics equipment of the engine valve driver system. The CO₂ solenoid valve could also be operated manually, providing a flexible injection system. The CO₂, supplied from a K bottle, was filtered by 20 μ and 1 μ filters, in order to minimize undesired contamination introduced in the chamber.

IV. INSTRUMENTATION

Quartz Crystal Microbalances were used to measure the contaminant mass deposits. Because of the particular characteristics of this experiment, two different types of temperature compensated QCMs were designed. The working principles and the details of the QCM design and operation follow.

A. QCM Working Principles

A QCM consists of an electronic oscillator whose resonance frequency is stabilized by the piezoelectric effect of a quartz crystal. The resulting resonance frequency depends on several parameters, but if one fixes the oscillator circuit constants and polarization voltages, the specific modes of crystal vibration will depend only on the orientation of the cut plate with respect to the crystal axes. For QCM action the AT cut is used, which yields a thickness vibration resonant mode of about 5 MHz. Depending on the angle of the AT cut, the precise resonance frequencies will depend both on the mass deposited on the surface of the crystal and the temperature. If the crystal experiences a variation in temperature ΔT and a mass variation ΔM , the frequency shift can be expressed as:

$$\Delta f = C_M \Delta M + C_T \Delta T \quad (1)$$

where C_M and C_T are the mass coefficient and temperature coefficient of the crystal, respectively.

In general, C_M and C_T depend on the temperature and cut angles of the crystals. If a cut angle is chosen such that $C_T = 0$ for some range of temperature, then $\Delta f = C_M \Delta M$ and the crystal can be used as a delicate microbalance to detect and measure small masses deposited on the surface. It turns out that for a considerable change in temperature and cut angle, the mass coefficient does not vary more than 5%, and one can use the expression

$$\Delta M = \frac{\Delta f}{F_c^2} 4.30 \times 10^{-7} \quad (2)$$

for all practical purposes, where ΔM = mass deposits in g/cm^2 , Δf = frequency shift in Hz, and F_c = resonant frequency in MHz. A derivation of Equation (2) is found in Appendix A.

An illustration of the crystal, along with the location of one of the electrodes and the thickness vibration mode, can be seen in Figure 8. For an

elementary treatment of the crystal oscillators, as well as crystal nomenclature, one can consult any standard electronics textbook. An accounting of microbalance applications can be found in References 6-12.

B. Temperature Compensation

As indicated above, since mass deposits correlate with frequency shift, it is necessary to select a crystal cut that makes $C_T = 0$ for the anticipated temperature variation range. Although this is obtainable for some applications, in most cases the frequency spectrum of the crystal becomes so complicated that the interpretation of the readings is very difficult. Bartera (Ref. 13) has designed a particular arrangement that, in spite of its simplicity provides a very efficient temperature compensation (see Fig. 9).

Consider two crystals, No. 1 and No. 2, both exposed to mass deposit and temperature variation. The corresponding change in frequency can be written as:

$$\begin{aligned}\Delta f_1 &= C_{M_1} \Delta M_1 + C_{T_1} \Delta T_1 \\ \Delta f_2 &= C_{M_2} \Delta M_2 + C_{T_2} \Delta T_2\end{aligned}\tag{3}$$

If both crystals have identical piezoelectric properties and are kept at the same temperature, then

$$C_{M_1} = C_{M_2}, C_{T_1} = C_{T_2}, \text{ and } \Delta T_1 = \Delta T_2\tag{4}$$

Subtracting Equations (3) and taking Equation (4) into account, we have

$$\Delta F = \Delta f_1 - \Delta f_2 = C_{M_1} (\Delta M_1 - \Delta M_2)\tag{5}$$

and if one of the crystals is protected from mass deposits in such a way that $\Delta M_2 = 0$, we then have

$$\Delta F = C_{M_1} \Delta M_1 \quad (6)$$

that is, the beat frequency shift ΔF of both crystals can be easily correlated with the mass deposits on one of them. The conditions just described, namely $T_1 = T_2$, identical piezoelectric constants and $M_2 = 0$ are achieved if one adopts the arrangement described in Figure 9. A doublet crystal plate is cut and polished. Gold electrodes are deposited on one side, in the form indicated by the figure, while a rectangular electrode which is common to both parts of the doublet is used on the other side. Under these premises, and if the crystals are driven at low voltage, one can have two independent crystal oscillators. By protecting one of them from mass deposit with a screen optically thin to the environment radiation, the beat frequency shift of both crystals can be expressed as

$$\Delta F = C_{M_1} \Delta M_1 \quad (7)$$

as it was originally intended.

C. QCM Unit Design

The design criteria of QCMs are very much dependent on the particular application for which the QCM is intended, and the particular environmental and operating conditions under which it will be operating.

The two experiments of concern in the present task: plume far field mapping and rocket exhaust contaminant distribution measurements, require two different QCM concepts. In the mapping of the plume far field, one is interested in operating the QCM at extremely low temperatures in order to have sticking coefficients of the plume gases as close to 1 as possible. On the other hand, when investigating rocket exhaust contaminant distribution,

one is often interested in operating the QCMs at different constant temperatures, with the additional capability to sweep working temperatures from NH_3 condensation temperature to room temperature. These two kinds of applications give rise to two QCM concepts:

1. Low Temperature QCMs - The design responds to the need to measure small deposition rates of nitrogen. The plume of a certain thruster is simulated by blowing nitrogen through the nozzle in steady state. A set of very cold QCM's are positioned on the walls of the vacuum chamber and their readings monitored. From the slope of the frequency time curves, one can infer the mass flow rate per unit solid angle which is the function of interest in plume far-field studies. In order to accomplish these measurements, the mass collecting surface of the QCM, which is the electrode of the quartz crystal, has to be extremely cold. A general practice in MOLSINK environment has been to cool the QCM by thermally connecting it to the MOLSINK walls. Special care has to be adopted to retain good frequency stability at these very low temperatures. To this end, the components of the electronics used in these QCM units were carefully selected by observing the deviation of their design electronic constants when operated at liquid Helium temperatures, and rejecting those that showed excessive departure. The acceptance criterion was an overall stability of better than 1 Hz in 5 MHz in the output frequency. Figures 10a and 10b show two different views of a low temperature QCM unit. One can distinguish 4 main components: the crystal, the electronics, the thermal control parts, and mechanical mountings. The crystal consists of a doublet quartz plate (AT cut angle of $40^\circ 28'$) with two circular electrodes on one side and a common rectangular electrode on the other side (see Figures 11a and 11b). This crystal cut has a small C_T coefficient at low temperature. Additionally, temperature compensation is implemented by mounting them on an aluminum block by a set of "hairbrush" gold wires which are glued to the common electrode by a high thermal conductivity, low outgassing silver epoxy. Two gold wires connect the crystal electrodes to two heat sinks and from there they extend to the electronics package. A schematic diagram of the electronics circuit is given in Figure 12. In the same figure one can identify the solid state components that have been

used. The electronics were packaged in a small box attached to the QCM collimator and insulated from it by a small Teflon plate. Attached to the electronics box and for convenience of operations during actual measurements, there is a spot heater to control the temperature of the electronics in the event of some malfunction of the components due to extremely low temperatures. The QCM collimator consists of a copper plate that houses the quartz crystal. The copper plate has two apertures one of which exposes the sensitive area of half of the common electrode, and the other one is covered with a piece of mylar. The aluminum mounting block is equipped with a spot heater and one thermocouple connected to one of the heat sinks. With this arrangement, one can thermally desorb the QCM from any deposited material when the crystal surface is overloaded. (Overload on the crystal surface can cause false reading and eventually total damping.) The mounting block ends in a fork to conform with the wedge-shaped Molsink chamber wall fins. The whole unit is cooled by the chamber walls and when it operates in vacuum and at 10°K, stabilities of 0.1 Hz are often obtained. Seven of these units were fabricated and installed on the walls of the Molsink chamber with their active crystal face oriented towards the thruster. The details of their positions and wiring will be given in Section V.

2. Variable Temperature QCMs - This QCM design responds to the need to have very precise readings at different fixed temperatures. When a monopropellant rocket exhaust contains contaminants, one does not know in advance the condensation temperature of the contaminants. In order to selectively sample the contaminants by condensation trapping, the QCMs are exposed to the plume, and their outputs monitored while they are operated at consecutively decreasing isotherms.

A 35° 10' AT cut crystal doublet was prepared and mounted on a small aluminum block similar to the low temperature QCMs (see Fig. 13). The 35° 10' crystal cut is known to have a low temperature coefficient at room temperature. Temperature compensation is achieved by the technique described earlier and the gold wire hairbrush mounting absorbs any thermal

stresses that would otherwise cause mechanical failure of the crystal; notice that good thermal conductance from the block to the crystal is still maintained. Two photographs of a variable temperature QCM can be seen in Figures 14a and 14b. The QCM unit was provided with heaters which were controlled by a copper-constantan thermocouple located in the proximity of one of the heaters, while the crystal temperature was monitored by a similar thermocouple located in the crystal mounting block. The unit was covered with a teflon block collimator provided with two circular apertures. One of these apertures was used to collect and collimate the oncoming gases while the other was covered with a transparent piece of mylar. A small coupon of Kapton was attached to the teflon block near the collimating hole. The QCM readings will indicate the amount of mass deposit on them, but they do not give any information about the nature of the contaminants, other than the vaporization rates. As an aid to the identification of the contaminants, and because of its preferential chemical activity to N_2H_4 vapors while being inert to NH_3 , Kapton coupons were thought helpful in identifying traces of hydrazine.

V. GENERAL ARRANGEMENT OF THE EXPERIMENT

A. Propulsion Systems

The propulsion systems, as described in Section III were installed in the chamber as depicted in Figure 4. The engine was located at the axis of the chamber, with the nozzle exit located 71.2 cm (28") from the top of the chamber and pointed downwards. A perspective of the thruster, its instrumentation and thermal insulation is presented in Figure 15. The thruster was mounted on a vertical bracket supported by a horizontal set of bars in "T" form. The fuel lines and thruster valve were covered by aluminum foil in order to prevent excessive radiative losses. Maximum thermal insulation was utilized for all components to minimize heat leaks to the walls. Heater wiring and solenoid valve cabling were collected between the propellant-lines tube protector and the aluminum foil wrapping (see Figure 6b). They were extracted from the chamber by feed-throughs located

at the top door of the MOLSINK. Figure 16a shows a view of the MOLSINK top door during installation, and Figure 16b shows a view of the arrangement of the propellant feed-module fuel lines and chamber top door during operations. The cabling of the four chromel-alumel thermocouples installed on the thruster were passed through the top door and fed into a cold reference junction located near the propellant feed module. The wires of the copper-constantan thermocouples located on the fuel lines were passed inside the supporting tube and collected together with the wires of similar thermocouples associated with the thermal control of the propulsion systems. The cables were collected in a 36 pin connector feed-through at the bottom door of the MOLSINK, from there to the cold reference junctions, and then to the data systems. Periodic readouts and dynamic thermal controls were installed for convenience and safety of the operations.

B. QCM Systems

Seven low temperature QCMs were installed in the chamber as shown in Figures 17a and 17b. Five of them were mounted on the same vertical section of the chamber (Fig. 17a), and two others on another vertical section located in a plane perpendicular to the first section (Figure 17b). Figure 18 shows a photograph, looking upwards, of the thruster and several low temperature QCM's. The QCM's were mounted on the fins of the walls and oriented towards the thruster. Details of a QCM mounted on the fins, its wiring and nearby environment, can be seen in Figure 19. All the materials used in its construction, mounting and wiring have extremely low outgassing rates in vacuum. Notice the absence of any non-functional items in its proximity, and the general compactness and cleanness of any surface exposed to plume impingement.

Five variable temperature QCMs were mounted on an aluminum bar located across the chamber as depicted in Figures 4 and 17b. A view of the set of QCMs as seen from the thruster (looking downward) is seen in Figure 20. The QCMs are identified with the letters A, B, C, D, E. The electronics and heater wiring of all the QCM units were extracted through the bottom

door, and from there channeled to the data systems and control panels. The copper-constantan thermocouples of all the QCMs (a total of 18) were fed through a 36 pin connector and then sent to the reference junctions of the data systems and thermal controllers. The heater controlling thermocouples of the variable temperature QCMs dynamically controlled the temperature of the QCMs units. The actual setting of the control point for these heaters was determined by readings from thermocouples located near the crystals. A backup data system was continuously displaying the frequency and temperature readings of the 5 QCMs used for contaminant mapping.

C. Data Acquisition System

1. DC Signals. Signals from the thermocouples and pressure transducers were fed into a cross-bar switch and then into a digital voltmeter. The digitized signal then entered a Hewlett-Package Data Acquisition System which drives a teletype. Only the printing option of the teletype was used in this experiment.
2. AC Signals. The signals from the QCMs were input into a board of RF relays, which are controlled by the same cross-bar switch used for DC signals. The actual readings were made with a fixed delay to avoid the noise from the relay closure. The signal was fed into a differential amplifier (which eliminated the chamber ground noise) and which had a good selectivity in band amplification. A programmable counter digitized the signal and fed it into the data systems in an analagous manner as the digitized DC signals.

The data systems could handle these numerous AC and DC signals by multiplexing them through the cross-bar switch and the RF relays.

VI. PROCEDURES

All the thermal controls were set at nominal temperatures. The chamber doors were closed although conductance between the inner and outer

chambers was maintained through the upper and lower intermediate doors. The facility is equipped with a mechanical pump and diffusion pump. The mechanical pump brought the vacuum to $1.33 \times 10^{-1} \text{ N/m}^2$ (10^{-3} torr) and the diffusion pump continued it to $1.33 \times 10^{-3} \text{ N/m}^2$ (10^{-5} torr). After leak checking, liquid nitrogen was introduced into the inner liner of the chamber. This brought the temperature of the inner liner and molecular trap to 80°K at the end of another 24 hours. At this point, the pressure in the chamber was down to $1.33 \times 10^{-3} \text{ N/m}^2$ (10^{-5} torr), and the helium refrigeration system was started. At the end of 8 hours the moltrap temperature reached 10°K and the pressure in the inner chamber had an overall low of $1.33 \times 10^{-7} \text{ N/m}^2$ (10^{-9} torr) pressure. At this time the facility was at its nominal high-vacuum operating mode and the calibration and test procedures were started. The systems were checked by flowing gases through the auxiliary CO_2 injection system nozzle and several runs on the data systems were obtained until all the systems were debugged, coordinated and properly interfaced. Details of the test itself are given in Sect VII.

VII. RESULTS

A. Far-Field Plume Mapping Test

The mapping of the far-field of the thruster plume for large turning angles has considerable interest in contamination studies. Also for calibration purposes, it is convenient to take measurements for smaller turning angles. To this end, seven low temperature QCMs were placed in the chamber as shown in Figures 17a and 17b. These QCMs are mounted in the chamber in very good thermal contact with the tubings of GHe that cool the moltrap. In this manner temperatures as low as 10°K are reached on the crystals, and condensation trapping with sticking coefficients of 1 are not unusual if no hydrogen or helium trapping is attempted. Hydrazine thrusters, however, contain in their exhaust a significant portion of hydrogen (up to 55% in the plume) and although trapping of the nitrogen and ammonia is very effective, the hydrogen is only partially cryosorbed on the crystal face, distorting the readings. Past analysis of backflow from

small nozzles (see Ref. 14) indicates that the type of gas does not influence the backflow data drastically. For these reasons, one would think that a practical way to define the extent of the plume could be implemented by flowing an inert gas through the thruster and then conduct the measurements. Nitrogen appears to be the most convenient gas to work with from the operational point of view. A set of steady state runs were performed by running the engine at 200°C and varying the plenum pressure. The data of each run was cyclically recorded every 11 seconds by six of the QCMs (one of them, crystal V, became quickly saturated and unoperational due to high deposition rate). The signal of each QCM in each run was then plotted versus time (see Fig. 21) and a characteristic number,

$$\dot{f}_i = \frac{\sum_{j=1}^N n_j \dot{f}_{ji}}{\sum_{j=1}^N n_j} \quad (7)$$

was assigned to each QCM for each run, where \dot{f}_{ji} is the slope of frequency-time curve encountered n_j times during the run for QCM i and where N is the total number of readings. Also, $(\dot{f}_{ji})_{\max}$ and $(\dot{f}_{ji})_{\min}$ are recorded. The rates of frequency change \dot{f}_i , $(\dot{f}_{ji})_{\max}$, $(\dot{f}_{ji})_{\min}$ are converted to mass deposition rates by formula (2), i. e.,

$$\frac{dM}{dt} = \frac{df/dt}{F_c^2} 4.3 \times 10^{-7} \quad (8)$$

where $\frac{dM}{dt}$ is now the mass deposition rate on the crystal surface in $g/cm^2/sec$. If one corrects this reading for the distance r and orientation angle ϕ (see Fig. 22), the mass flux per unit solid angle is obtained if radial flow is assumed in the far field.

$$\left(\frac{d\dot{m}}{d\Omega}\right) = \frac{df/dt}{F_c^2} (4.3 \times 10^{-7}) \left(\frac{r^2}{\cos\phi}\right) \quad (9)$$

One of the functions of interest in far-field plume definition is the mass flow rate per unit solid angle normalized at the centerline of the plume

$$\left(\frac{d\dot{m}}{d\Omega} \right) / \left(\frac{d\dot{m}}{d\Omega} \right)_{\theta=0} = f(\theta) \quad (10)$$

where θ is the turning angle (see Fig. 22).

The function $f(\theta)$ has received considerable attention in the literature, and the data in this report has been reduced to provide information about this function. The value of $(d\dot{m}/d\Omega)_{\theta=0}$ obtained by the Hill and Draper scheme (Reference 15) has been adopted, and the resulting data compared with the $f(\theta)$ proposed by those investigators, i. e.,

$$f(\theta) = \exp \left\{ -[\lambda^2 (1 - \cos \theta^2)] \right\} \quad (11)$$

where

$$\lambda = \left[\pi^{1/2} (1 - C_F/C_{F \max}) \right]^{-1} \quad (12)$$

where C_F , the thrust coefficient, is given by

$$C_F = \sqrt{\frac{2\gamma^2}{\gamma-1} \left(\frac{2}{\gamma+1} \right)^{\frac{\gamma+1}{\gamma-1}} \left[1 - \left(\frac{P_e}{P_o} \right)^{\frac{\gamma-1}{\gamma}} \right]} + \frac{P_e}{P_o} A_e$$

and $C_{F \max}$ is given by

$$C_{F \max} = \sqrt{\frac{2\gamma^2}{\gamma-1} \left(\frac{2}{\gamma+1} \right)^{\frac{\gamma+1}{\gamma-1}} \left[1 - \left(\frac{P_e}{P_o} \right)^{\frac{\gamma-1}{\gamma}} \right]}$$

is the plume slenderness coefficient, and

$$\left(\frac{d\dot{m}}{d\Omega} \right)_{\theta=0} = \frac{\dot{m}_w \lambda}{\pi^{3/2}} \quad (13)$$

is the mass normalization factor at the axis centerline and m_w = nozzle total mass flow rate. The data is presented in Figure 23 in semilogarithmic scale, i. e.,

$$f(\theta) = 10^{-K_M(\theta)} \quad (14)$$

where K_M is the mass coefficient.

Four different plenum pressures were run, and the results have been plotted (see Figures 23) versus the Hill and Draper approximation only as a reference, and no intention of correlation with theory has been attempted at this point.

B. Plume Contaminant Mapping Results

The data was collected at fixed intervals (10 minutes during standby procedures and 3 minutes during thruster operation). Due to the complexity of the experiment, approximately 100 parameters were printed. Only the temperature and frequency readings of QCMs A, B, C, D, E will be presented in this report, since the other parameters are connected only with the surveillance of the propulsion and facility systems, and the low temperature QCMs were promptly saturated. The QCM outputs have been arranged in such a manner that an increase in beat frequency corresponds to mass deposit on the crystal, except in QCM/D, where a decrease in frequency correlated with a mass deposit. The frequency is expressed in Hz and an approximate equivalence between Hz and molecular layers for several gases is given in Table 3. The table has been obtained by assuming a 0.3 nm (3Å) separation between molecules and applying equation (2) for ΔM given in Section IV. The data are presented graphically in Figures 24-36. They are presented by calendar days with an 8 hr. overlap i. e., from 0000 hr to 0800 hr of the following day. In each graph one can see the temperature and beat frequency variations during the day, together with the engine duty cycle and facility activities. One graph is presented for each QCM, with a total of five graphs per day.

Table 3. Frequency-Mass Equivalence

$$F_c = 5 \text{ MHz}$$

(Approximate Resonant
Frequency of Single Crystal)
1 Hz Equals X Molecular Layers

Gas	X
H ₂	4
N ₂	0.52
NH ₃	1.21
CO ₂	0.50
H ₂ O	1.23
N ₂ H ₄	2.80

The measurements took place at two different temperatures. Figures 24-27 display the results for the QCM temperatures in the neighborhood of 255° K, and Figures 28-33 correspond to values of 228° K. The rest of the data shown in Figures 34-36 show the history of the chamber when bringing it back to room temperature and one atmosphere when it was backfilled with nitrogen. Details of the logging of operations can be seen in Appendix B, as well as indications of facility parameters and engine operating conditions.

At the time of the beginning of the contamination experiment, the facility had been operating for one week. Gases such as nitrogen, carbon dioxide, hydrogen and ammonia had been injected in the chamber for plume far field mapping purposes. There was evidence that at the beginning of the contaminant mapping experiment all the systems had outgassed all volatile materials when maintained at the nominal operating temperatures.

Water was injected into the chamber at the end of the test in two modes, 1) as a wet mixture of GN_2 and H_2O with container of the order of 1% and flowed through the thruster, 2) as liquid water through auxiliary nozzles. In both cases the QCMs were affected by mass deposits (see Figures 32 and 33).

When the chamber was open, no traces of hydrazine reaction were encountered on the Kapton coupons that were positioned on the collimators of the variable temperature QCMs.

C. Discussion of Results

The results as described in this section have been summarized in Table 4a and 4b.

One can classify these results in two groups according to the temperature of the crystals.

1) Table 4a contains a summary of the QCM's frequency changes when the crystals were maintained at 255.23°K (0°F). No significant changes are observed at this temperature, which leads to the conclusions that the vaporization rate of the contaminants at 255°K is far higher than their deposition rates for the thruster duty cycles explored in this matrix.

Due to a malfunction of the QCM electronics at low temperatures, the filtering system of the QCMs had to be adjusted, which caused a frequency shift in the QCMs during May 15, 1974. Therefore, the priming of the thruster (one of the operating points of interest from the contamination point of view) was purposely not monitored. This is a special precaution to be taken when using a QCM for measuring mass deposits: the setting points of the instrumentation polarization voltages and narrow pass band amplifiers used in the handling of the frequency signals should not be operated during the experiment.

The variable temperature QCMs are compensated for temperature effects as described in Section IVB. One of the conditions for temperature compensation was the uniformity of temperature through the entire crystal doublet. This condition should be nearly fulfilled with the design adopted in this experiment, and described in Section IVC. Because of the particular departures of each QCM unit from the optimum conditions, small gradients of temperature are encountered between each half of the crystal doublet. These gradients depend on the particular thermal balance of the QCM units, and when multiplied by the temperature coefficient may give rise to frequency changes. These effects account for the frequency changes observed in the QCMs when temperature is changed drastically, as in Figure 25a and 28a, b, c, d, e. The same effect accounts for the frequency changes observed during the MOLSINK avalanches where the presence of hydrogen in the chamber substantially alters (by convective heat transfer) the thermal flow through the crystal doublet. Note also that the response to temperature changes and avalanche have different polarity at different temperatures and for different units.

Although the results of the data summarized in Table 4a are not very conclusive, an observation of Figure 25a shows that the frequency of crystal A does not stabilize to the same value that it had before it was heated. Initially the crystal temperature was 255.23° K. It was heated to 373° K, then cooled back to 255.23° K. During this temperature excursion the frequency increased from an initial value of 2560 Hz to over 2620 Hz, and then down to about 2485 Hz. This behavior suggests that the material that was previously deposited on the crystal was vaporized during the baking of the crystal. Only in the sequence of firings of May 18, 1974 was there seen some accumulation of mass on some crystals. More pulses were fired on this day and the results seem to confirm the hypothesis of balance between vaporization rates and deposition rates established above.

2) In view of the small amount of mass collected when running the QCMs at 255.23° K (0° F) attempts were made to operate the QCMs at much lower temperatures. The circuitry used in these QCMs, however, produced

electrical noise at temperatures below about 233°K (-40°F). Thus the lowest temperature at which the contaminants could be collected was set by the limiting operating temperature of the electronics used in the design of the variable temperature QCMs. Right from the beginning one can see in Figure 29 that at this temperature the crystals begin to hold the deposited contaminants quite steadily. All the QCMs reacted as expected to thruster operation, mostly during the heavy duty cycles of days May 20-21, 1974. The following day, May 22, 1974, also shows some small mass deposits in spite of the moderate number of thruster firings (see Figures 29, 30, 31). One anomaly appears when the frequency of some QCMs does not return to values below or equal to those that were present before the warming and cooling of the QCM (see Figures 29 and 30). Instead (compare Figures 29b and 30b) an increase in mass deposit occurs, which does not agree with the vaporization induced by the warm up of the QCMs. Although there are no grounds to confirm it, migratory phenomena could be responsible for such a behavior. Another of the working principles of temperature compensation consists of shielding half of the doublet from mass deposit. Although the mylar strip prevented the direct deposit of contaminants on the covered side of the doublet crystal, it did not prevent the migration of mass from the active side to the passive (covered) side. There is not much known about migration, but it seems that a trapped gas (or liquid) on a surface, will move on the surface when the surface temperature approaches the vaporization temperature of the trapped material. It should, in general, move toward regions of lower energy. There is no mechanism in the present QCM configuration to prevent such a phenomenon of happening, although in certain circumstances anything as small as a 10µm notch will prevent migration across it.

Another point of interest is the behavior of the QCMs during the long pulsing of the 1% mixture of nitrogen and water (see Figure 32) that was injected through the thruster into the chamber during the night of May 23, 1974 and early morning of May 24, 1974. Only QCMs B and C (closer to the center of the chamber) showed mass deposits, which demonstrates that the QCMs were operational, and that they were within the sensitivity range of the water

naturally resident in the hydrazine. The rest of events on May 24, 1974 were associated with the procedures for ending this test series, and no interpretation of the QCM readings is attempted after this date because of the complexity of the operational procedures. It may be pointed out, however, that the QCMs always showed sensitivity to chamber operations, and they could be used to monitor the chamber environment. A final check of the operation of the QCMs as reliable wall deposit instrumentation was demonstrated when water vapor was introduced in the chamber (see Figures 32 and 33).

VIII. CONCLUSIONS AND RECOMMENDATIONS

Based on the above considerations, the following conclusions are offered:

- 1) The low temperature QCMs performed nominally and can be used to measure the plume far field for large turning angles.
- 2) The variable temperature QCMs need improvement. Their electronics should be designed with carefully screened components, as was done with the low temperature QCMs.
- 3) Feasibility of the methods and the technology has been clearly demonstrated.
- 4) Although no significant amounts of contaminants were measured at QCM temperatures greater than -18°C , the lower temperatures (-45°C) did yield mass deposits for certain thruster operating conditions. These mass deposits have not been positively identified, but are probably water, hydrazine, or other trace impurities resident in the hydrazine. If the results of this experiment were to be extrapolated to long time durations, the contamination amount could jeopardize many planned long-life satellite missions.
- 5) Some of the contaminants have a vaporization point located between -40°C and -17.7°C , and a postmortem analysis of the QCMs still showed some traces of contaminants detectable with the naked eye.

In view of these results, the following recommendations are suggested and some of them are presently being implemented.

- 1) Improve electronics of variable temperature QCM. (Under way).
- 2) If possible use another crystal cut for temperatures below 200°K and above 100°K (this will minimize temperature sensitivity).
- 3) Conduct tests under controlled conditions by running the QCMs to a temperature as low as possible (around 80°K), and then identify contaminants using a thermal gravimetric desorption technique. (Under way).
- 4) Study methods of eliminating migration effects in QCMs.
- 5) Provide an efficient water injection scheme to calibrate QCMs in the MOI TANK. (Under way).

COPY AVAILABLE TO DDC DOES NOT
PERMIT FULLY LEGIBLE PRODUCTION

Table 4a. Summary of Results from the QCM Readings and Thruster Operations

Number of Pulses		180	180	600	600	300	300	300	1000	1000
Time Interval, hr		3	3	1	1	1-1/2	1-1/2	1-1/2	2	2-1/2
On-Time, sec		0.02	0.01	0.02	0.01	0.05	0.150	0.200	0.01	0.02
Off-Time, sec		60	60	6	6	20	20	20	0.1000	0.1000
QCM A	Temperature, °C	50	-18	-18	-18	-18	-18	-18	-18	-18
	Frequency, Hz	0	<8	1	0	3	3	0	0	0
QCM B	Temperature, °C	-18	-18	-18	-18	-18	-18	-18	-18	-18
	Frequency, Hz	<2	0	0	4	0	0	0	0	0
QCM C	Temperature, °C	-18	-18	-18	-18	-18	-18	-18	-18	-18
	Frequency, Hz	0	0	3	2	1	0	5	7	0
QCM D	Temperature, °C	-18	-18	-18	-18	-18	-18	-18	-18	-18
	Frequency, Hz	0	0	1	1	1	0	0	0	2
QCM E	Temperature, °C	-15	-15	-15	-15	-15	-15	-15	-15	-15
	Frequency, Hz	<4	0	3	0	3	0	0	0	-

Table 4b. Summary of Results from the QCM Readings and Thruster Operations

Number of Pulses		1000	600	1000	15	300	15	15	15	200	200	106
Time Interval, hr		3	2-1/2	1-1/2	1/4	1/6	1/4	1/4	1/4	1/4	3/4	1
On-Time, sec		0.100	0.050	0.05	0.01	0.01	0.02	0.05	0.10	0.02	0.05	0.10
Off-Time, sec		0.400	0.200	0.20	60	0.02	60	60	60	0.05	20	0.50
QCM A	Temperature, °C	-45	-45	-45	-45	-45	-45	-40	-40	-40	-40	-40
	Frequency, Hz	20	33	10	0	1	0	4	0	0	1	0
QCM B	Temperature, °C	-45	-45	-45	-45	-45	-45	-40	-40	-40	0	-40
	Frequency, Hz	40	40	7	0	4	0	1	1	0	8	1
QCM C	Temperature, °C	-45	-45	-45	-45	-45	-45	-40	-40	-40	-40	-40
	Frequency, Hz	10	45	28	0	13	0	2	8	9	4	4
QCM D	Temperature, °C	-45	-45	-45	-45	-45	-45	-40	-40	-40	-40	-40
	Frequency, Hz	17	30	5	0	0	0	2	4	7	2	1
QCM E	Temperature, °C	-45	-45	-40	-40	-40	-40	-40	-40	-40	-40	-40
	Frequency, Hz	50	35	2	0	0	0	1	0	0	0	3

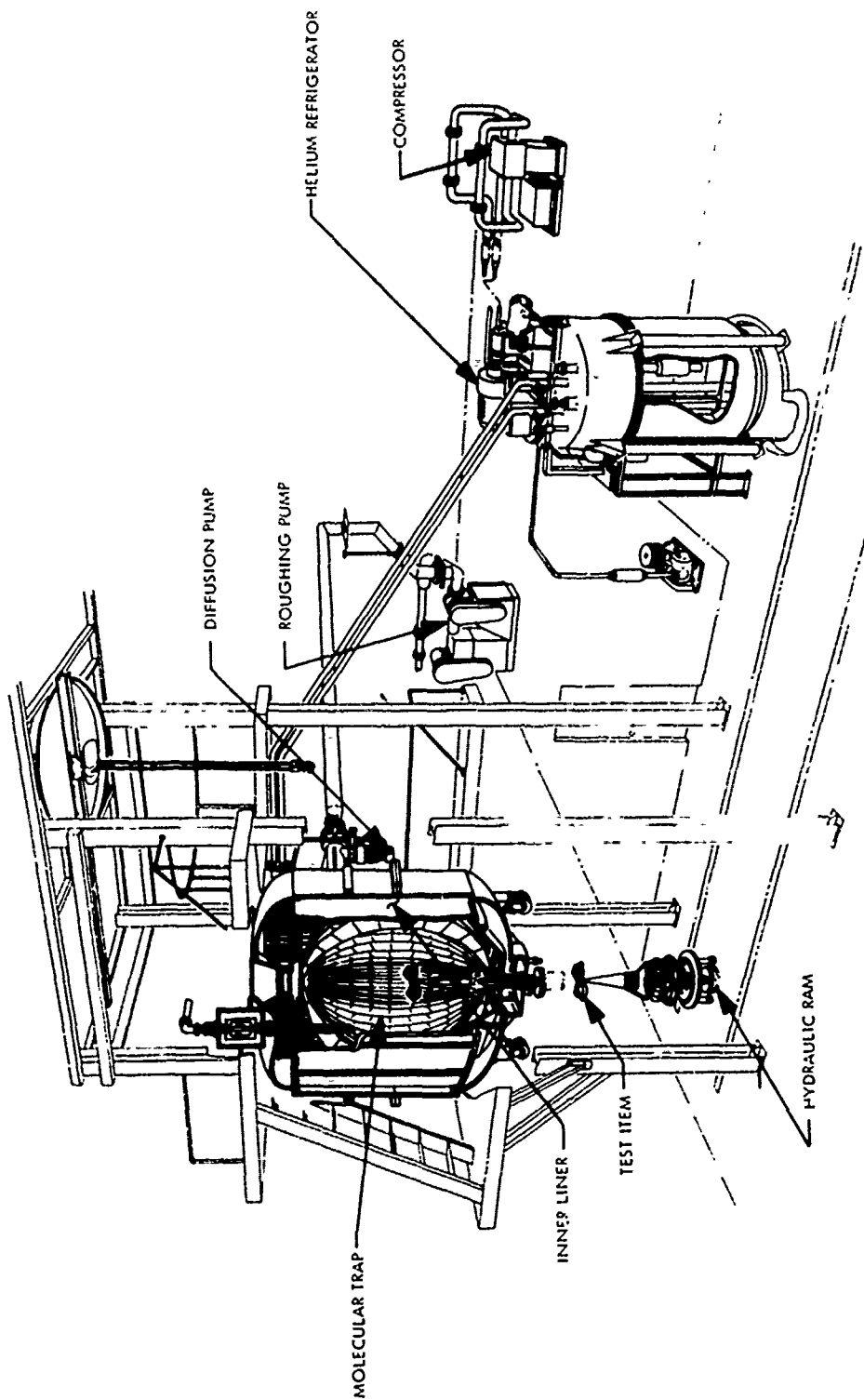


Figure 1. MOLSINK Vacuum Chamber and Auxiliary Equipment

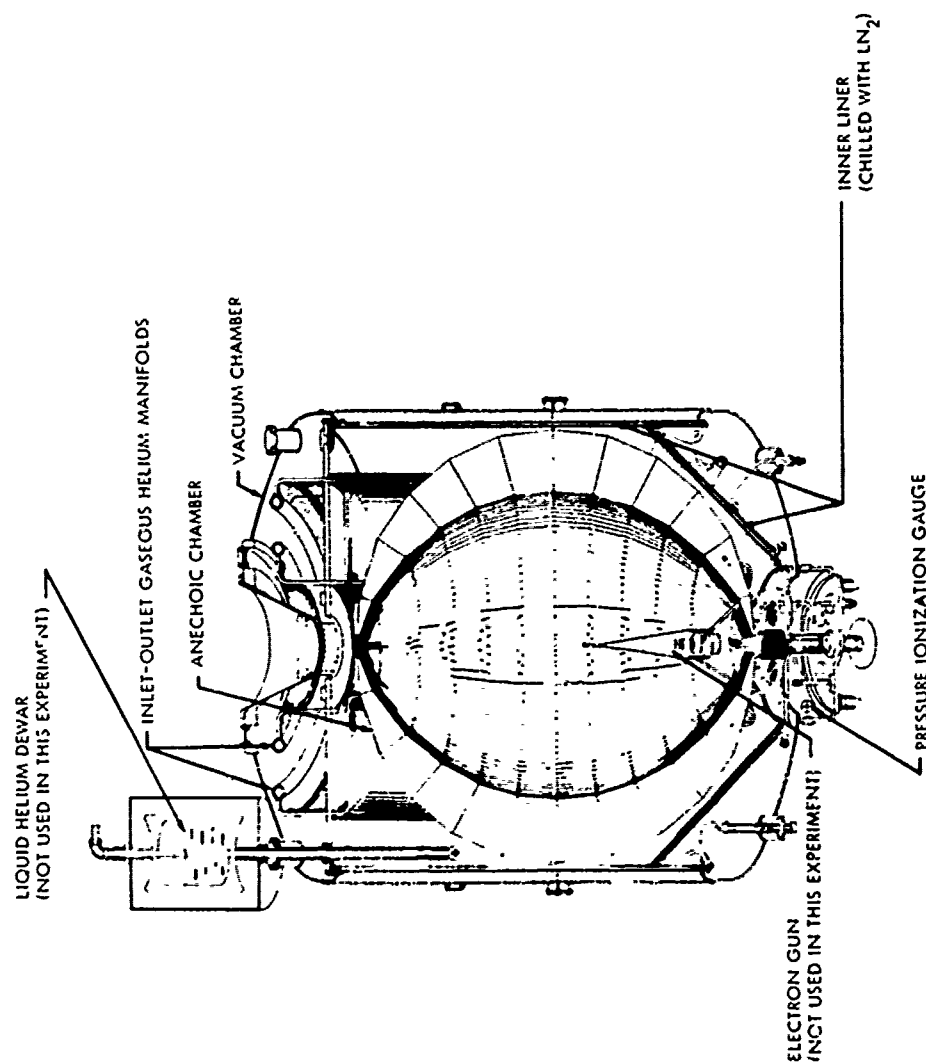


Figure 2. Molecular Sink (MOLSINK) Ultrahigh-Vacuum Chamber

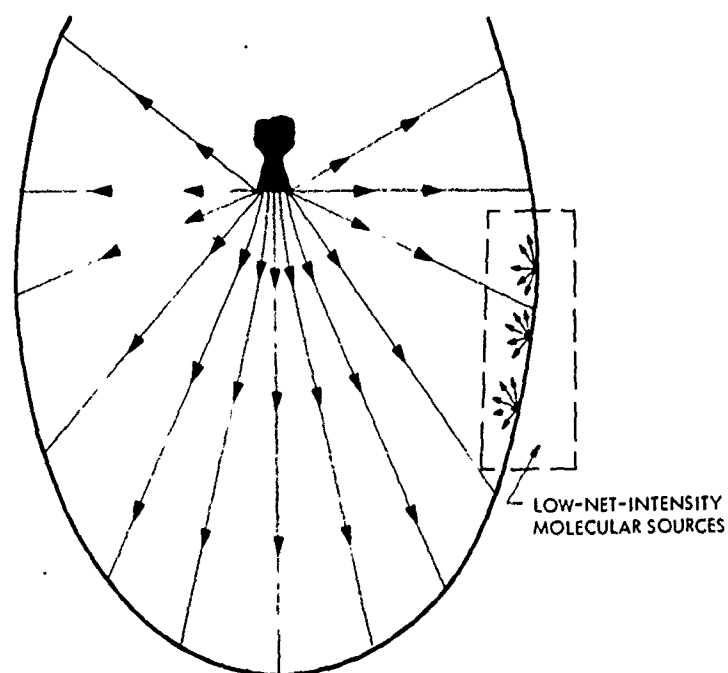


Figure 3. Rocket Plume in MOLSINK Chamber

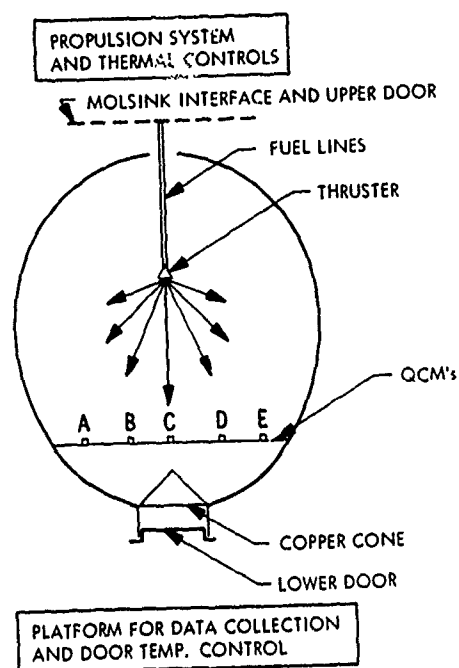


Figure 4. General Arrangement of the Different Systems at the MOLSINK (Not to Scale)

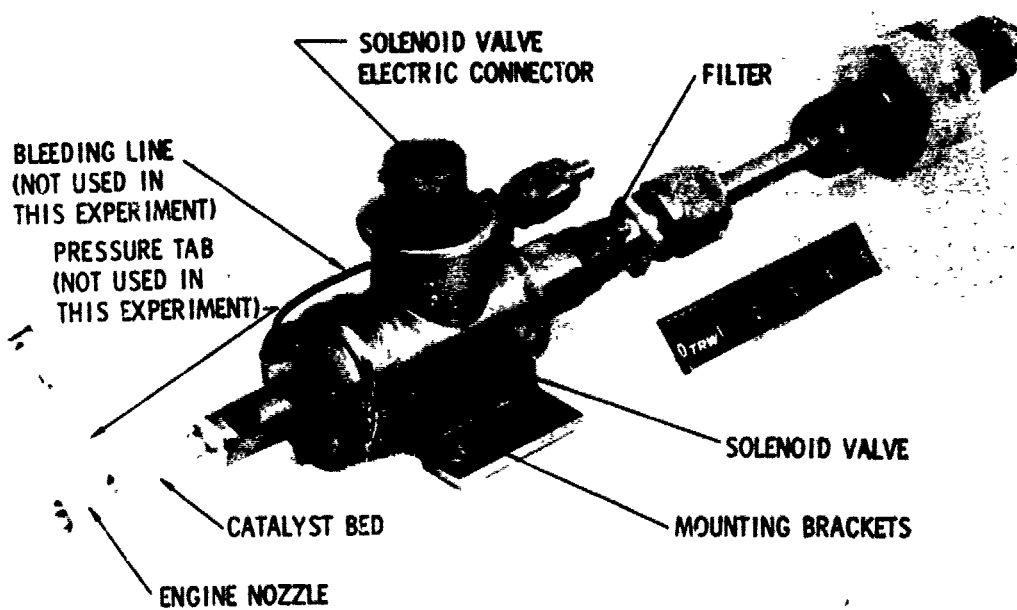


Figure 5. TRW-FLTSATCOM 0.44 N (0.1 lbf) Hydrazine Rocket Engine

INSTRUMENTATION

TFL	FEED LINE TEMPERATURE (MULTIPLE T/C'S)
TS1	THRUSTER SOLENOID VALVE MOUNTING BRACKET TEMPERATURE (4 TC's)
TS2	THRUSTER SOLENOID VALVE EXIT TEMPERATURE
TCB	THRUSTER CENTER CATALYST BED TEMPERATURE
TCC	NOZZLE INLET TEMPERATURE
TT	NOZZLE THROAT TEMPERATURE

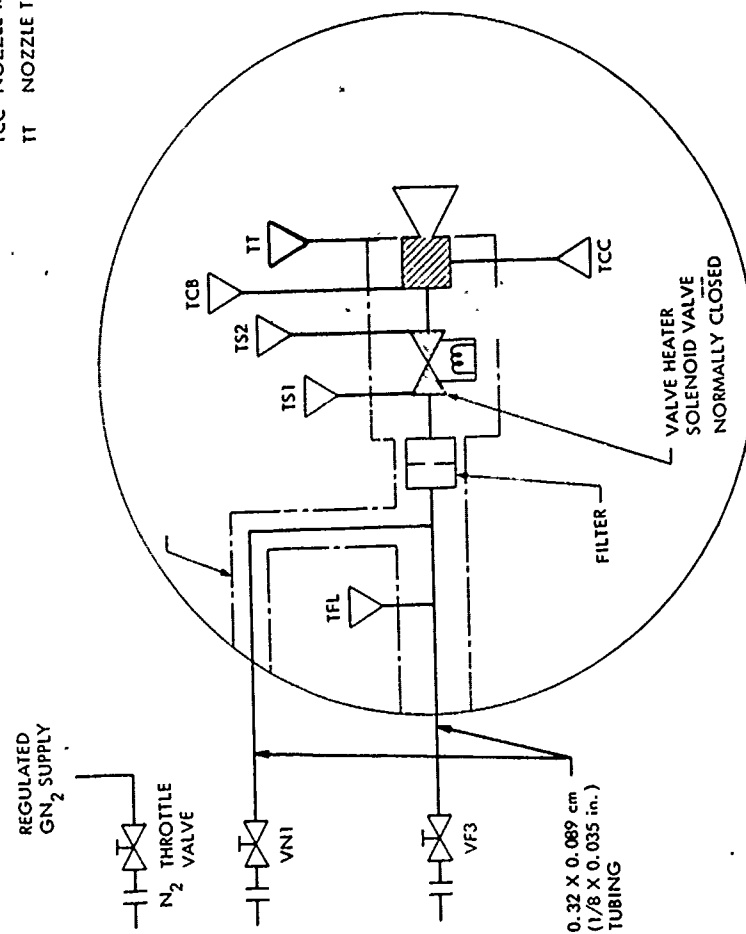


Figure 6a. Schematic Diagram of Propulsion Subsystem Inside the MOLSINK

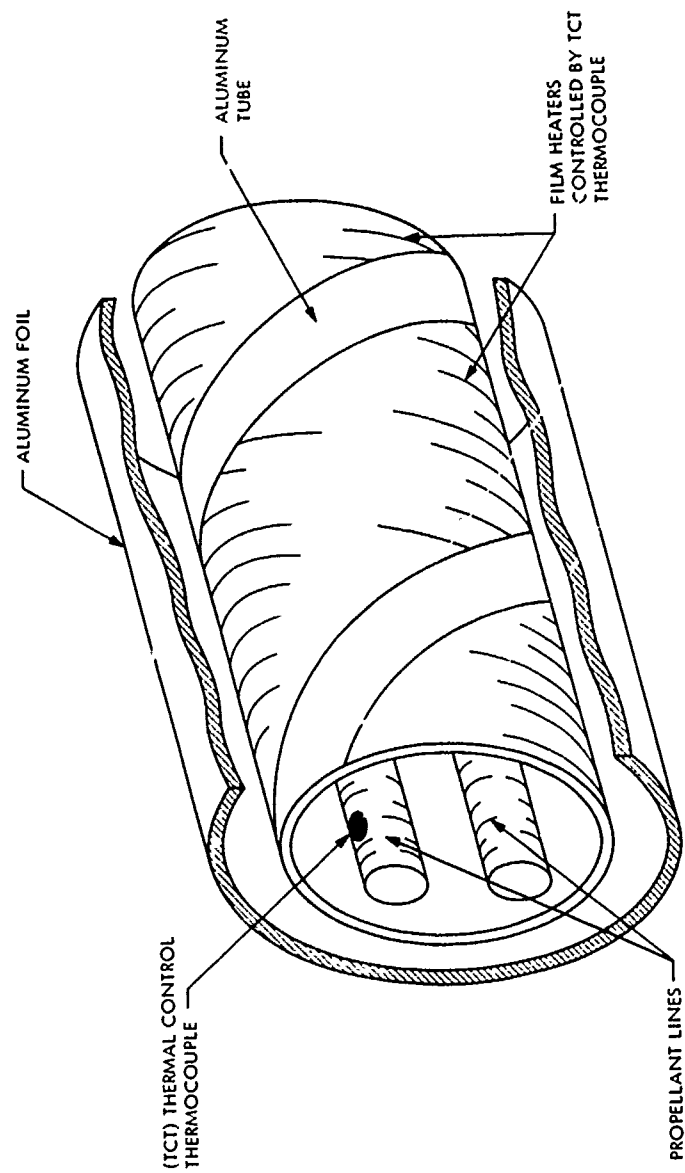


Figure 6b. Thermal Control System for Propellant Lines

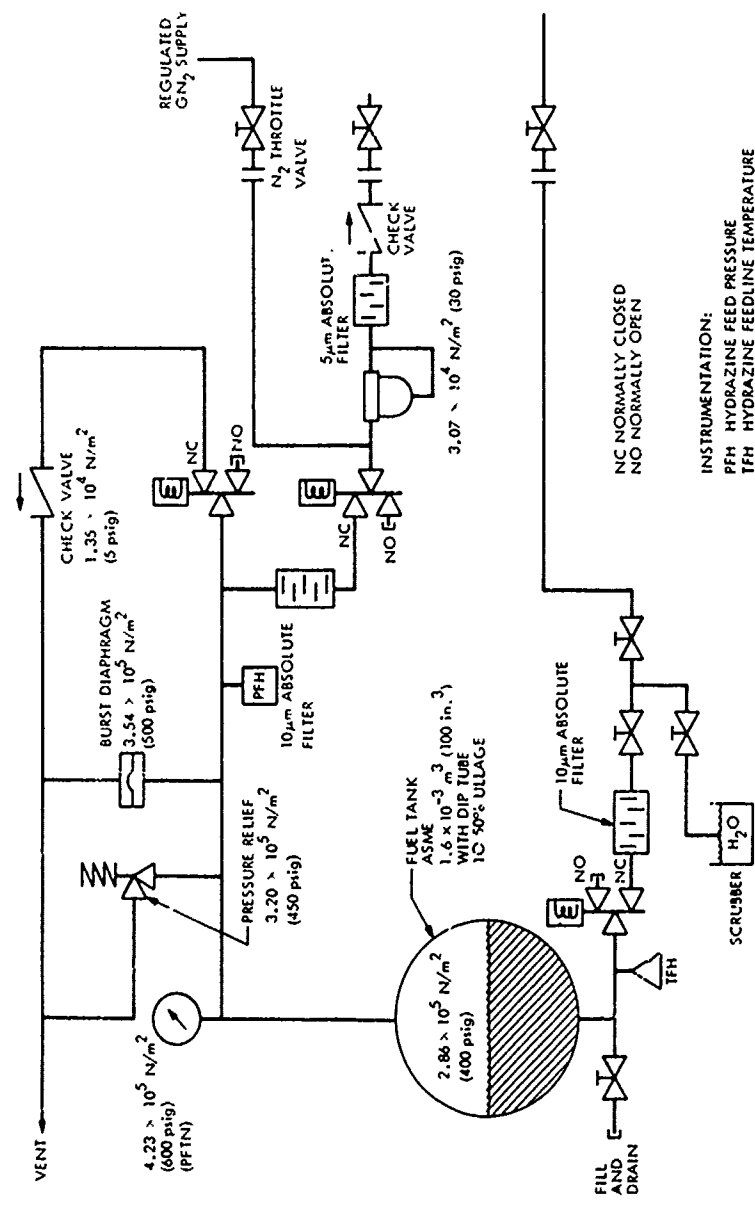


Figure 7. Propulsion System Schematic Diagram

$$\Delta f = C_M \Delta M + C_T \Delta T$$

$$C_M = \phi(T, \text{CUT ANGLES})$$

$$C_T = \psi(T, \text{CUT ANGLES})$$

$$\text{IF } C_T \approx 0, \Delta M = \frac{\Delta f}{F_c^2} \times 4.35 \times 10^{-7}$$

$$\Delta M (\text{gm/cm}^2)$$

$$\Delta f (\text{Hz})$$

$$F_c (\text{MHz})$$

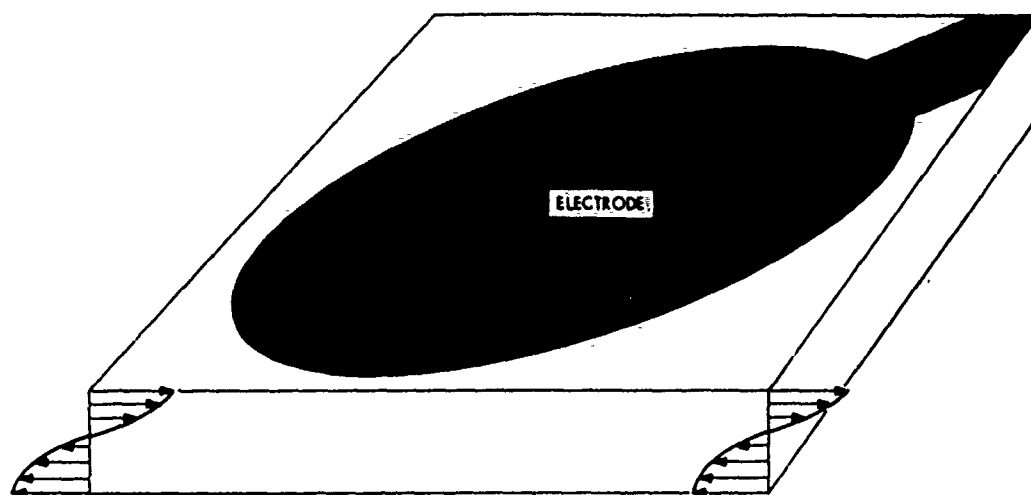


Figure 8. Quartz Crystal Electrodes and Demonstration of the Thickness Vibration Mode

$$\Delta f_1 = C_{M_1} \Delta M_1 + C_{T_1} \Delta T_1$$

$$\Delta f_2 = C_{M_2} \Delta M_2 + C_{T_2} \Delta T_2$$

$$\left. \begin{array}{l} C_{M_1} = C_{M_2} \\ C_{T_1} = C_{T_2} \end{array} \right\} \text{ IF } T_1 = T_2$$

$$\Delta F = \Delta f_1 - \Delta f_2 = C_{M_1} \Delta M_1$$

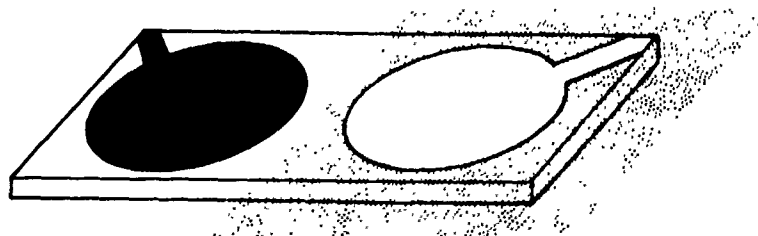


Figure 9. Doublet QCM

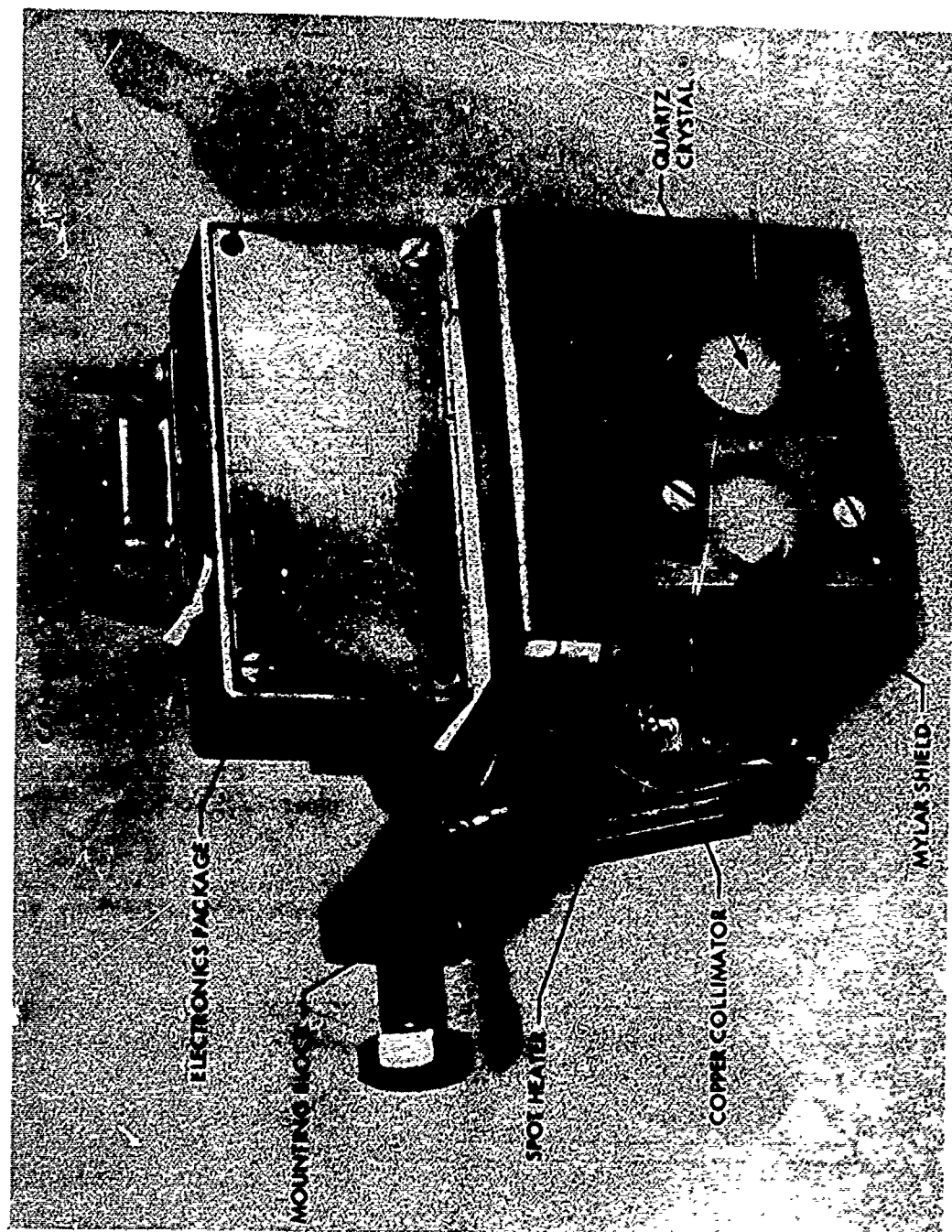


Figure 10a. Low Temperature Quartz Crystal Microbalance

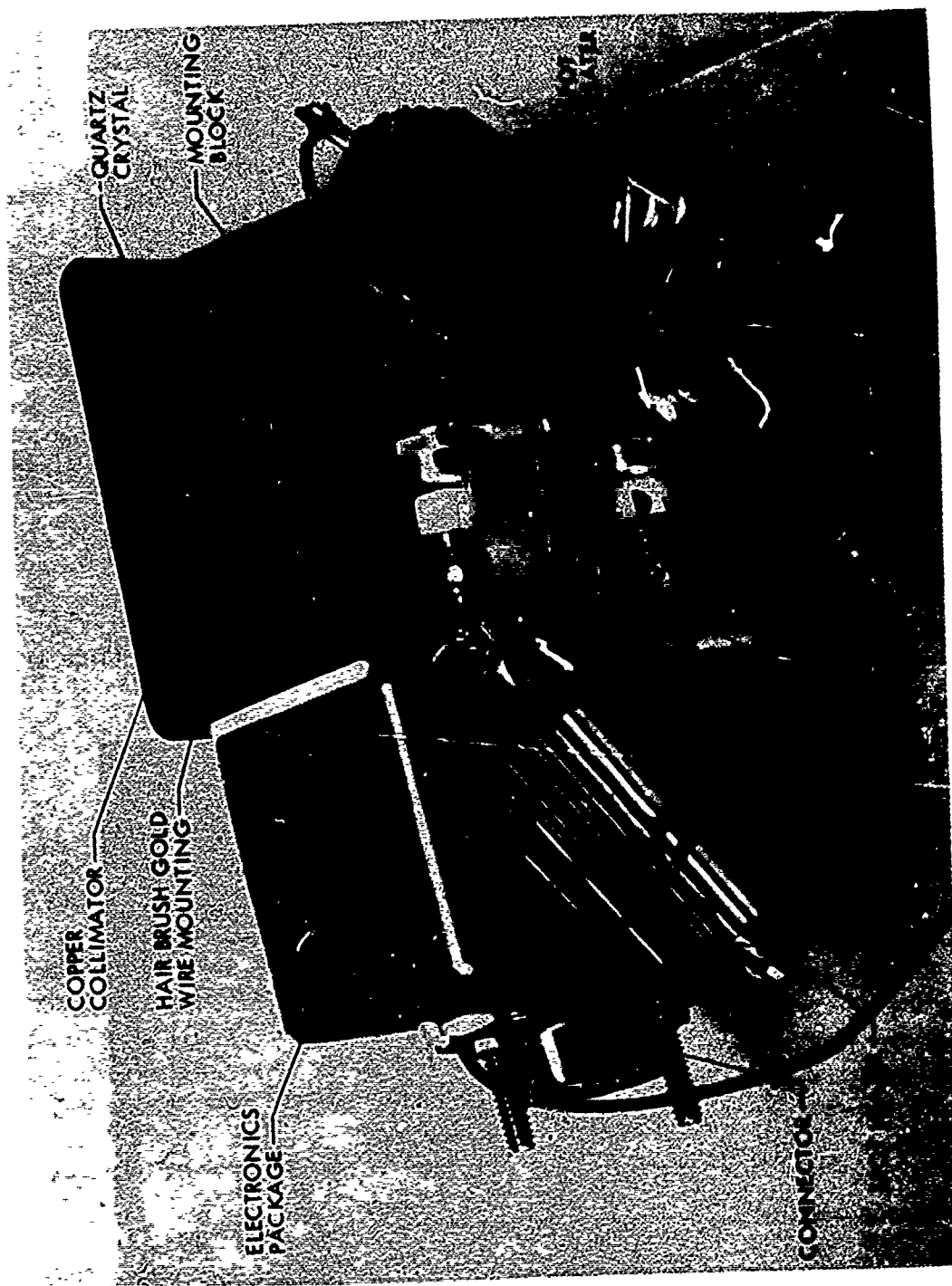


Figure 10b. Other Perspective of a Low Temperature QCM

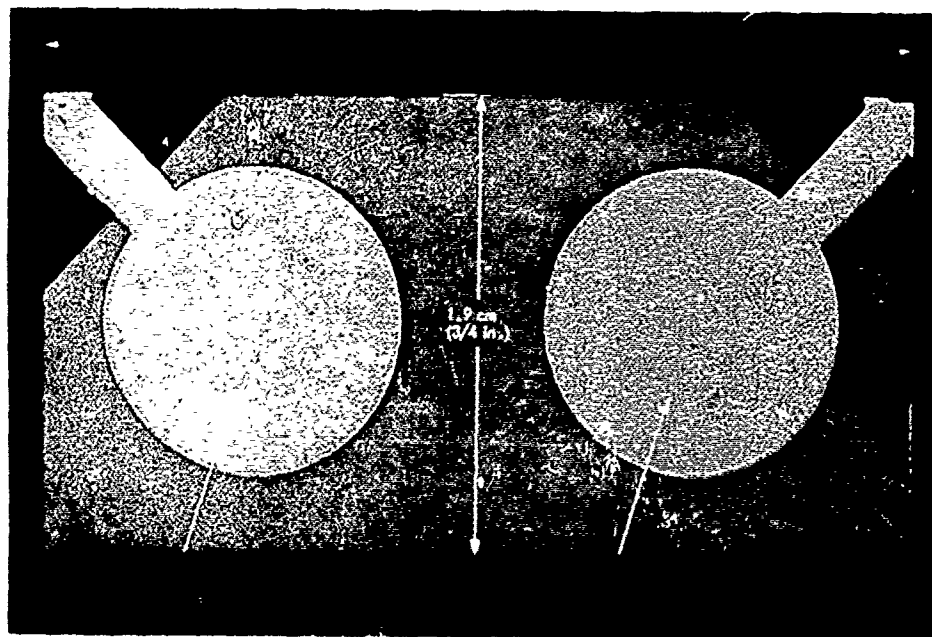


Figure 11a. Quartz Crystal Doublet with Two Independent Electrodes (Side 1)

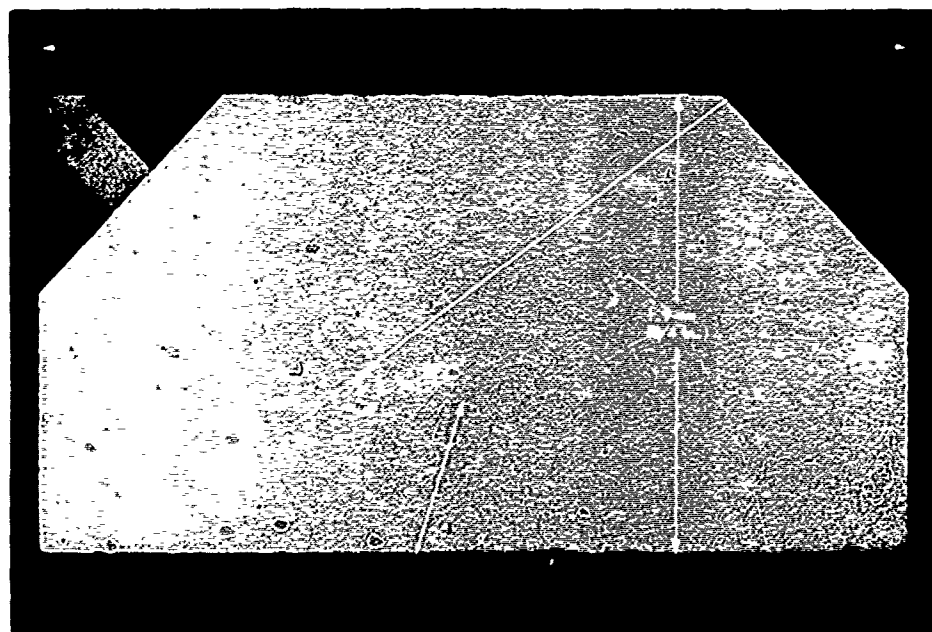


Figure 11b. Quartz Crystal Doublet with Common Electrode (Side 2)

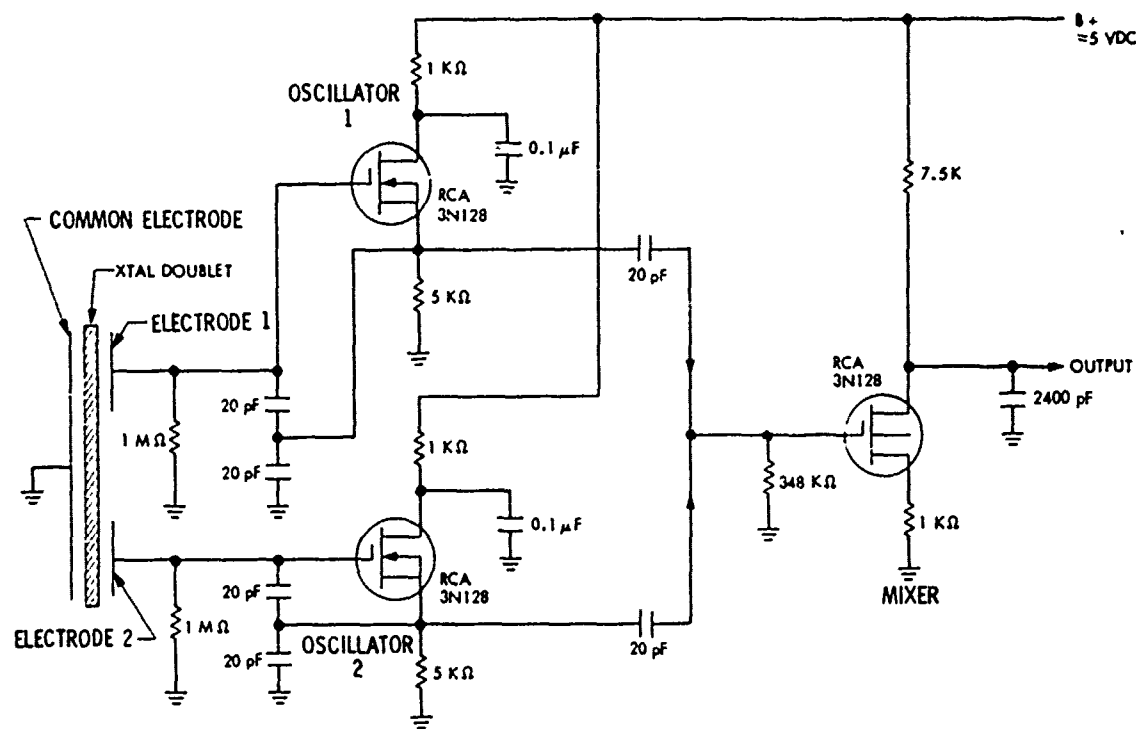


Figure 12. Schematic Diagram of the Circuitry Used for the Low Temperature QCM Units

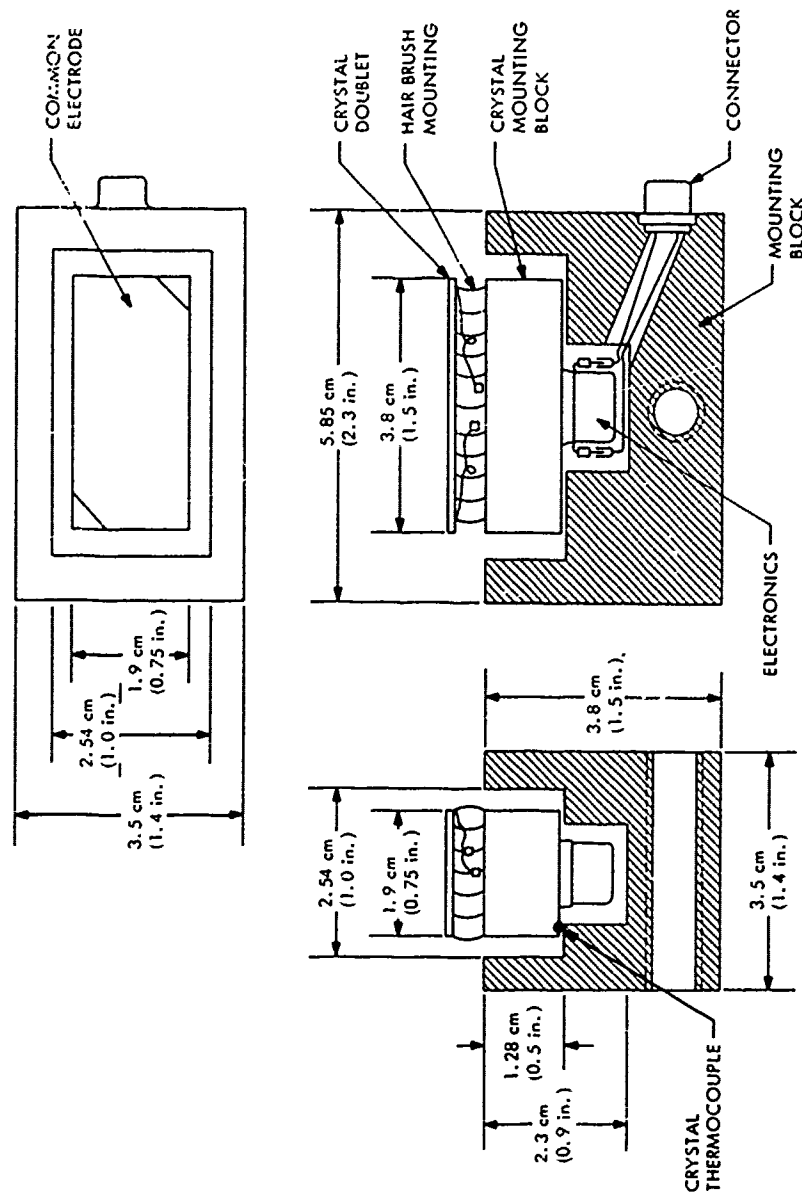


Figure 13. Schematic Diagram of a Variable Temperature QCM Unit

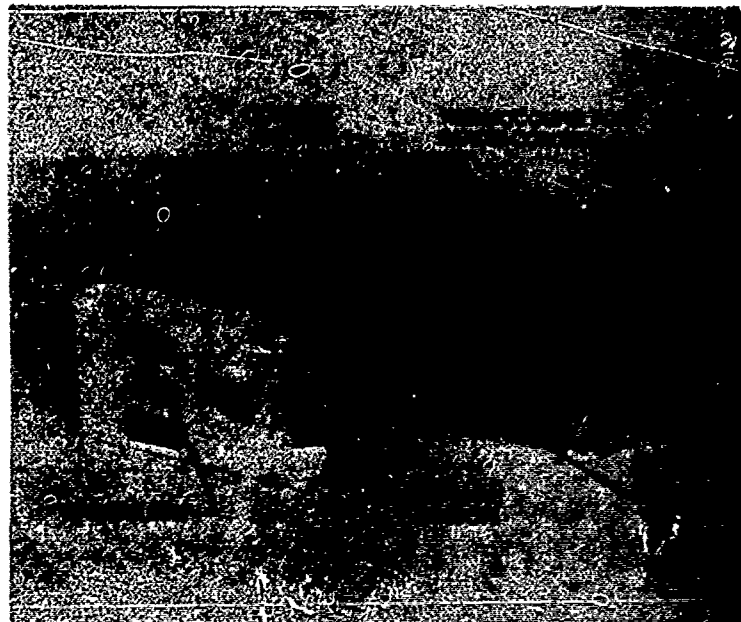


Figure 14a. A View of a QCM Unit with the Teflon Collimator Removed



Figure 14b. A View of a QCM Unit as it is Installed for Operation

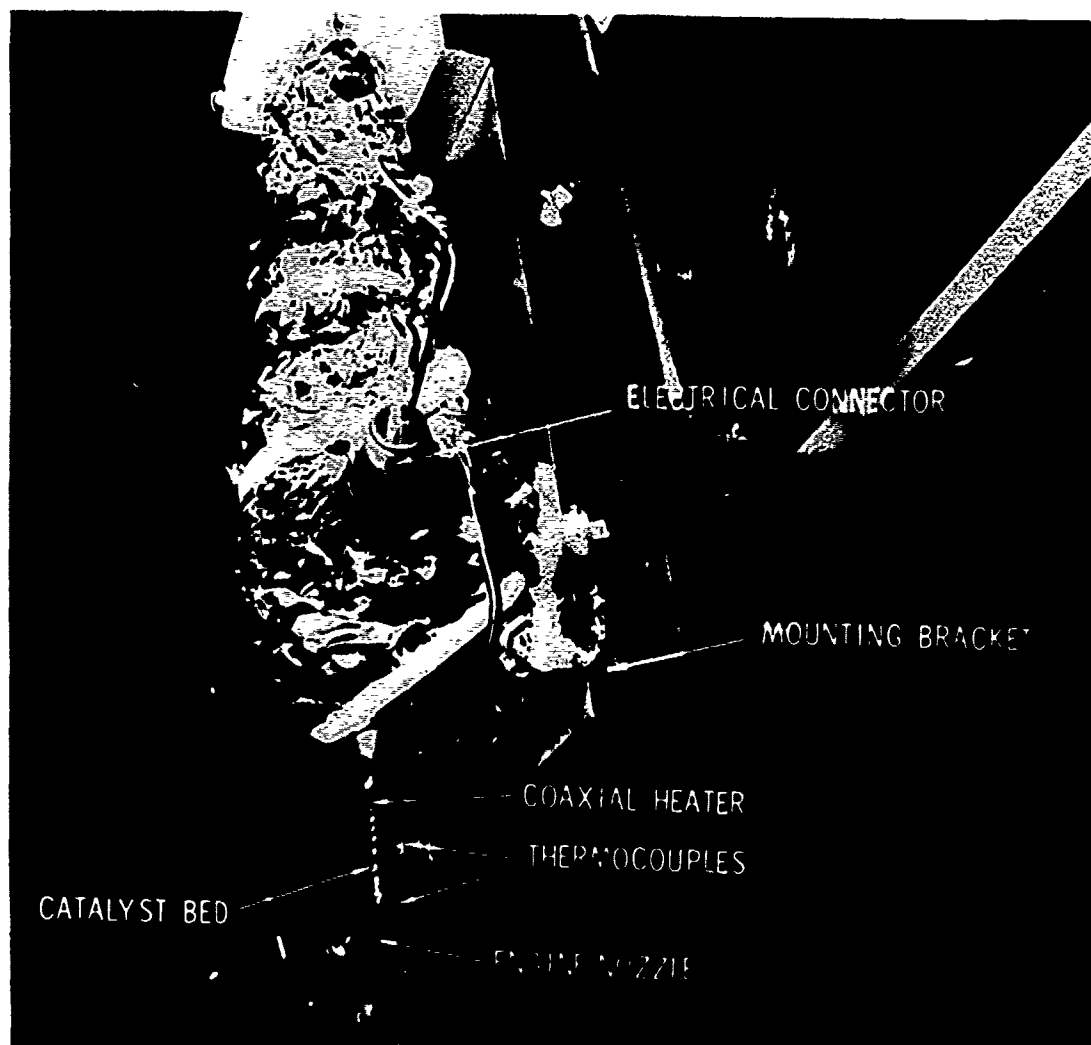


Figure 15. Perspective of Installation of the Thruster in the MOLSINK Chamber

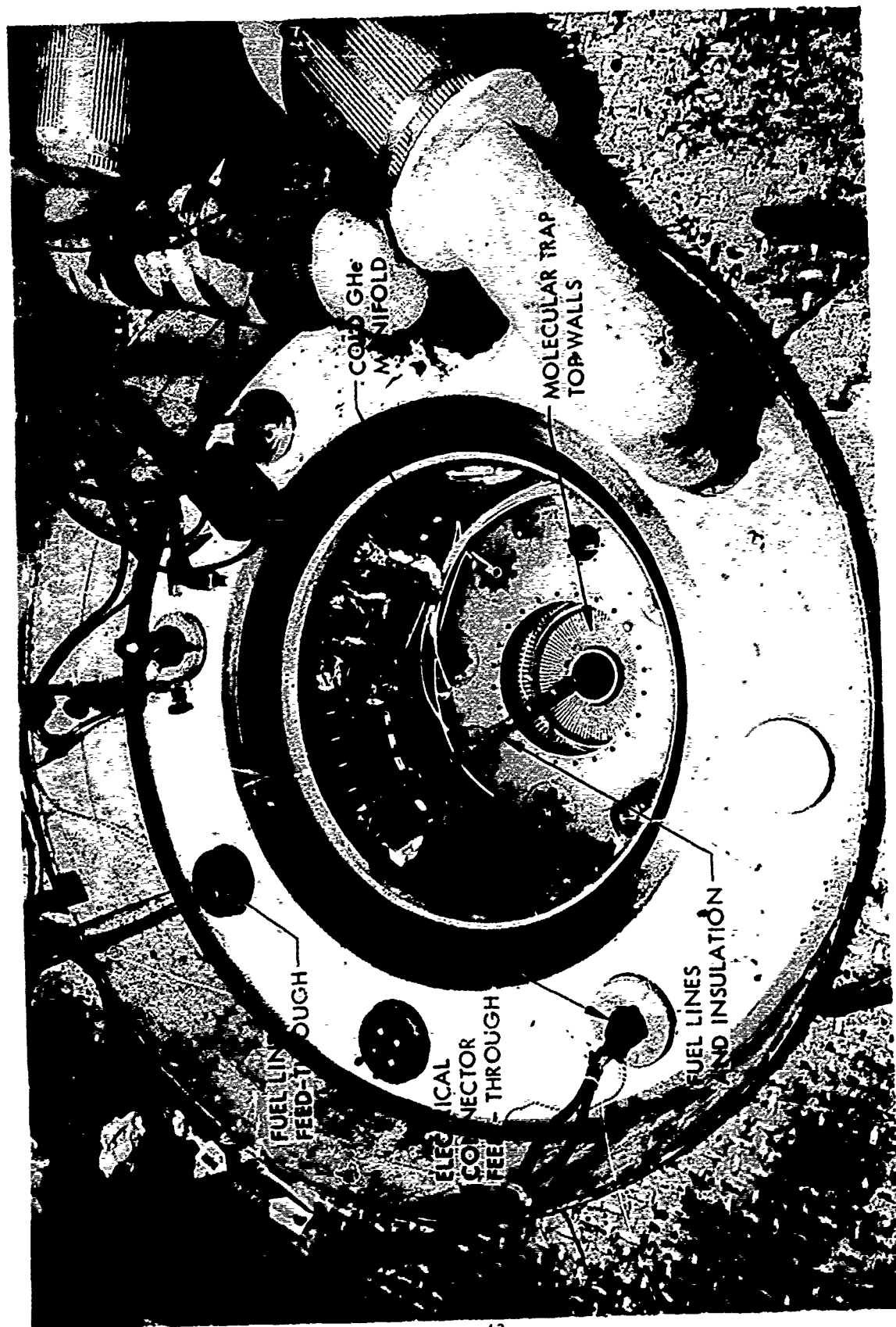


Figure 16a. Systems Arrangement at MOLSIK Top Door
(Viewed from Outside the Chamber)



Figure 16b. Propellant Feed Module

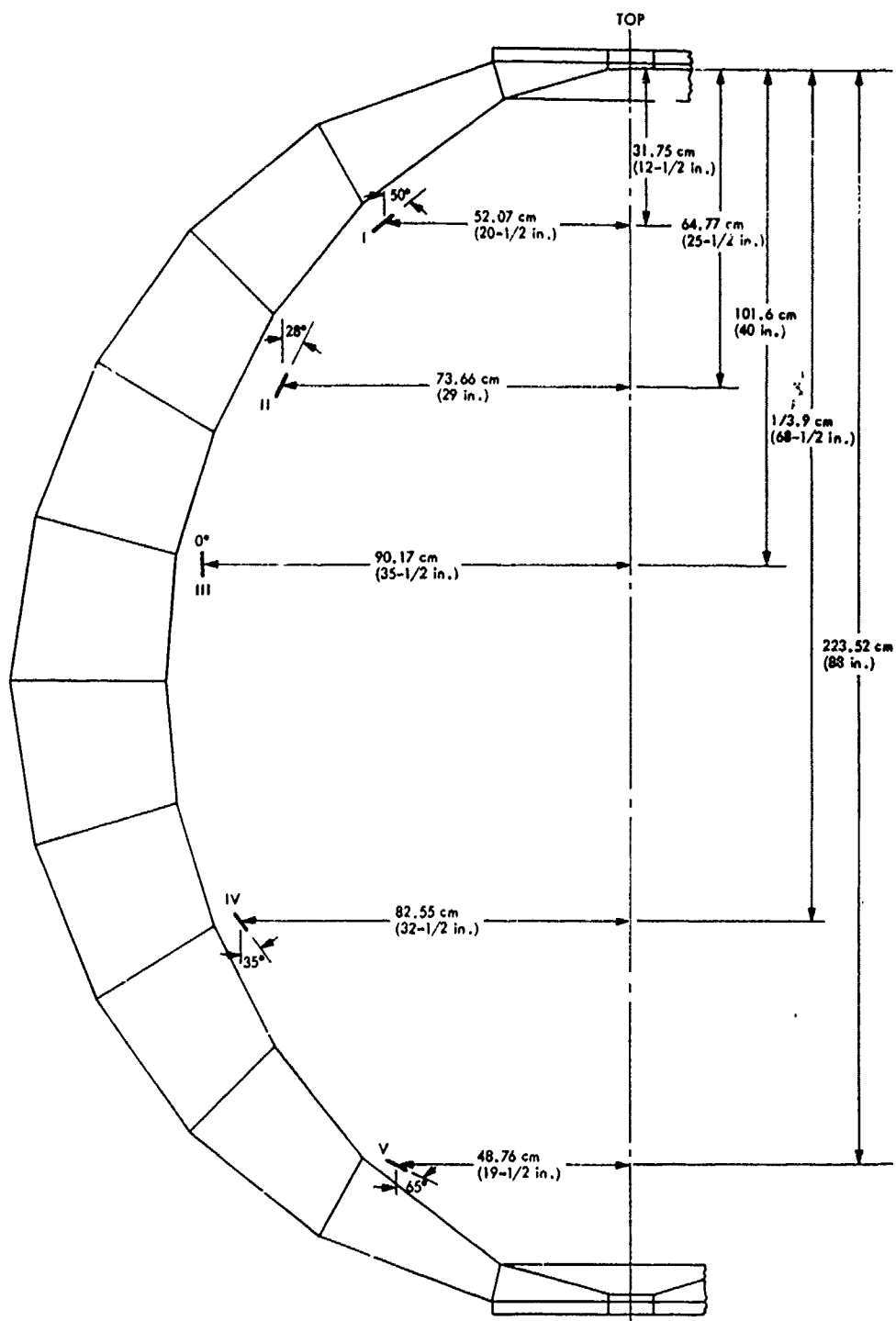


Figure 17a. QCM Orientation and Positions in MOLSINK Chamber

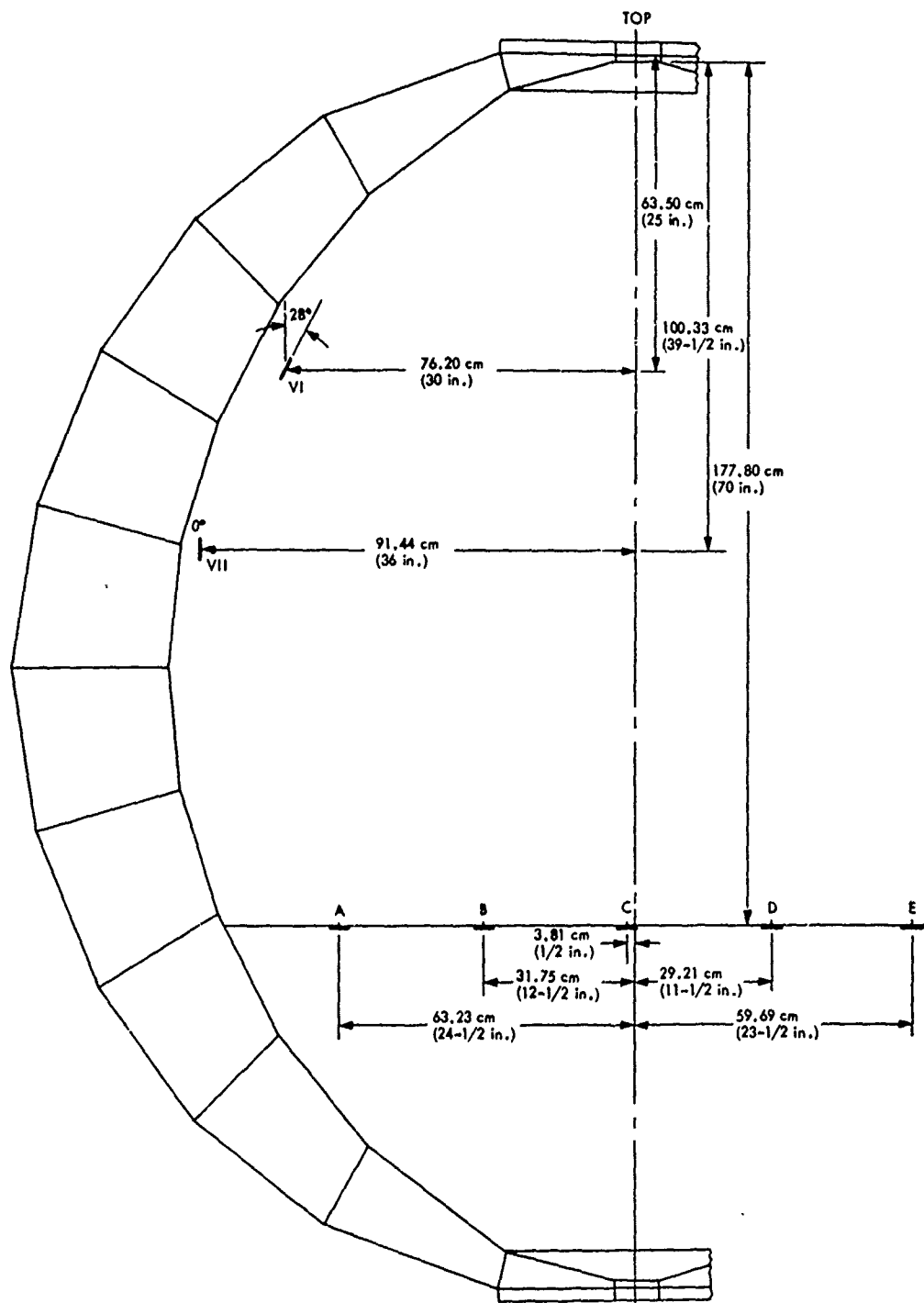


Figure 17b. QCM Orientation and Positions in MOLSINK Chamber. One Can See Also in This Figure the Locations of the Variable Temperature QCM's.

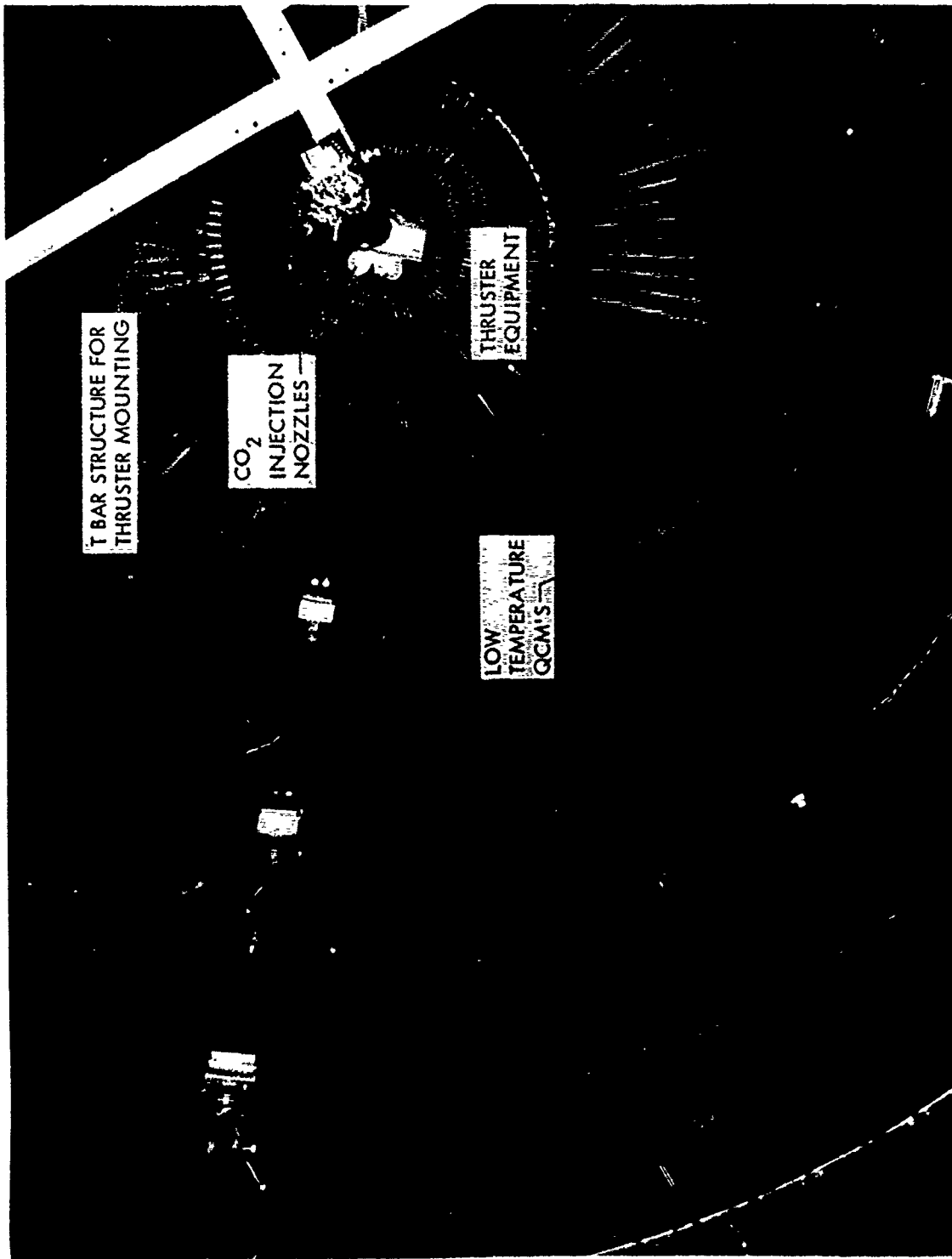


Figure 18. View of Top of the Chamber, Low Temperature QCM'S and Thruster
(The Photograph Has Been Taken Looking Upward)

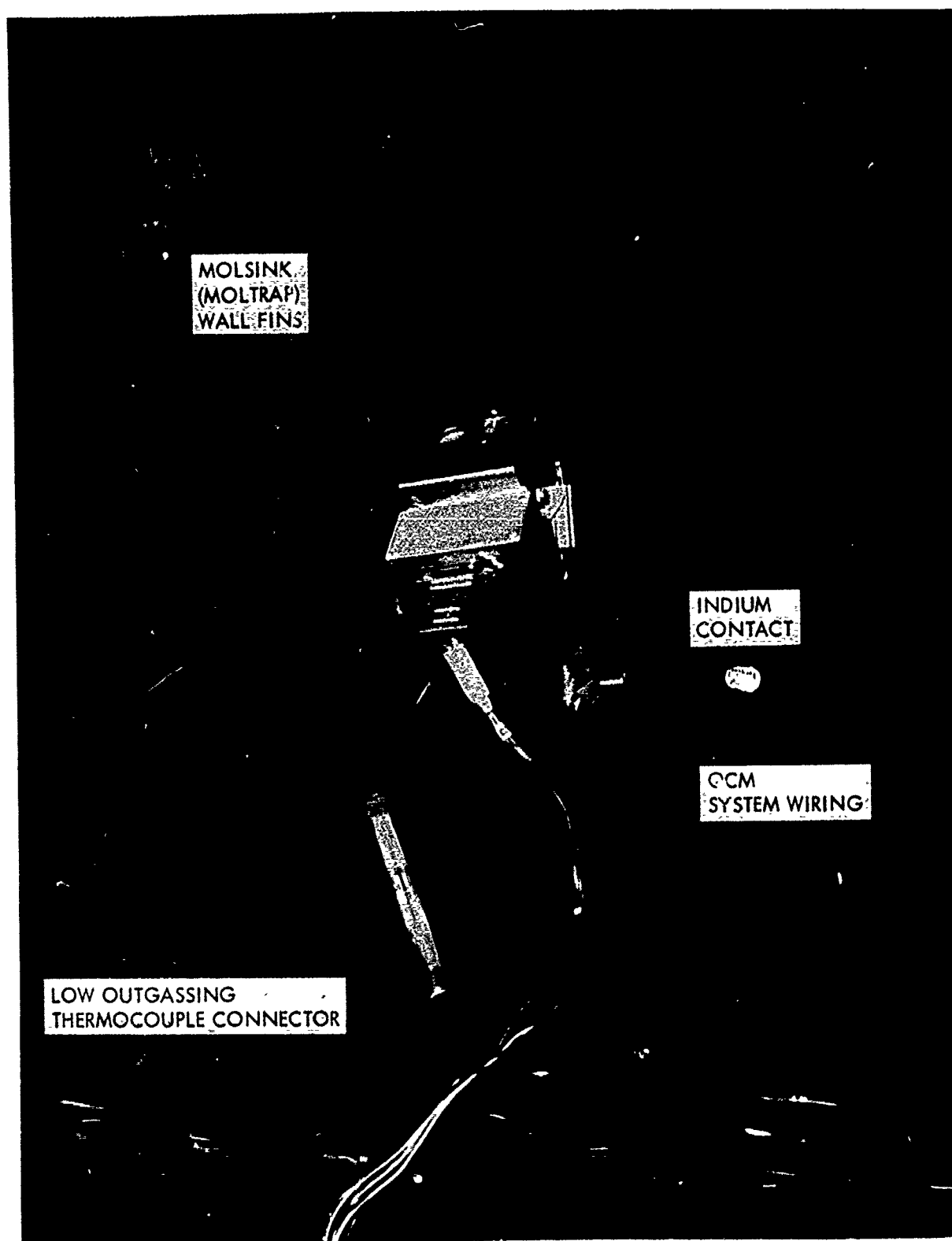


Figure 19. Low Temperature QCM Mounted on MOLSINK Walls

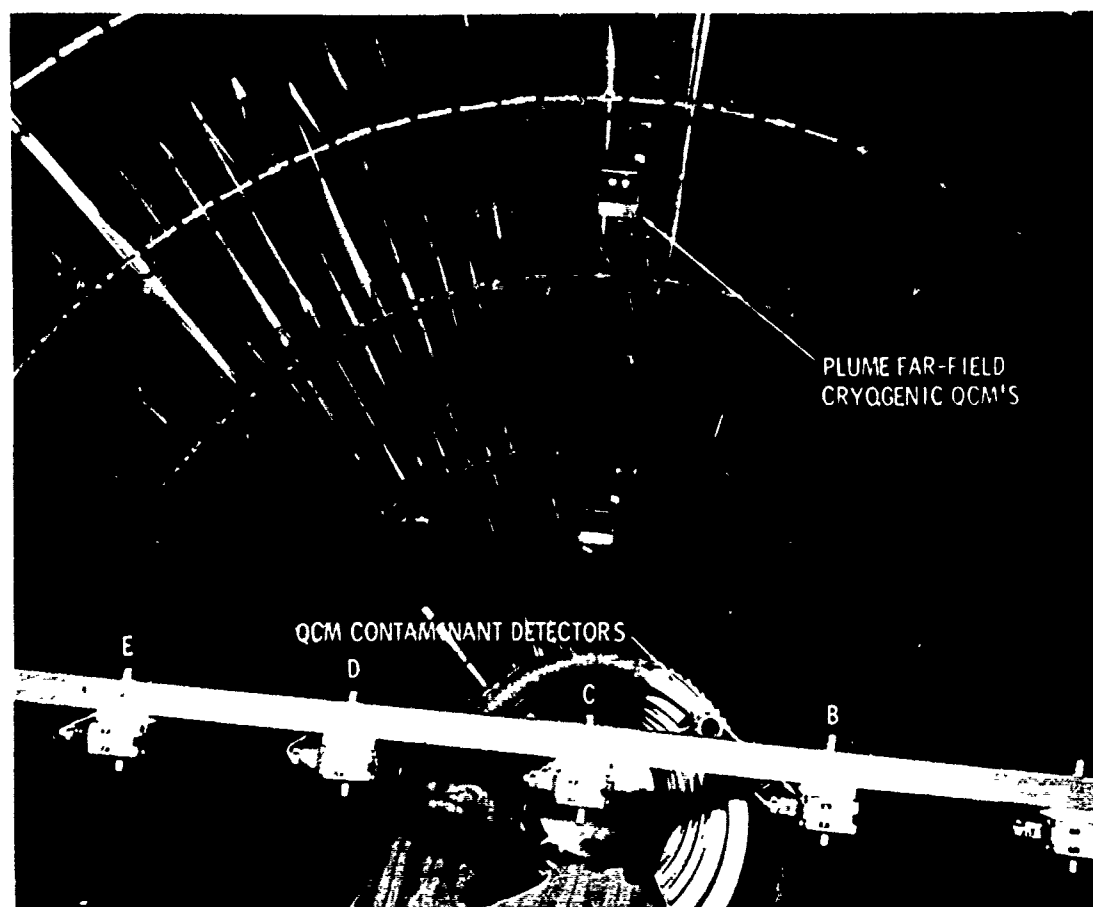


Figure 20. View of the 5 QCM's Used for Contamination Mapping and Their Location in the MOLSINK Chamber. The Photograph has been Taken from a Point Near the Engine.

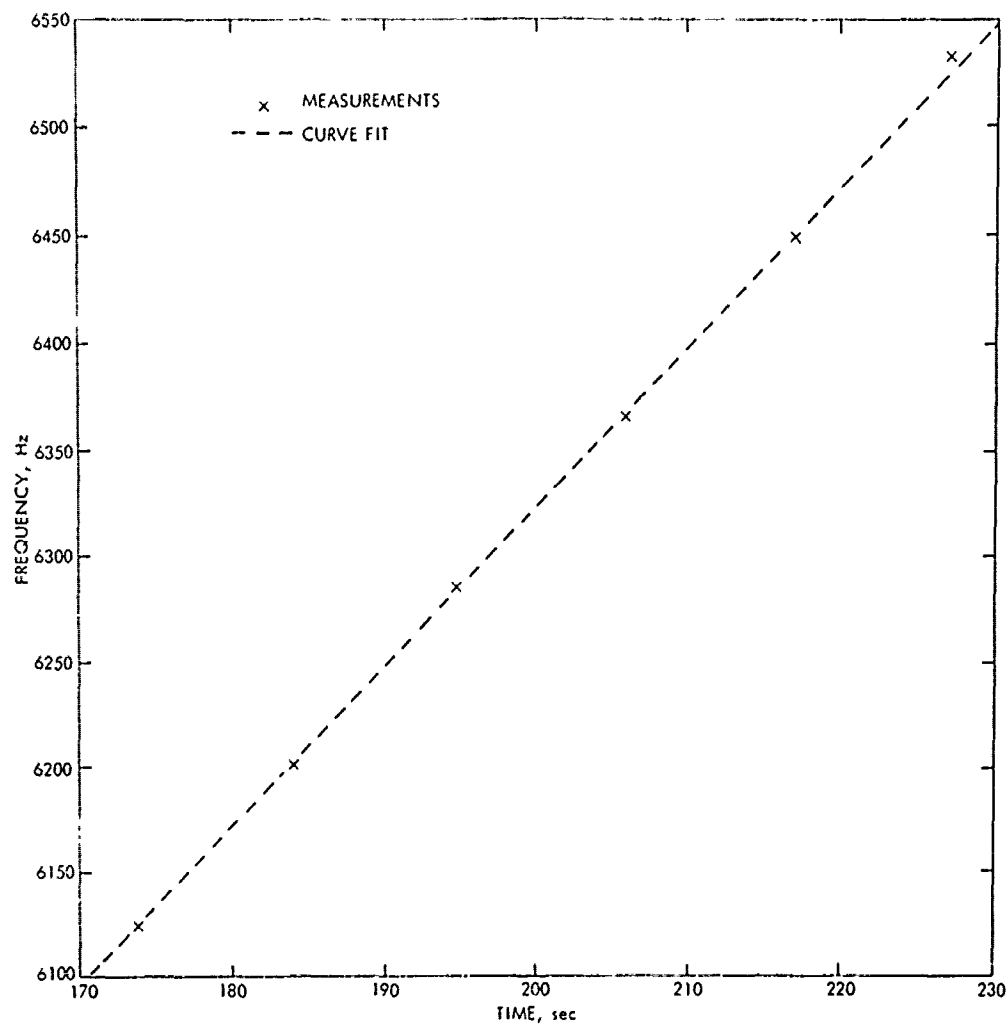


Figure 21. Frequency Shift of a Low Temperature QCM versus Time

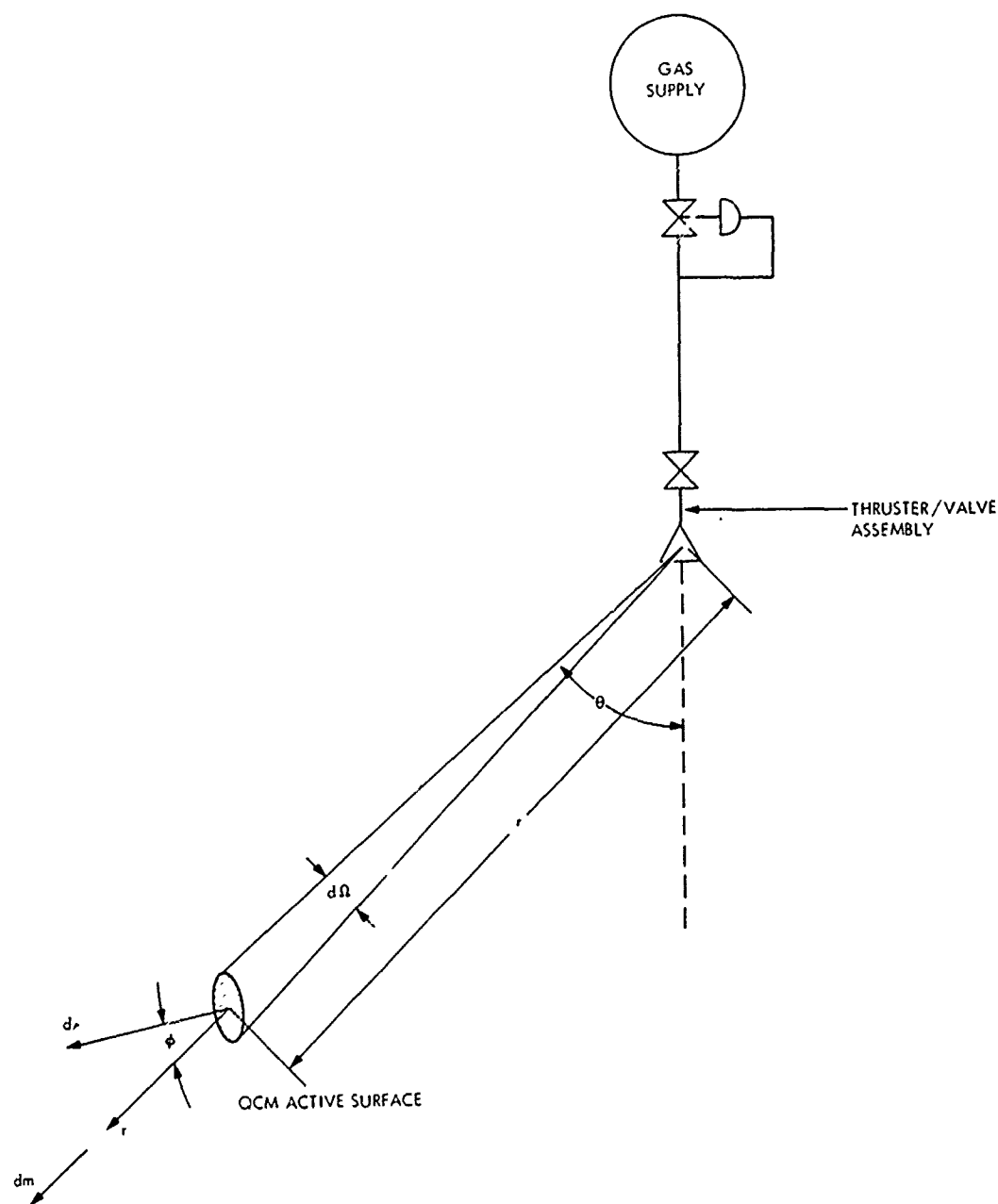


Figure 22. Solid Angle Subtended by the QCM Active Surface

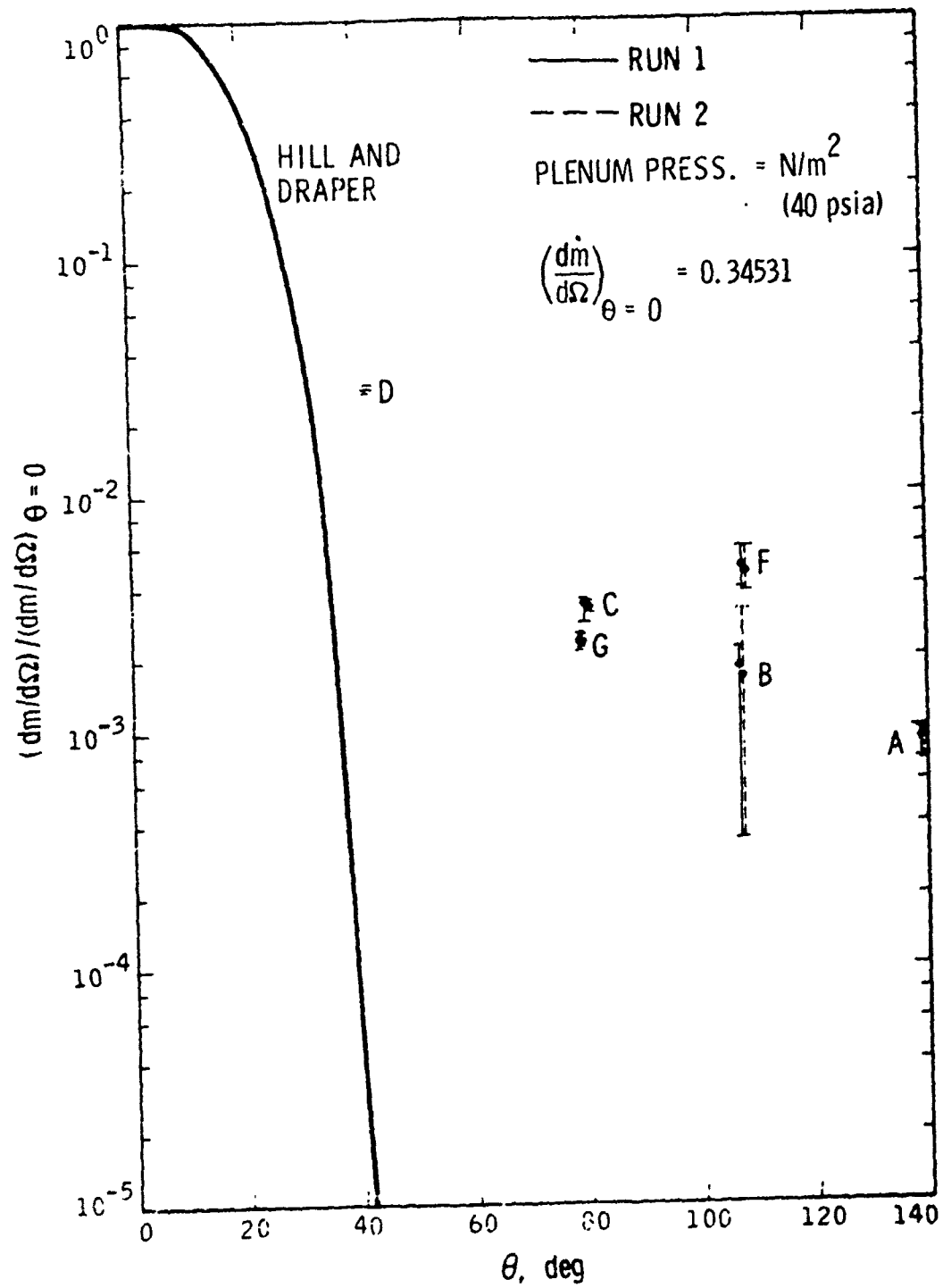


Fig. 23a. Mass Flux Measurements (Nitrogen)

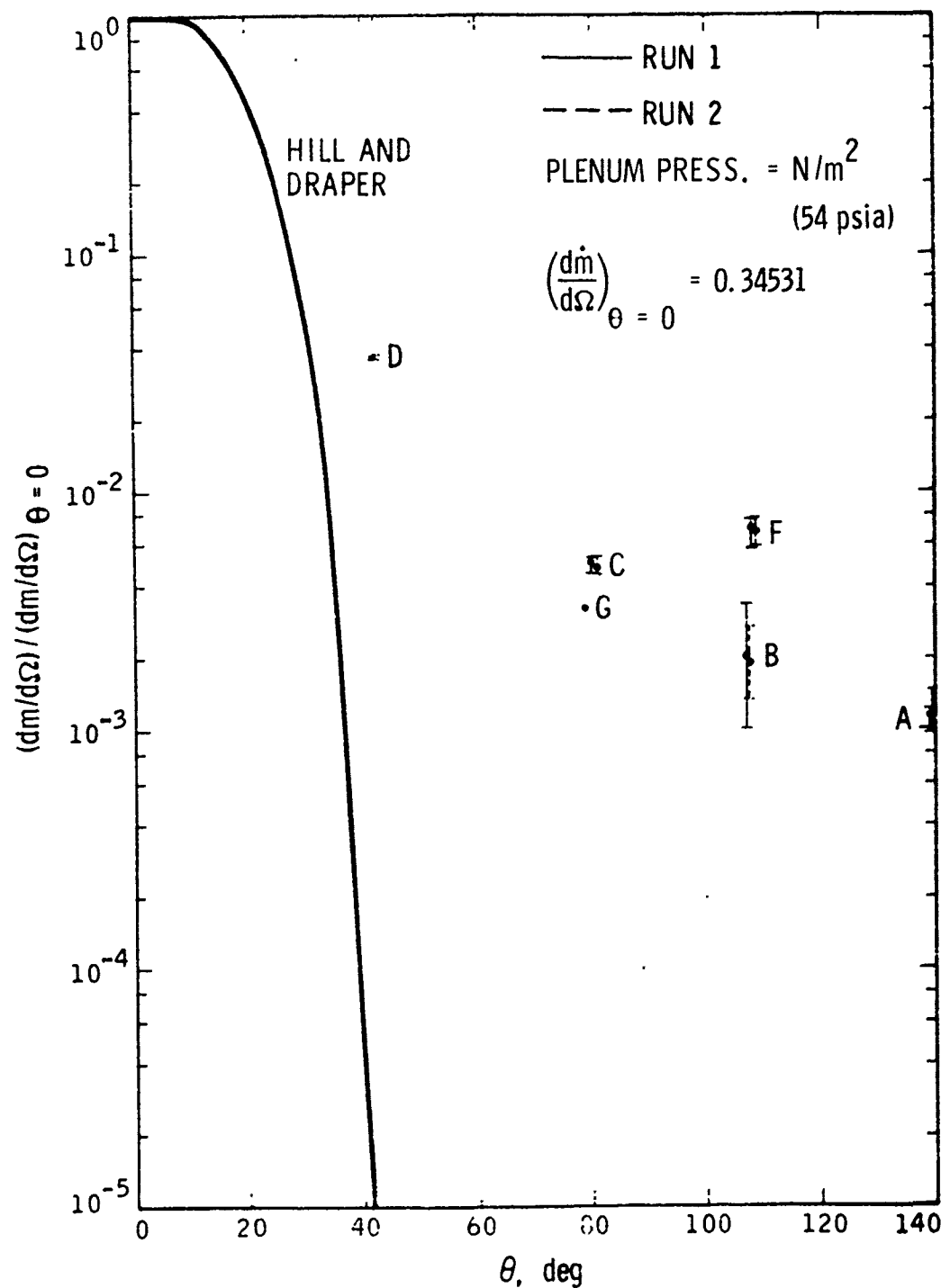


Fig. 23b. Mass Flux Measurements (Nitrogen)

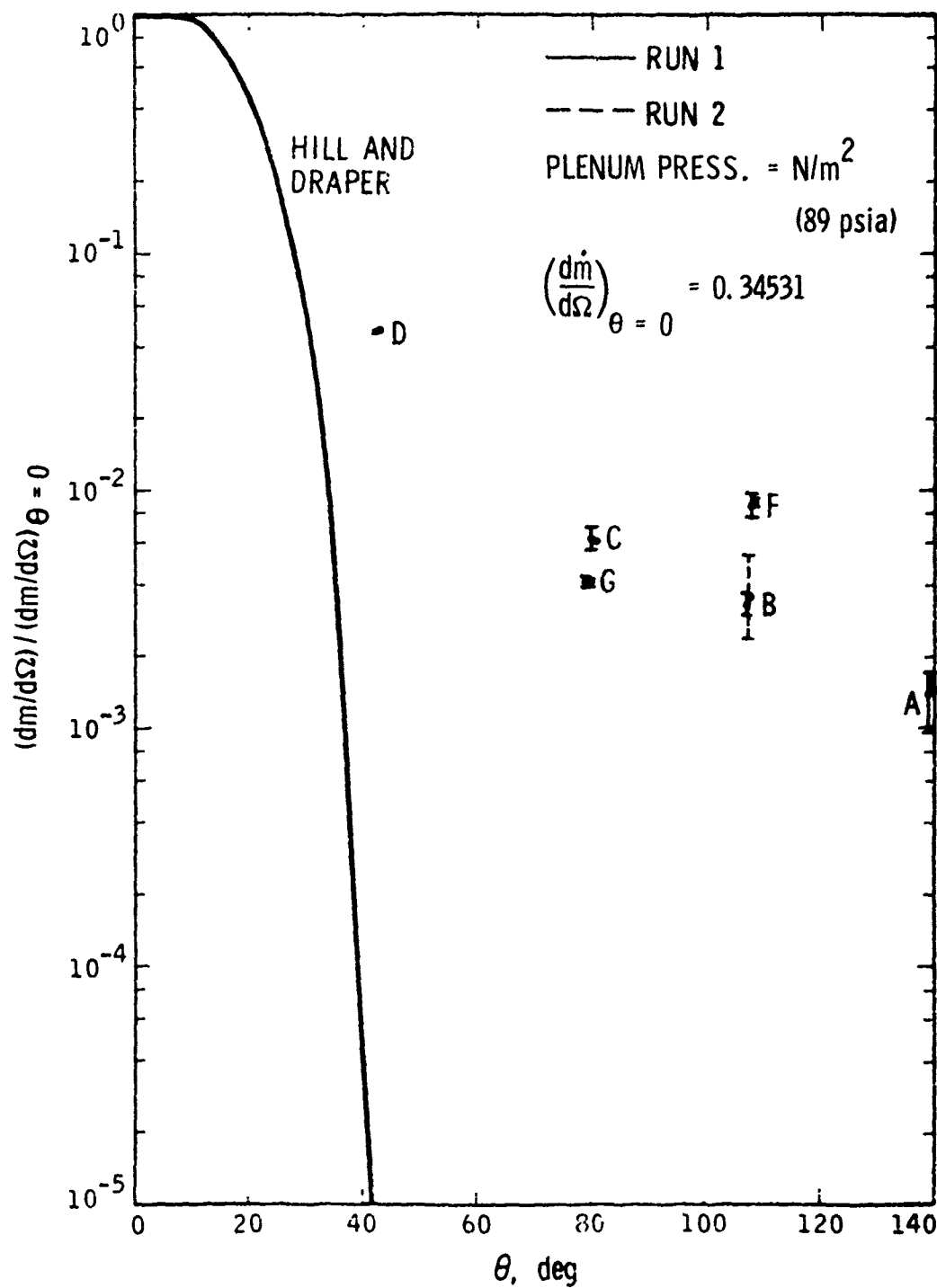


Fig. 23c. Mass Flux Measurements (Nitrogen)

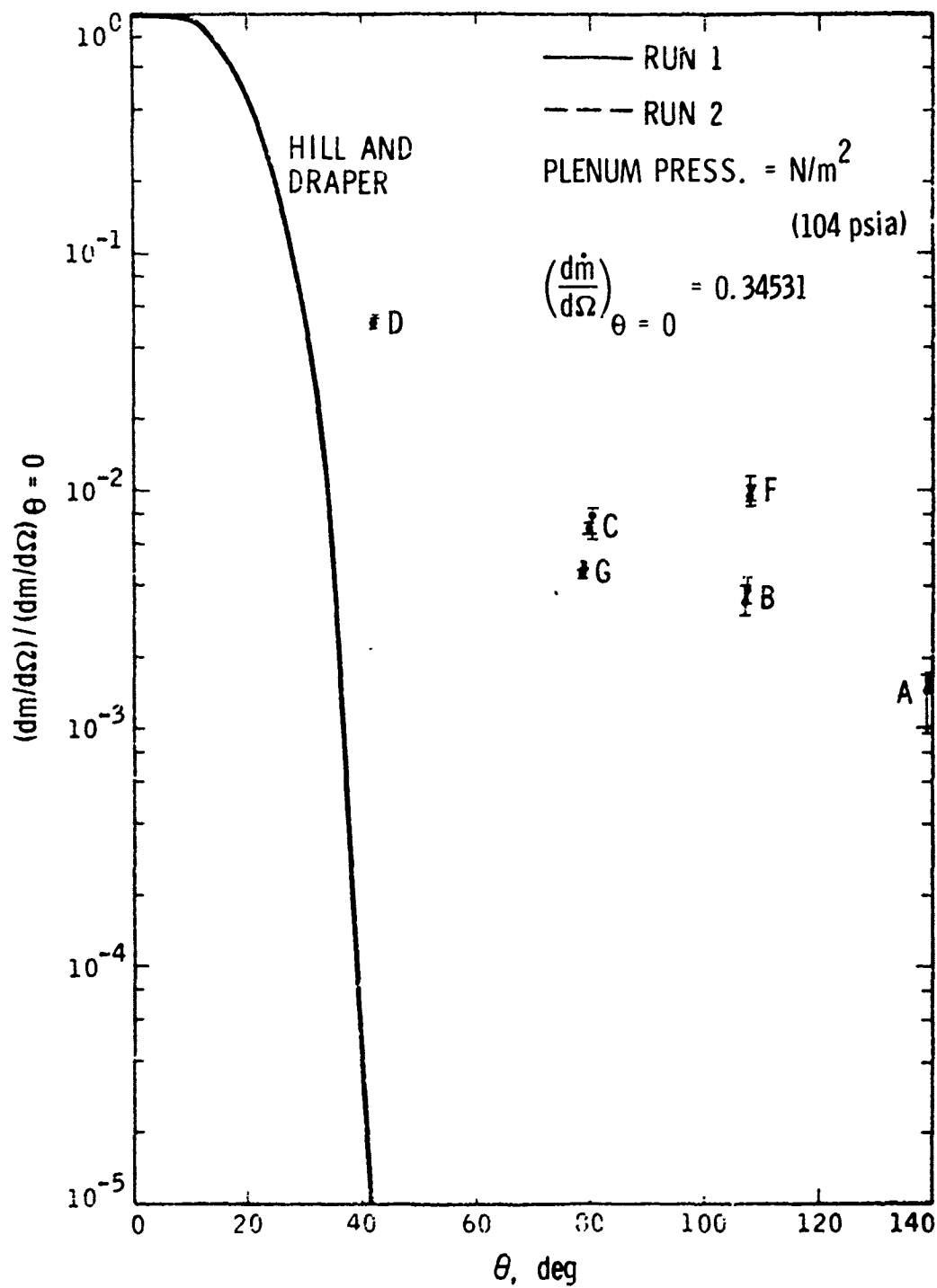


Fig. 23d. Mass Flux Measurements (Nitrogen)

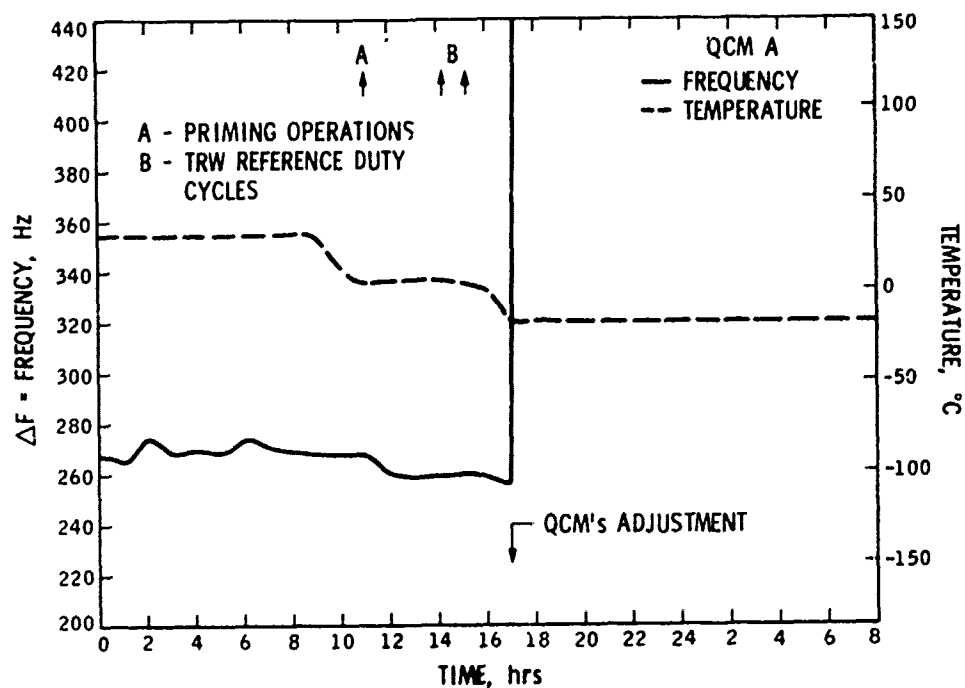


Figure 24a. Frequency and Temperature Readings for Crystal A, May 15, 1974

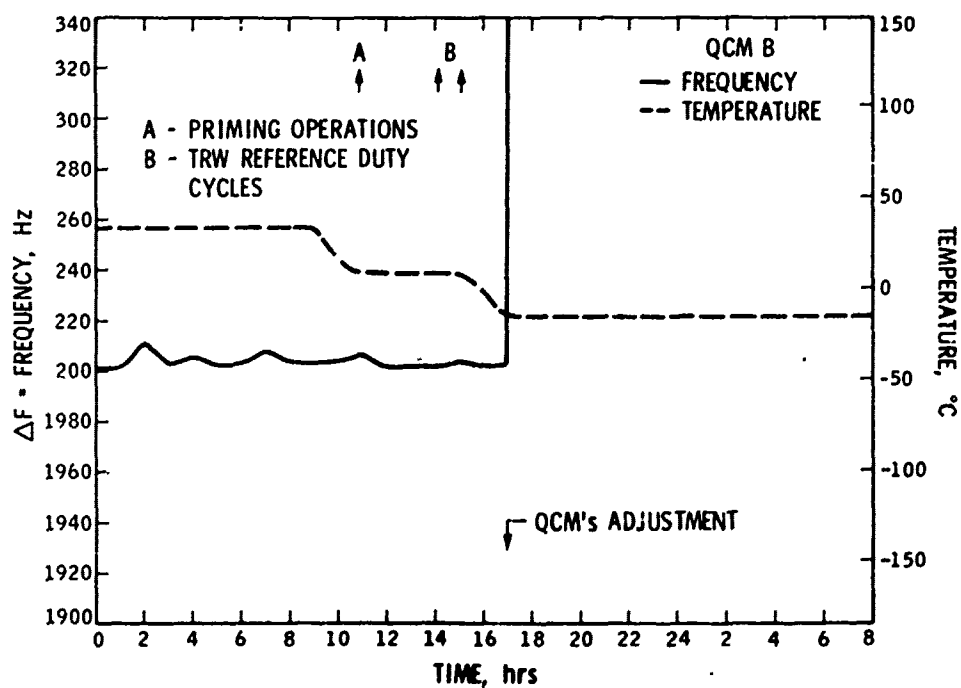


Figure 24b. Frequency and Temperature Readings for Crystal B, May 15, 1974

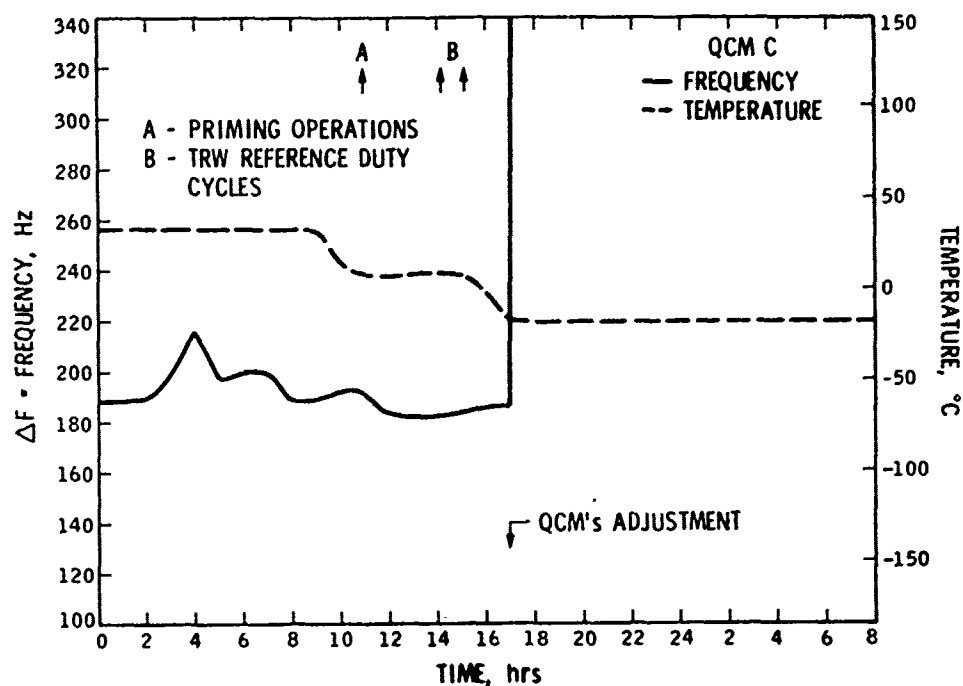


Figure 24c. Frequency and Temperature Readings for Crystal C, May 15, 1974

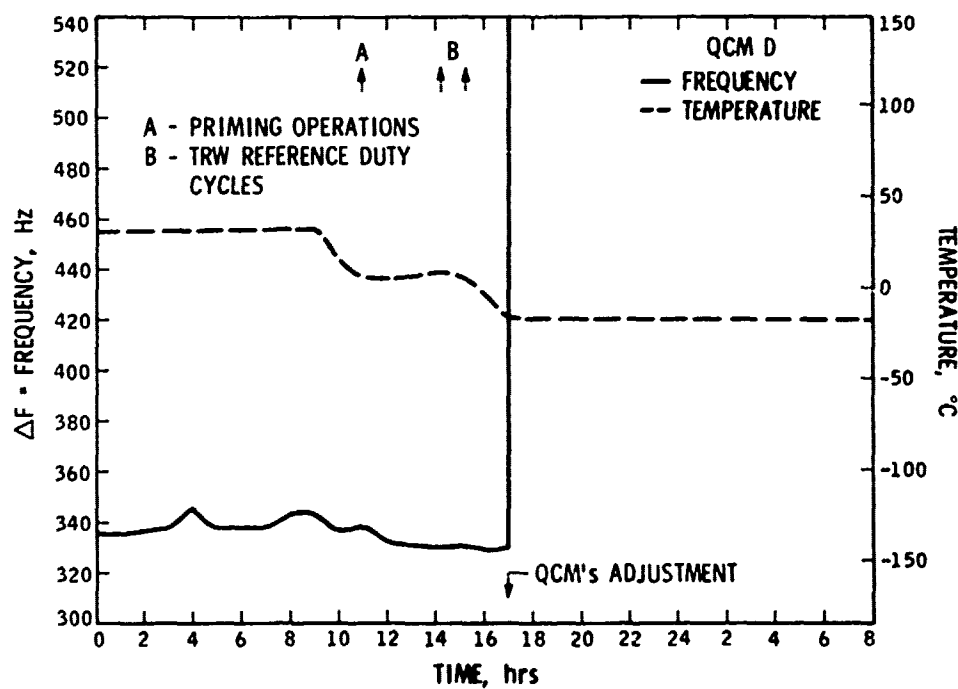


Figure 24d. Frequency and Temperature Readings for Crystal D, May 15, 1974

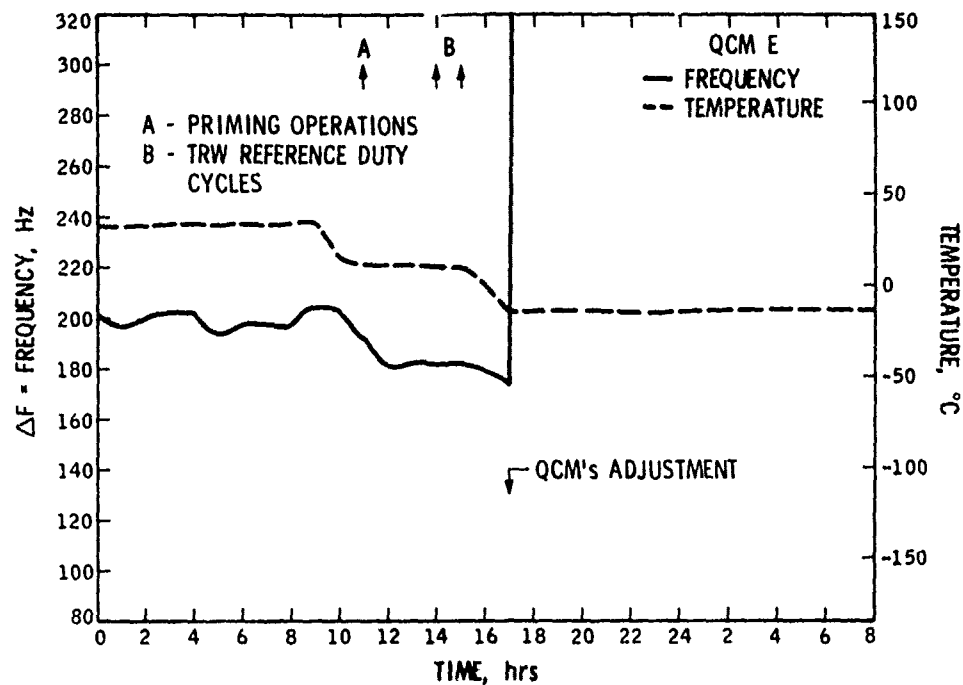


Figure 24e. Frequency and Temperature Readings for Crystal E, May 15, 1974

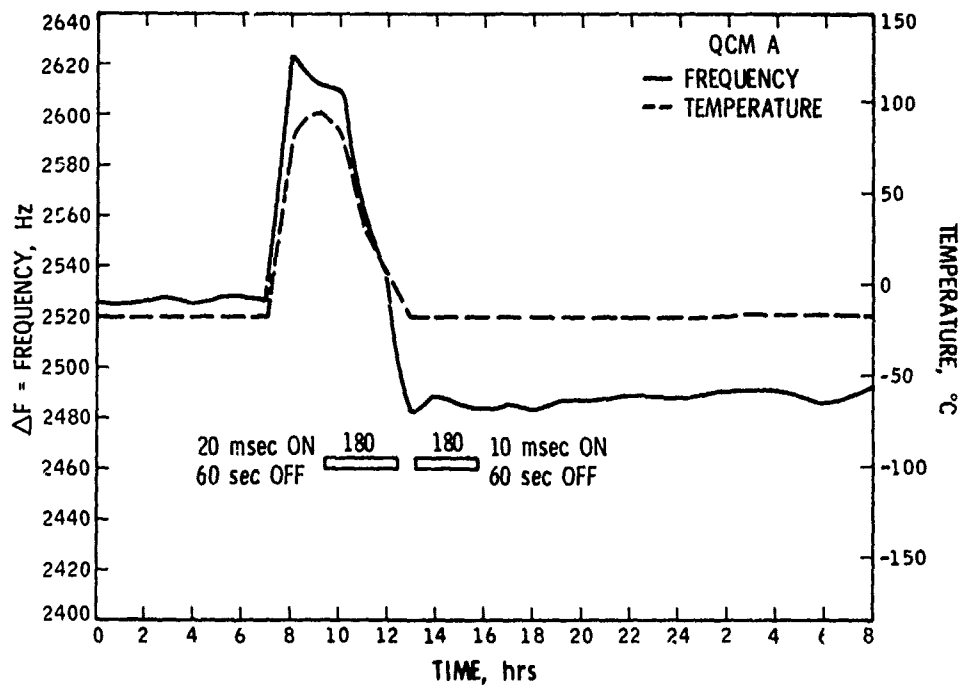


Figure 25a. Frequency and Temperature Readings for Crystal A, May 16, 1974

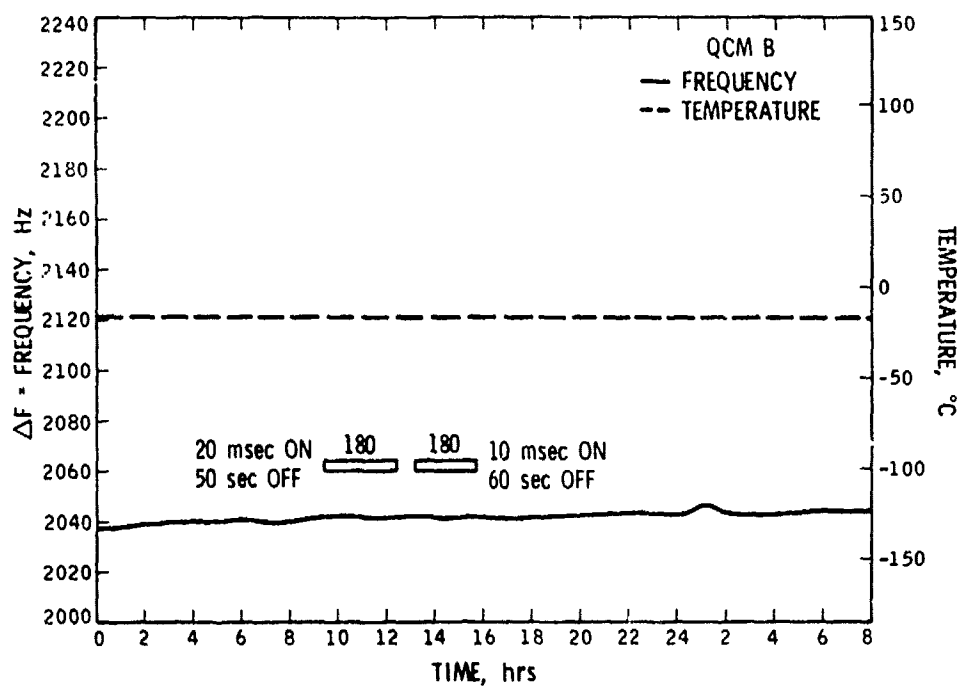


Figure 25b. Frequency and Temperature Readings for Crystal B, May 16, 1974

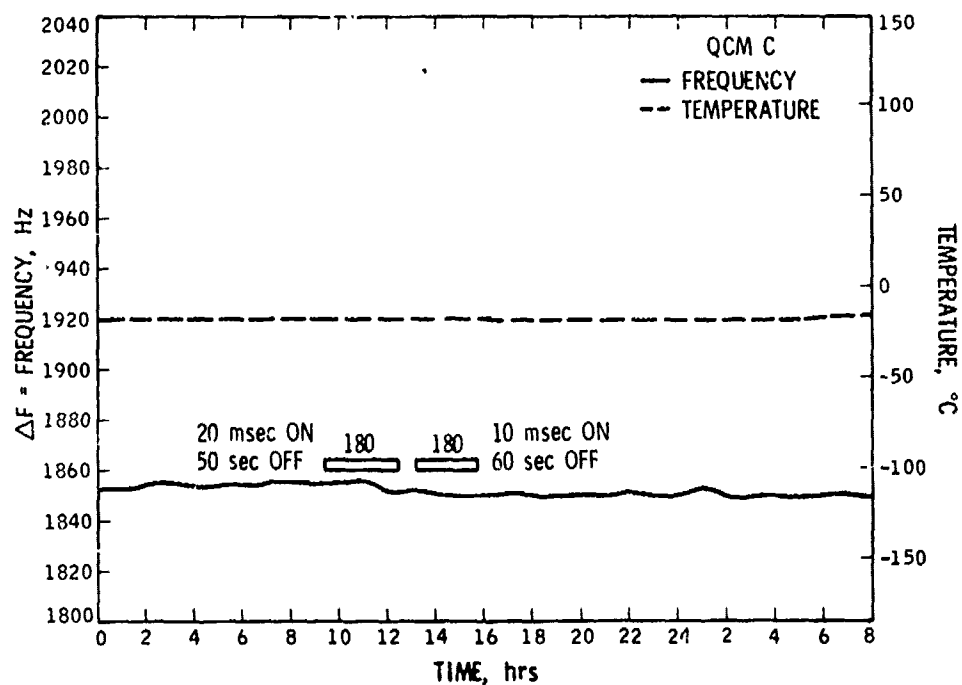


Figure 25c. Frequency and Temperature Readings for Crystal C, May 16, 1974

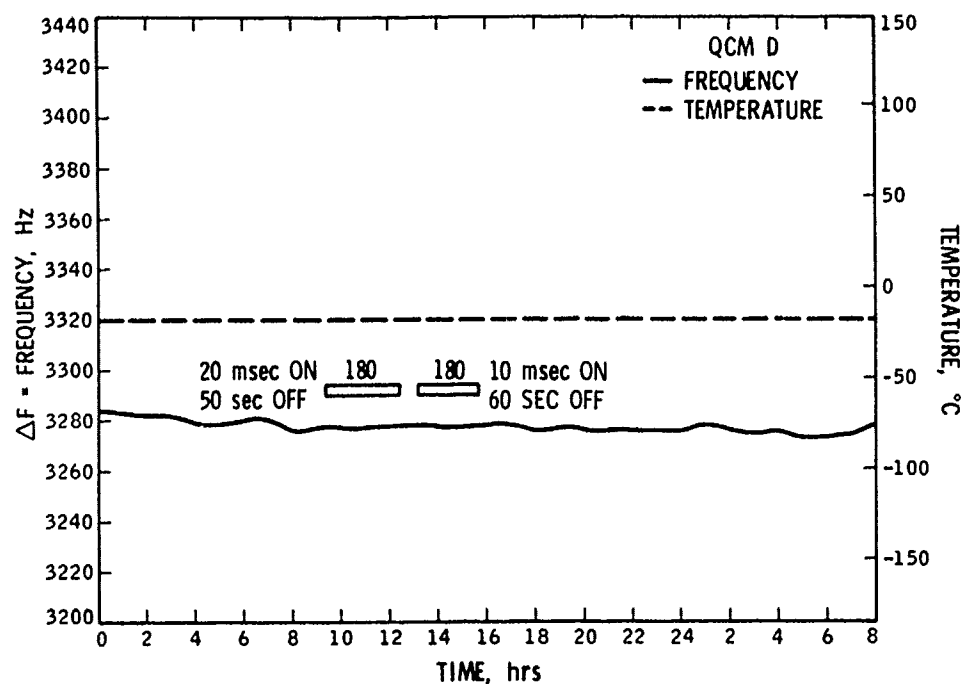


Figure 25d. Frequency and Temperature Readings for Crystal D, May 16, 1974

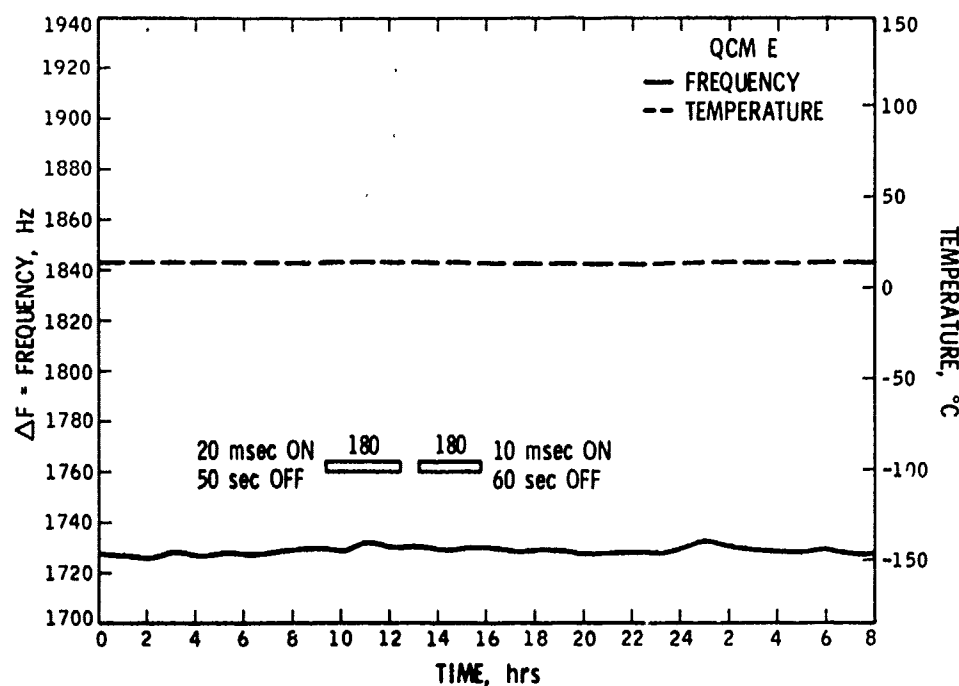


Figure 25e. Frequency and Temperature Readings for Crystal E, May 16, 1974

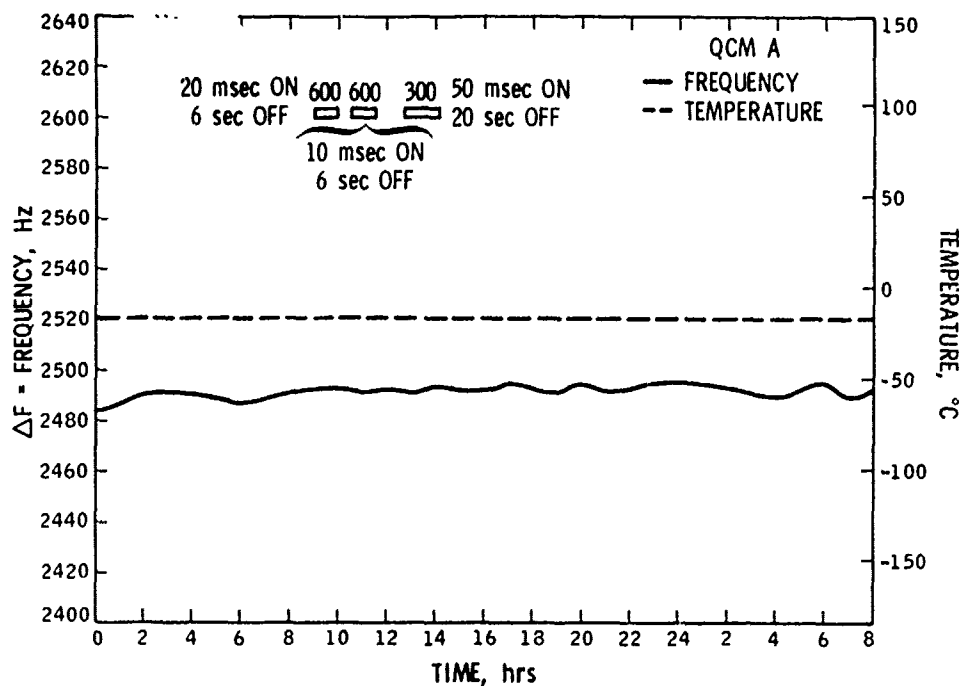


Figure 26a. Frequency and Temperature Readings for Crystal A, May 17, 1974

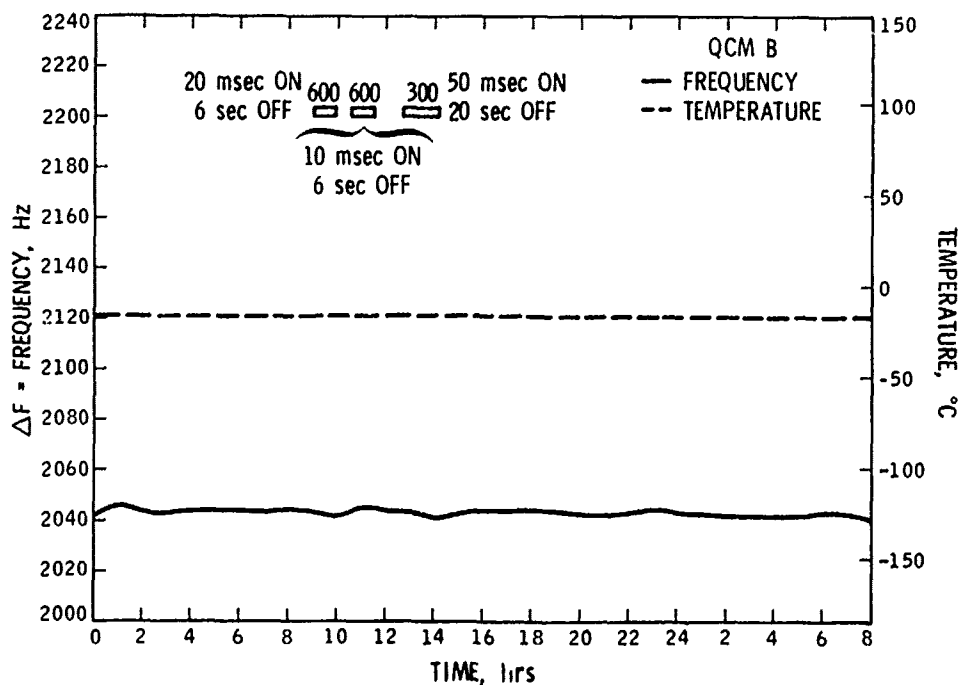


Figure 26b. Frequency and Temperature Readings for Crystal B, May 17, 1974

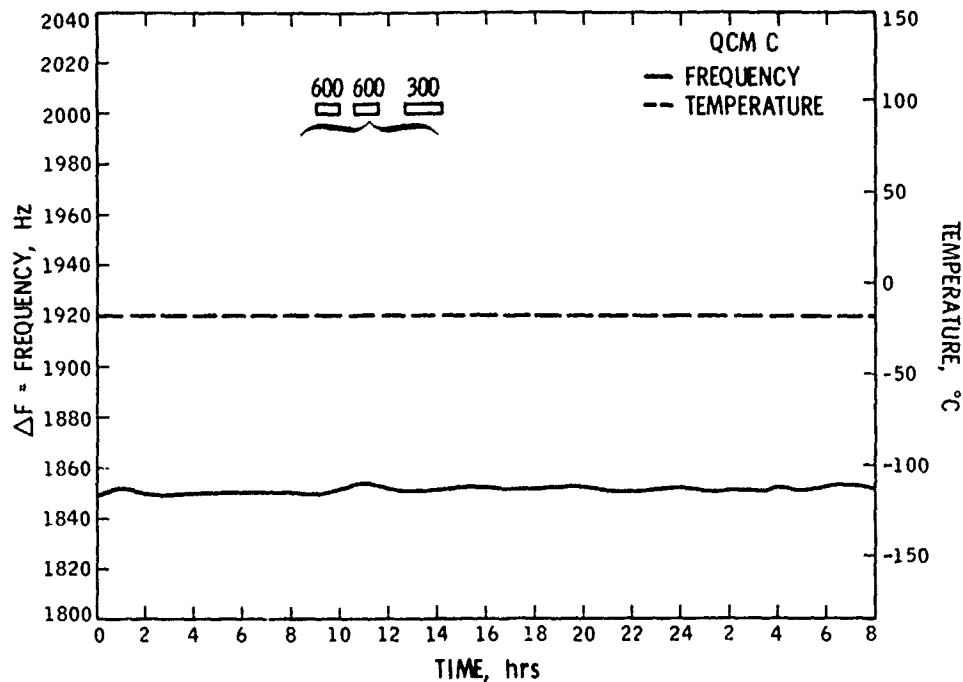


Figure 26c. Frequency and Temperature Readings for Crystal C, May 17, 1974

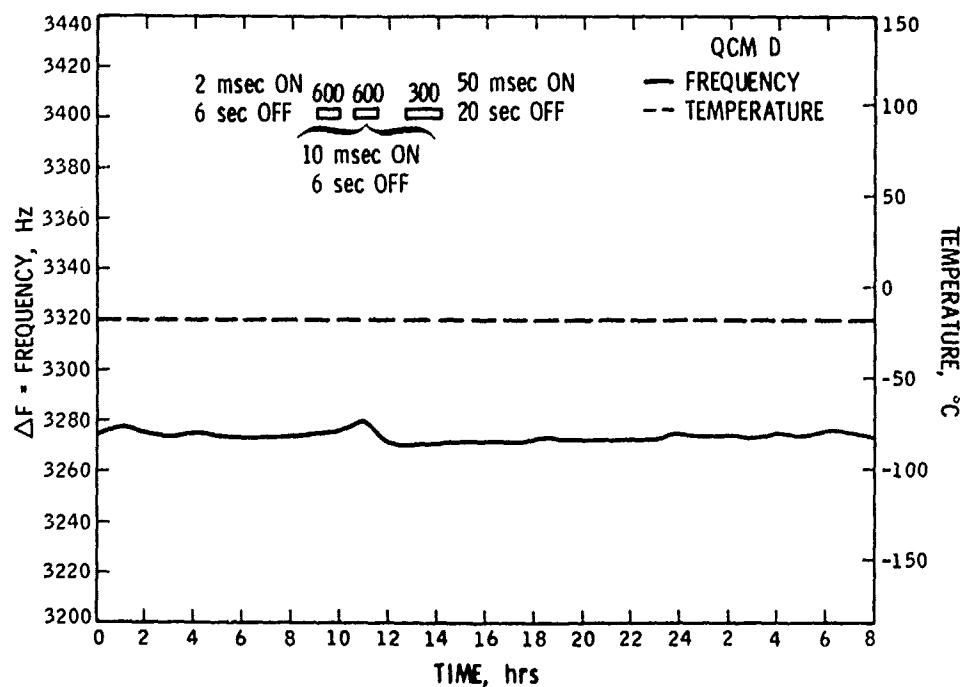


Figure 26d. Frequency and Temperature Readings for Crystal D, May 17, 1974

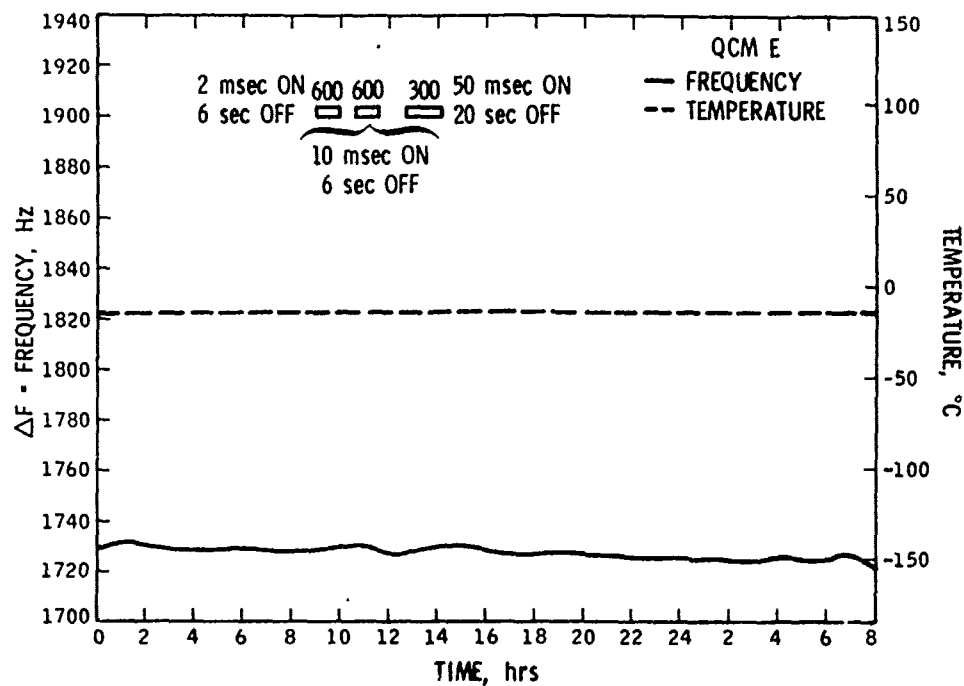


Figure 26e. Frequency and Temperature Readings for Crystal E, May 17, 1974

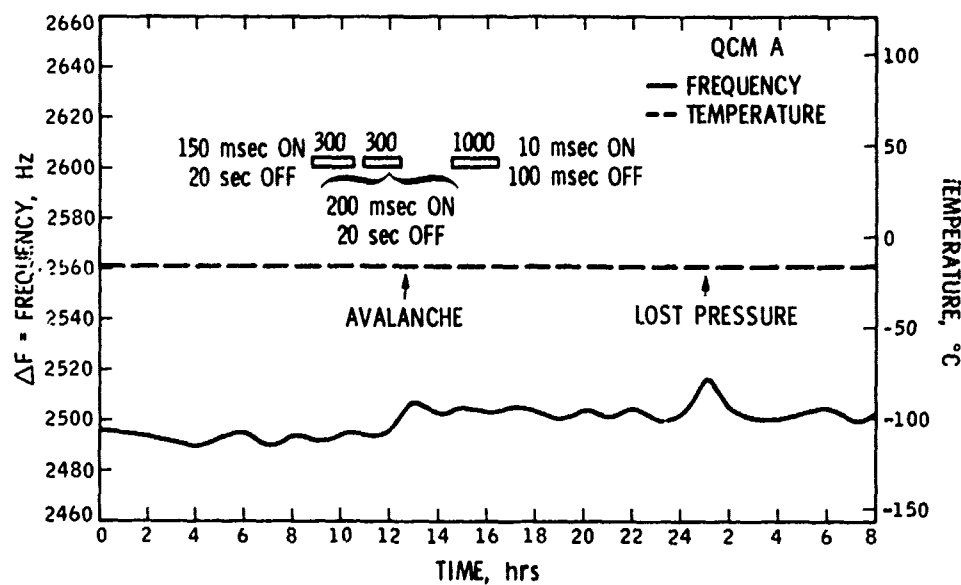


Figure 27a. Frequency and Temperature Readings for Crystal A, May 18, 1974

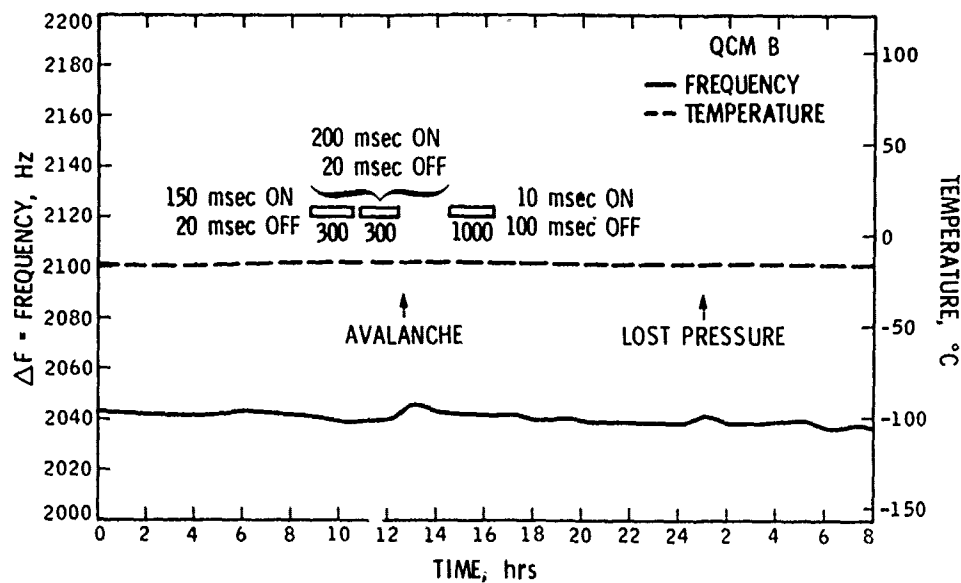


Figure 27b. Frequency and Temperature Readings for Crystal B, May 18, 1974

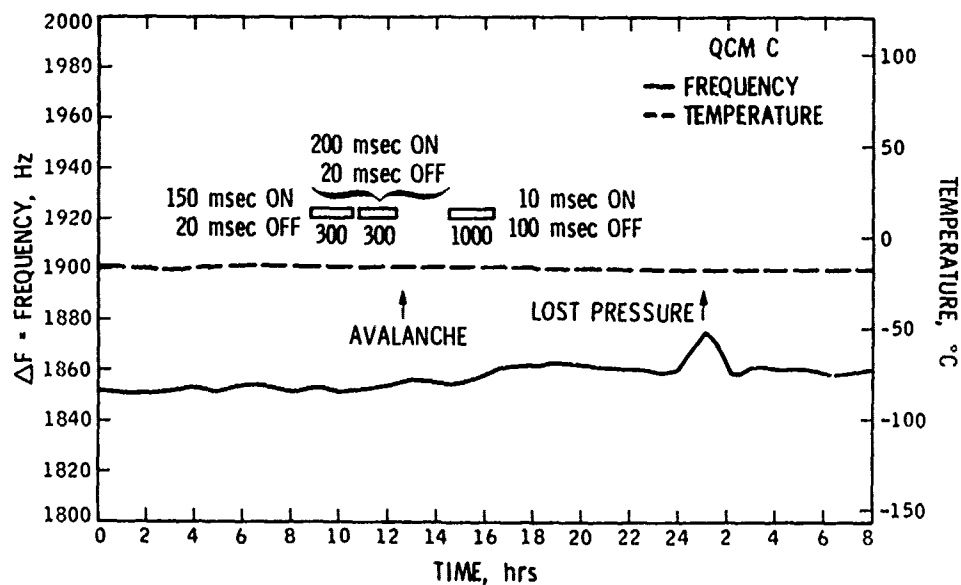


Figure 27c. Frequency and Temperature Readings for Crystal C, May 18, 1974

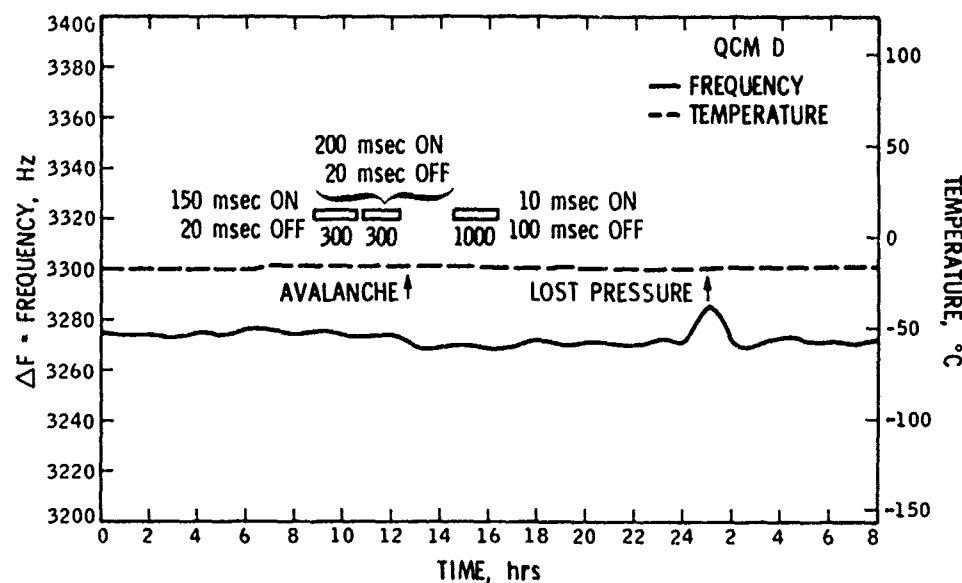


Figure 27d. Frequency and Temperature Readings for Crystal D, May 18, 1974

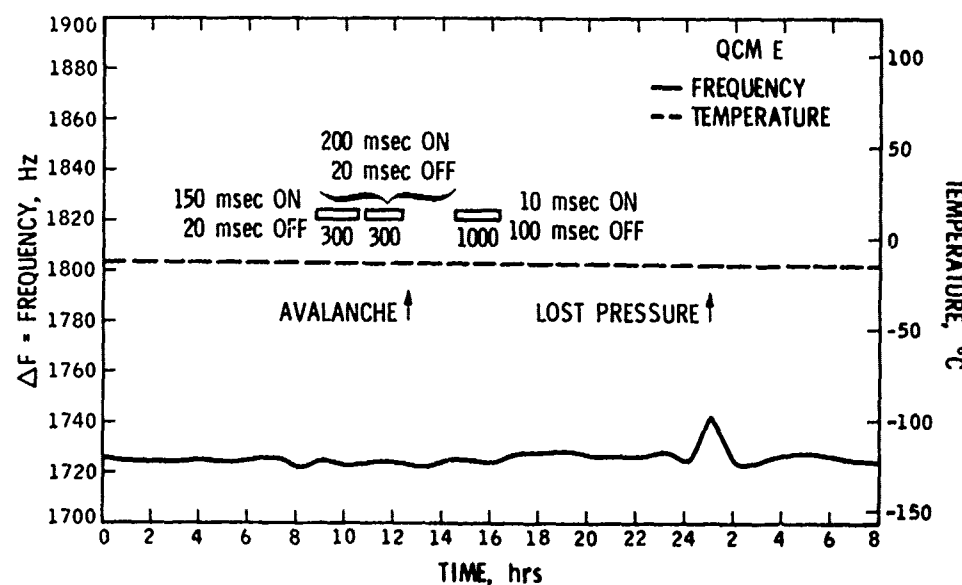


Figure 27e. Frequency and Temperature Readings for Crystal E, May 18, 1974

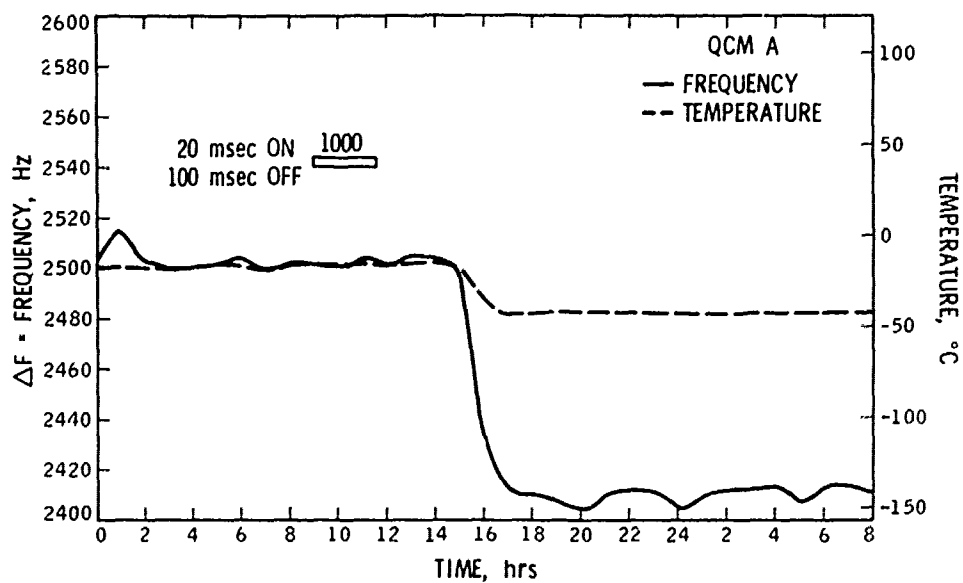


Figure 28a. Frequency and Temperature Readings for Crystal A, May 19, 1974

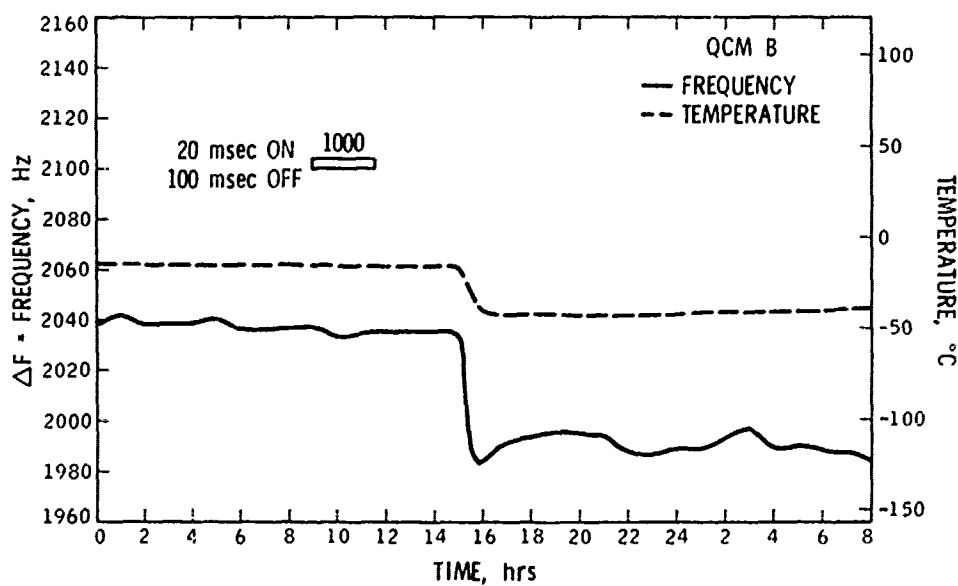


Figure 28b. Frequency and Temperature Readings for Crystal B, May 19, 1974

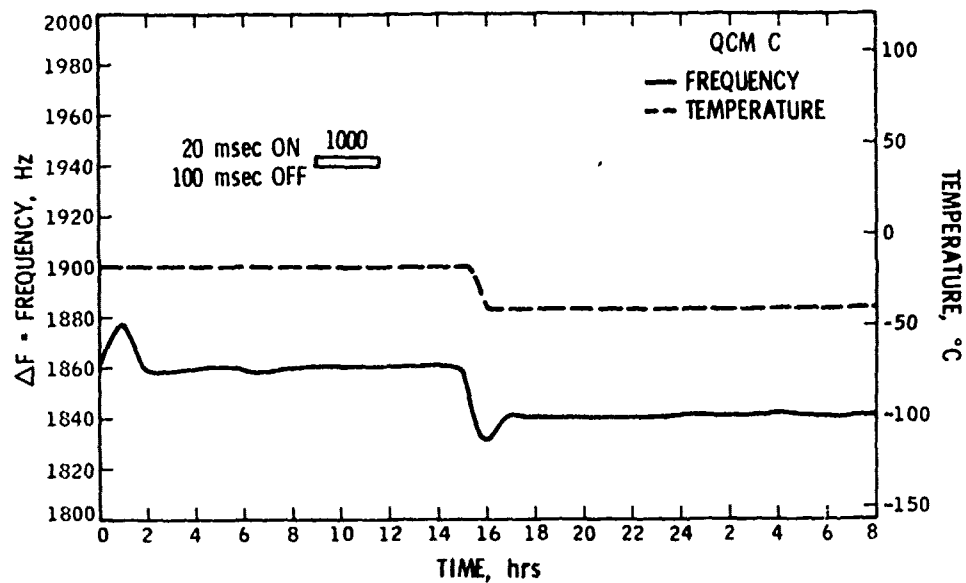


Figure 28c. Frequency and Temperature Readings for Crystal C, May 19, 1974

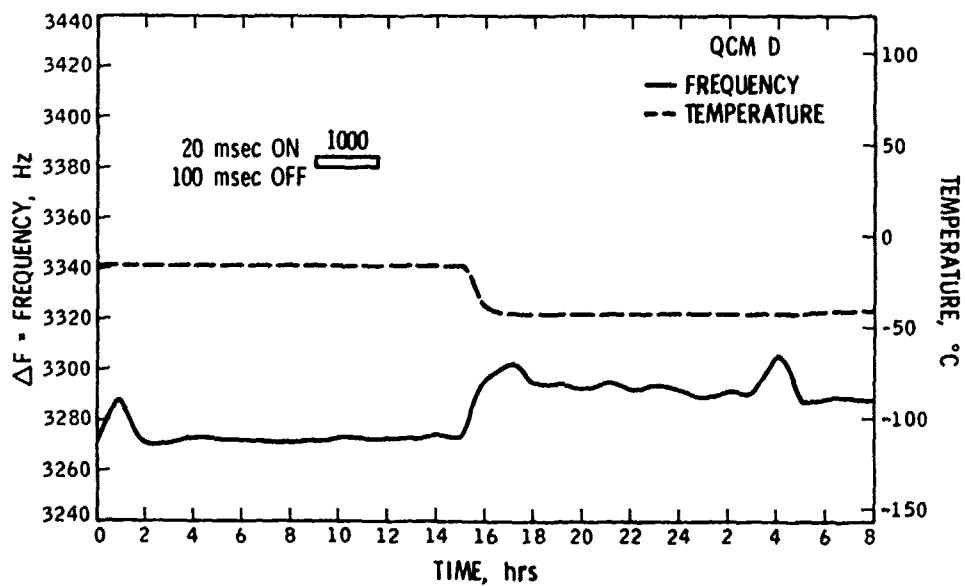


Figure 28d. Frequency and Temperature Readings for Crystal D, May 19, 1974

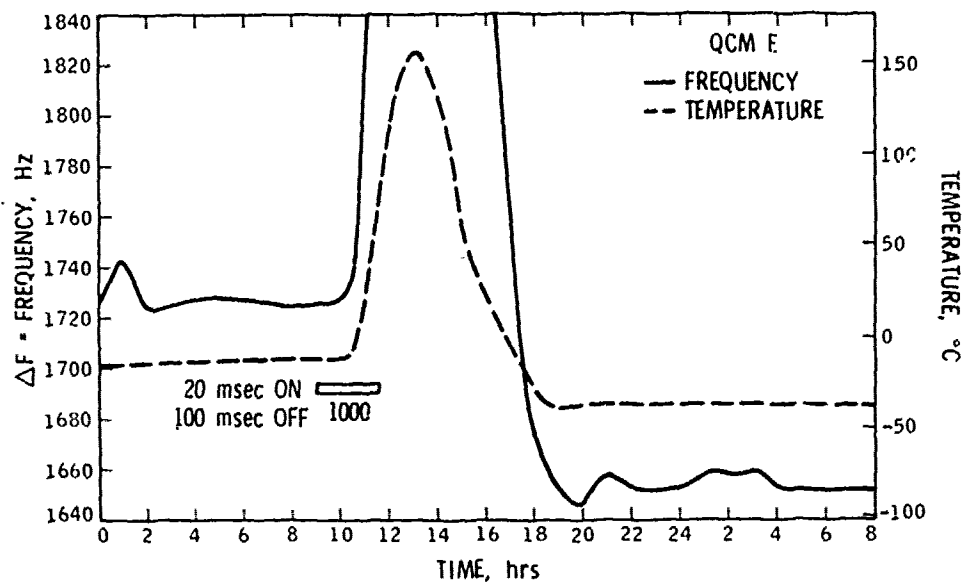


Figure 28e. Frequency and Temperature Readings for Crystal E,
May 19, 1974

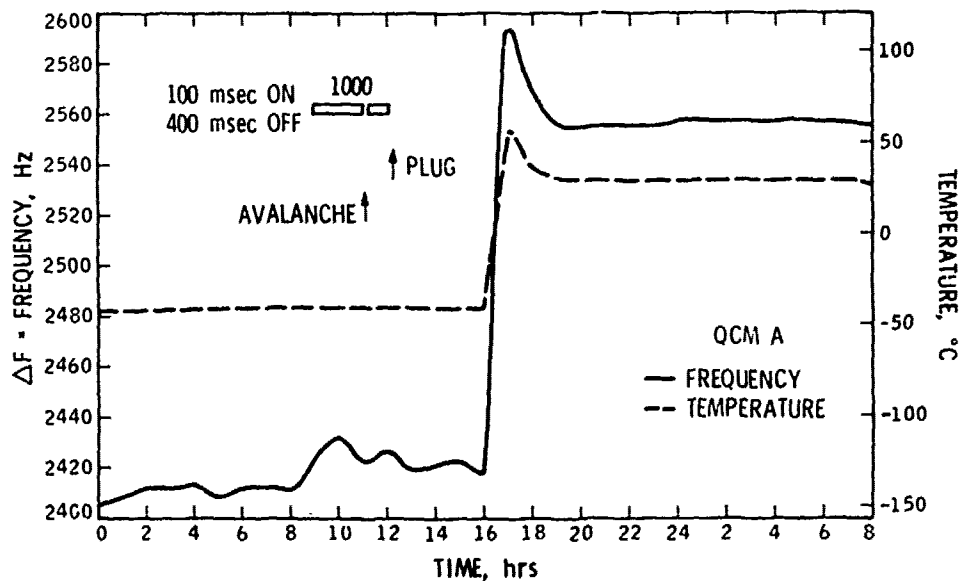


Figure 29a. Frequency and Temperature Readings for Crystal A,
May 20, 1974

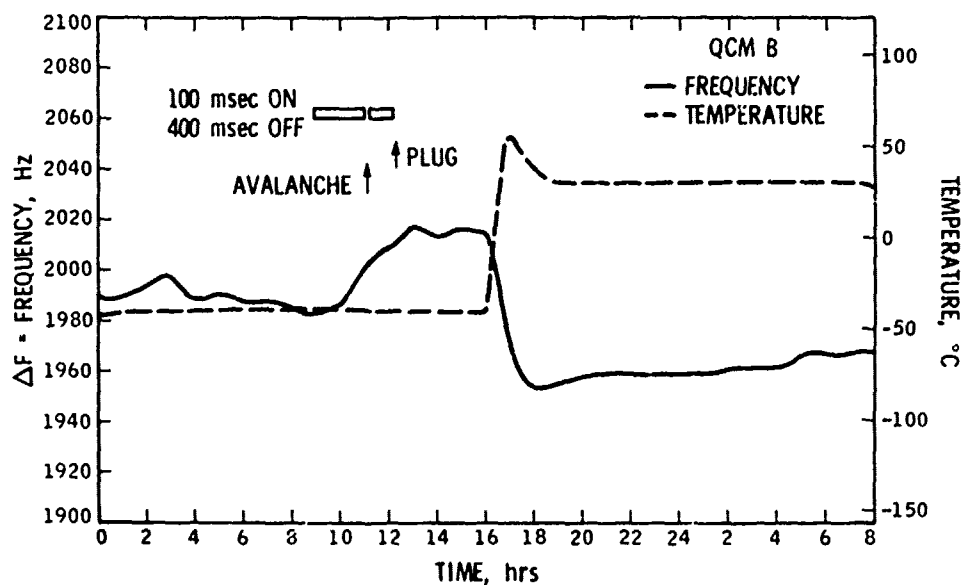


Figure 29b. Frequency and Temperature Readings for Crystal B, May 20, 1974

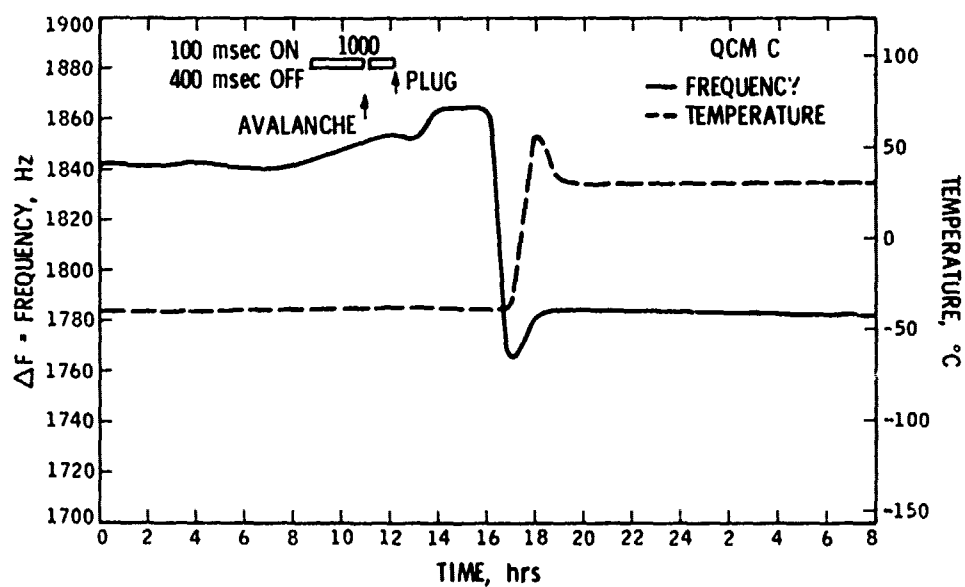


Figure 29c. Frequency and Temperature Readings for Crystal C, May 20, 1974

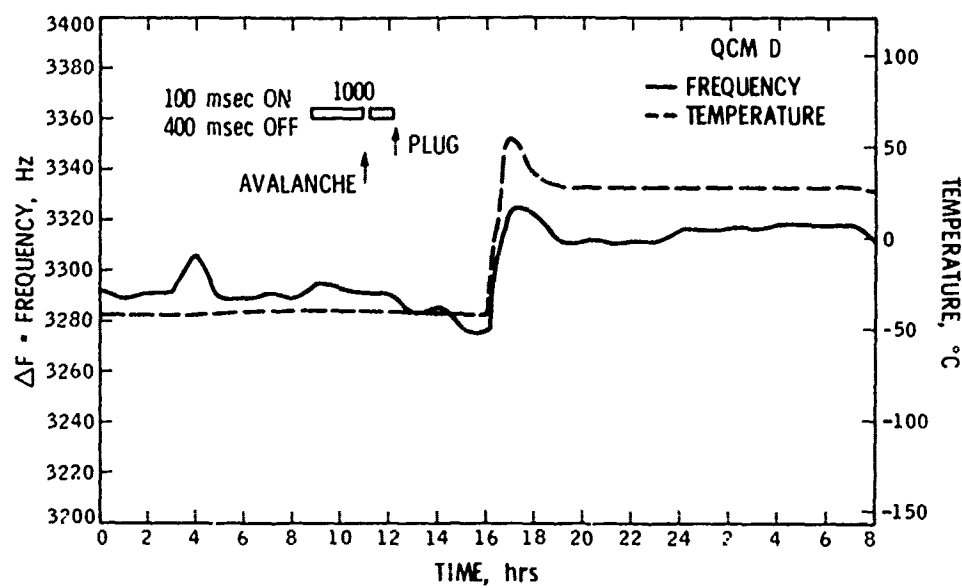


Figure 29d. Frequency and Temperature Readings for Crystal D, May 20, 1974

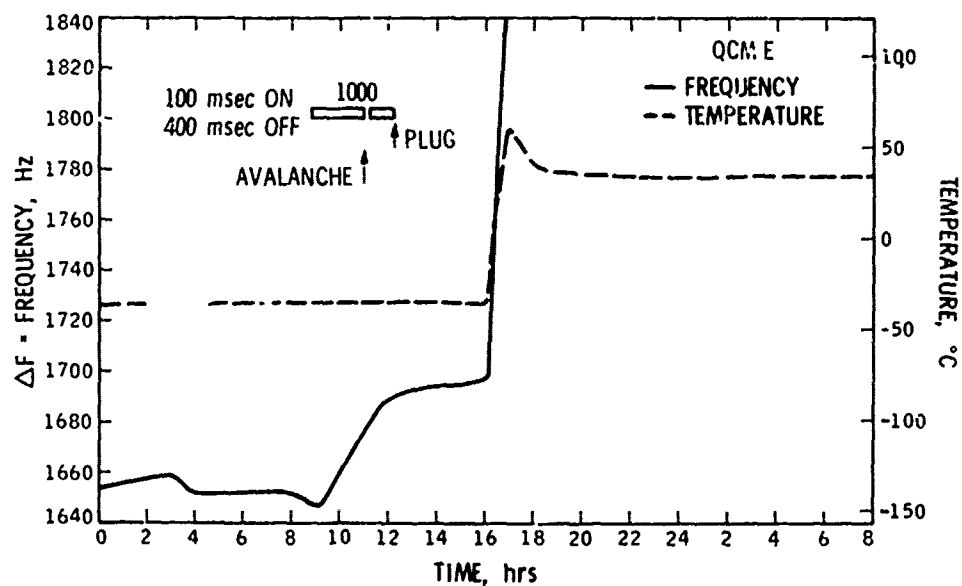


Figure 29e. Frequency and Temperature Readings for Crystal E, May 20, 1974

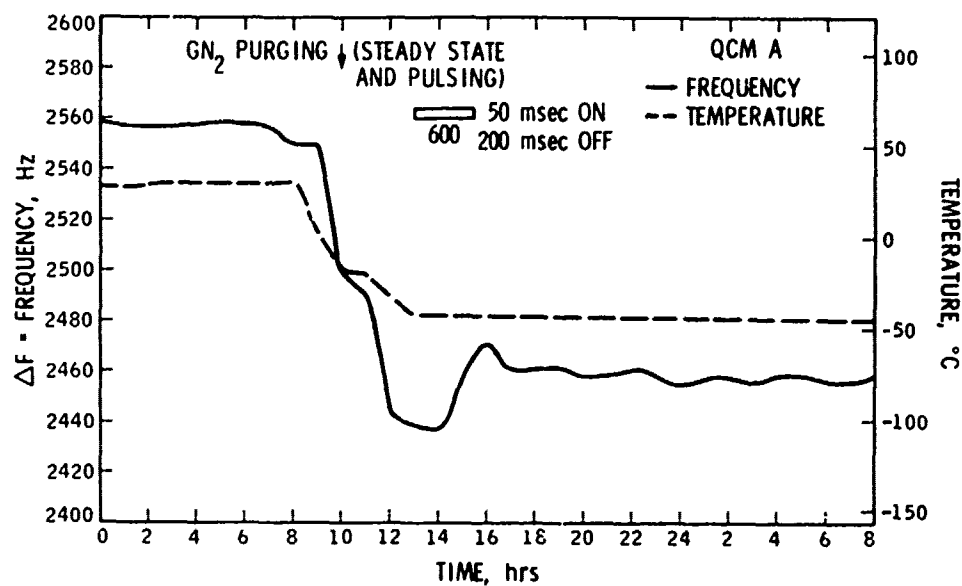


Figure 30a. Frequency and Temperature Readings for Crystal A, May 21, 1974

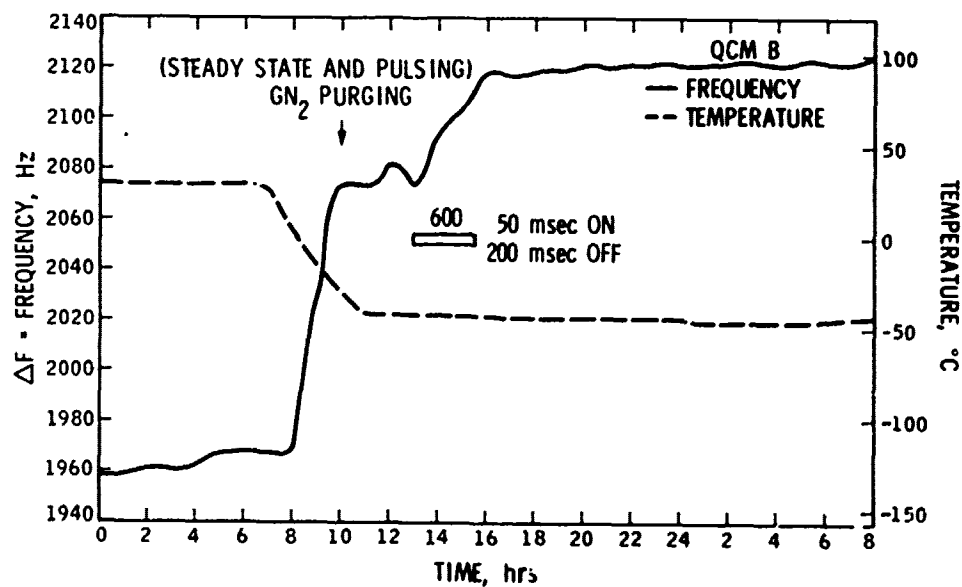


Figure 30b. Frequency and Temperature Readings for Crystal B, May 21, 1974

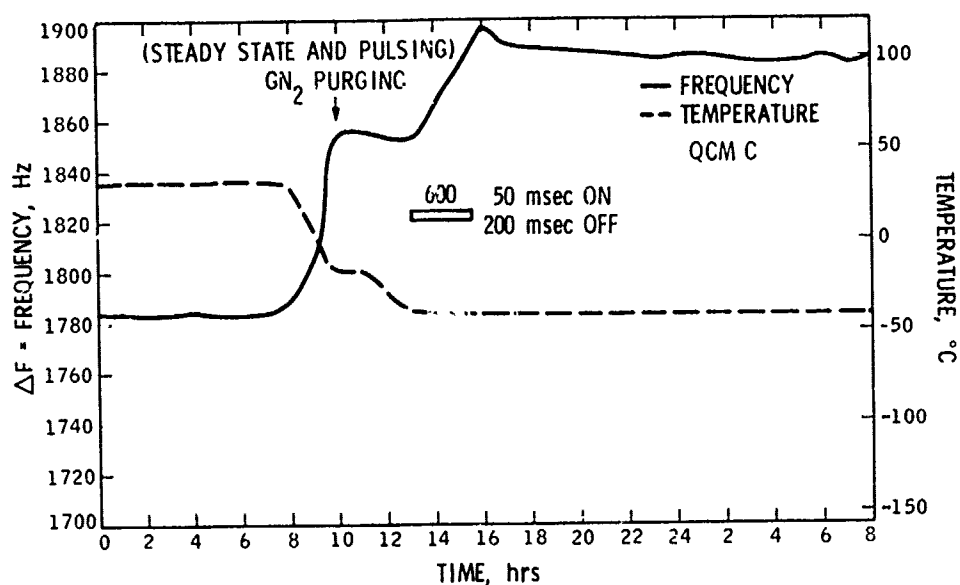


Figure 30c. Frequency and Temperature Readings for Crystal C, May 21, 1974

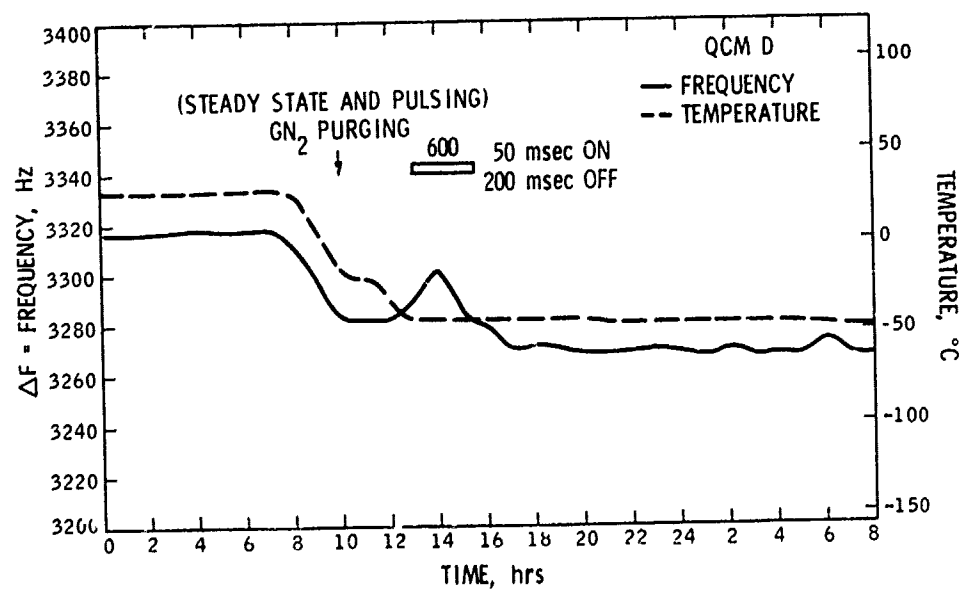


Figure 30d. Frequency and Temperature Readings for Crystal D, May 21, 1974

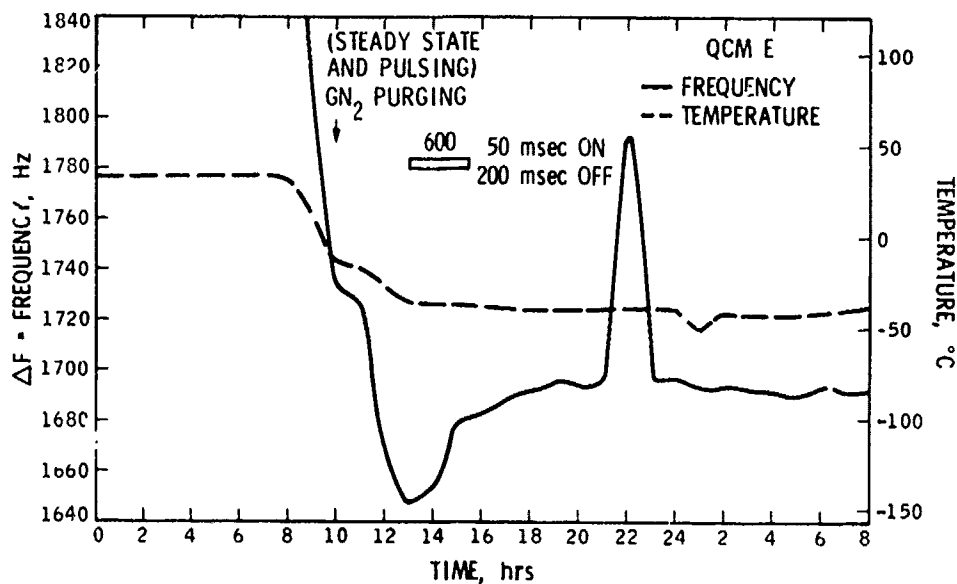


Figure 30e. Frequency and Temperature Readings for Crystal E, May 21, 1974

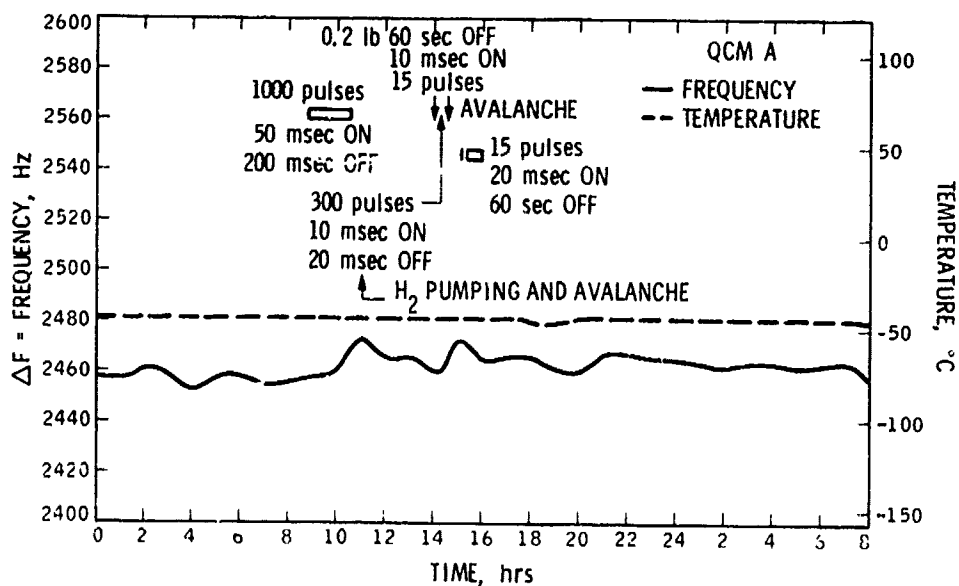


Figure 31a. Frequency and Temperature Readings for Crystal A, May 22, 1974

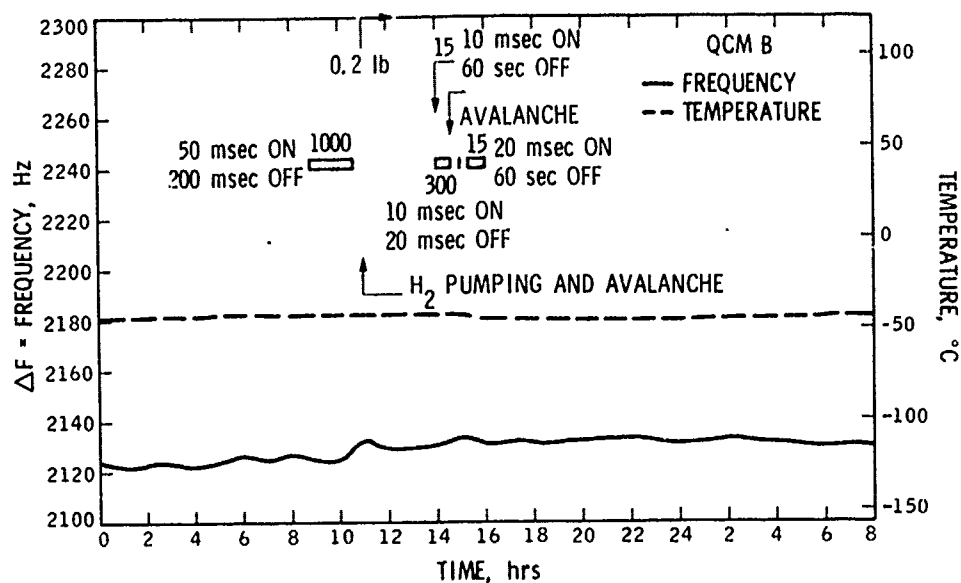


Figure 31b. Frequency and Temperature Readings for Crystal B, May 22, 1974

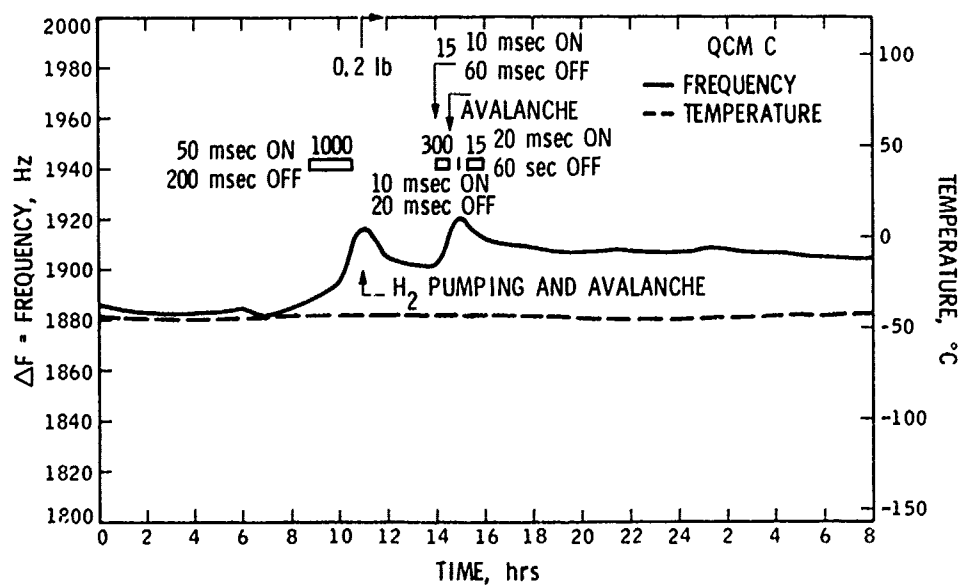


Figure 31c. Frequency and Temperature Readings for Crystal C, May 22, 1974

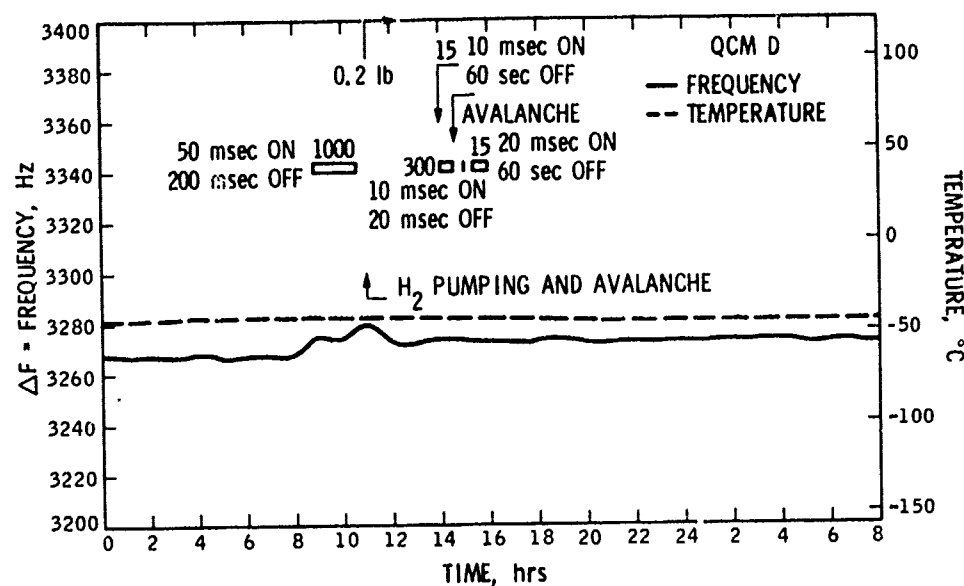


Figure 31d. Frequency and Temperature Readings for Crystal D, May 22, 1974

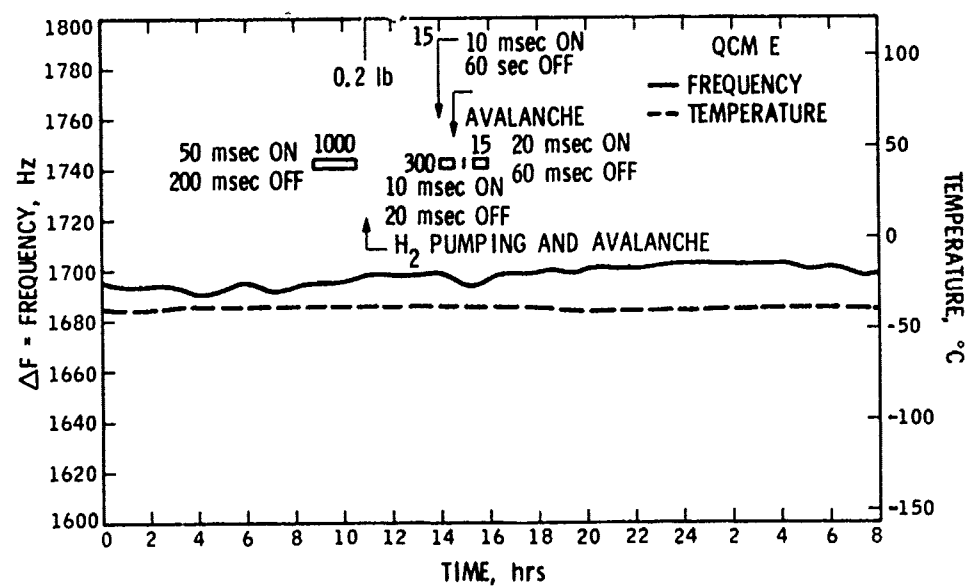


Figure 31e. Frequency and Temperature Readings for Crystal E, May 22, 1974

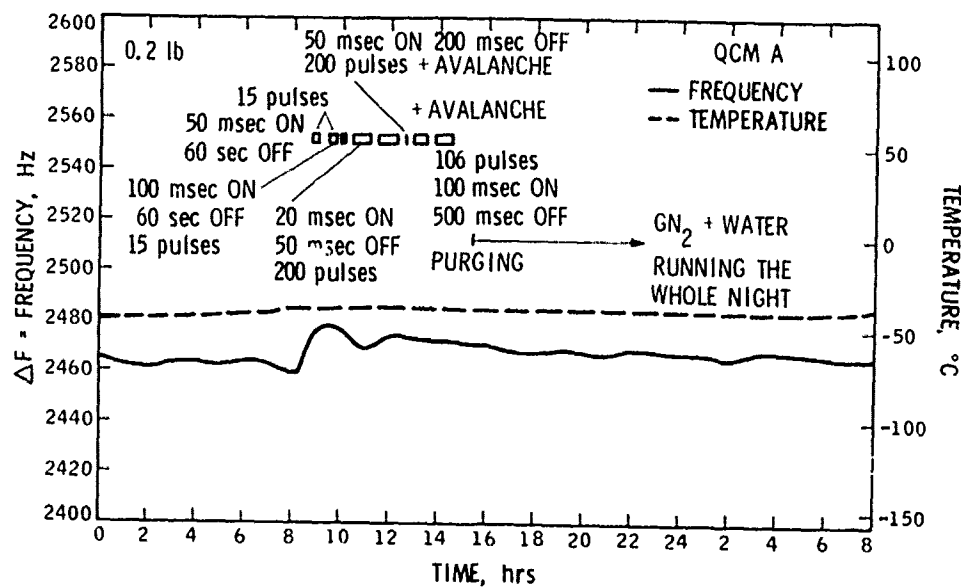


Figure 32a. Frequency and Temperature Readings for Crystal A, May 23, 1974

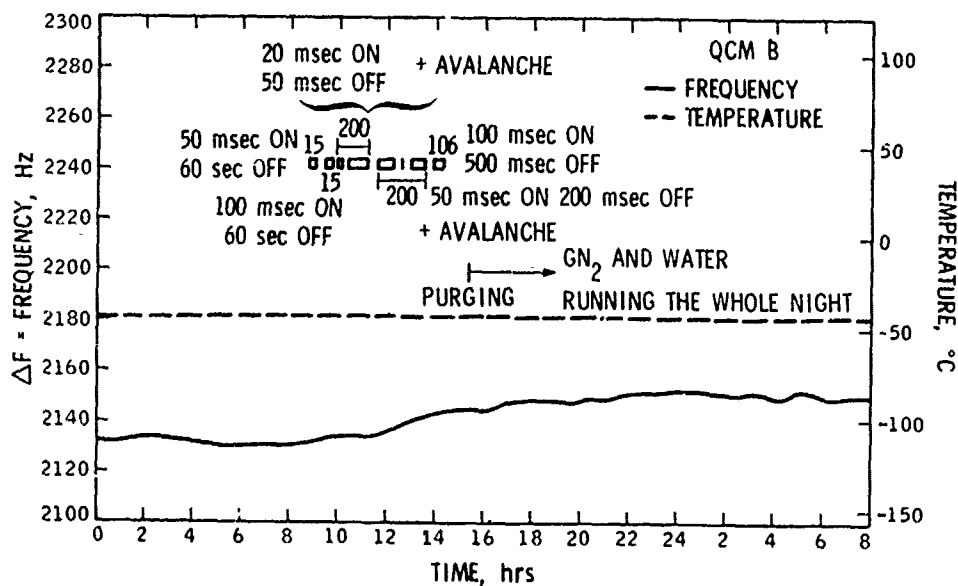


Figure 32b. Frequency and Temperature Readings for Crystal B, May 23, 1974

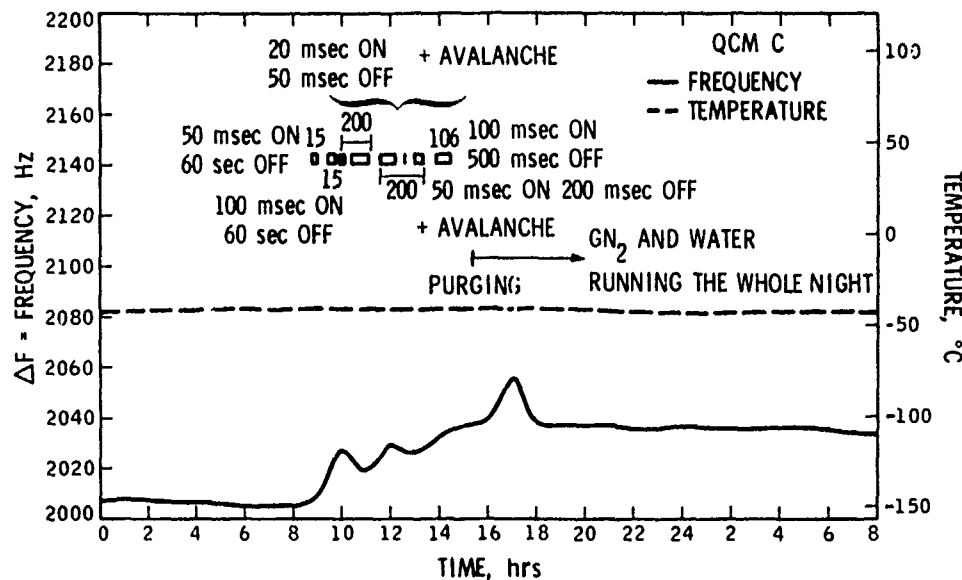


Figure 32c. Frequency and Temperature Readings for Crystal C, May 23, 1974

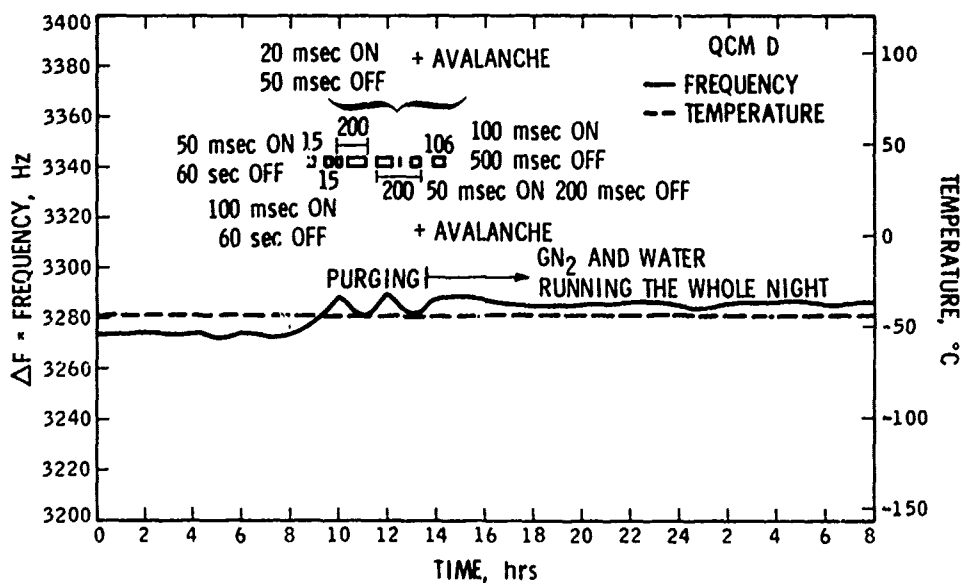


Figure 32d. Frequency and Temperature Readings for Crystal D, May 23, 1974

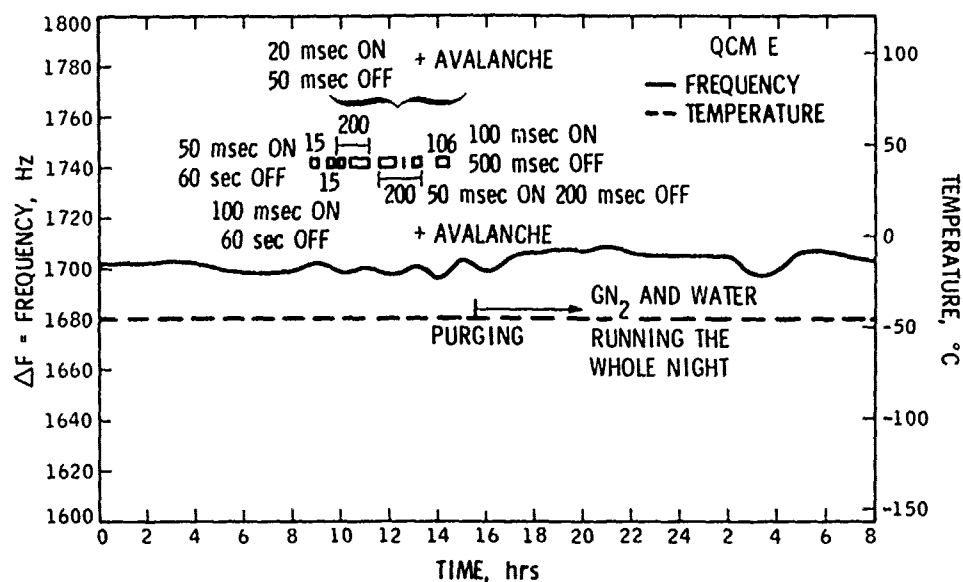


Figure 32e. Frequency and Temperature Readings for Crystal E, May 23, 1974

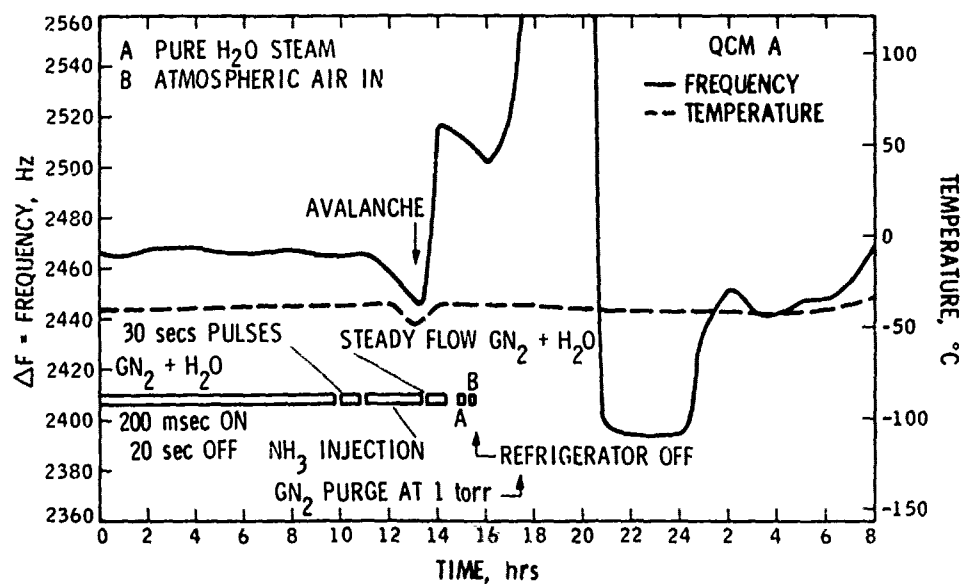


Figure 33a. Frequency and Temperature Readings for Crystal A, May 24, 1974

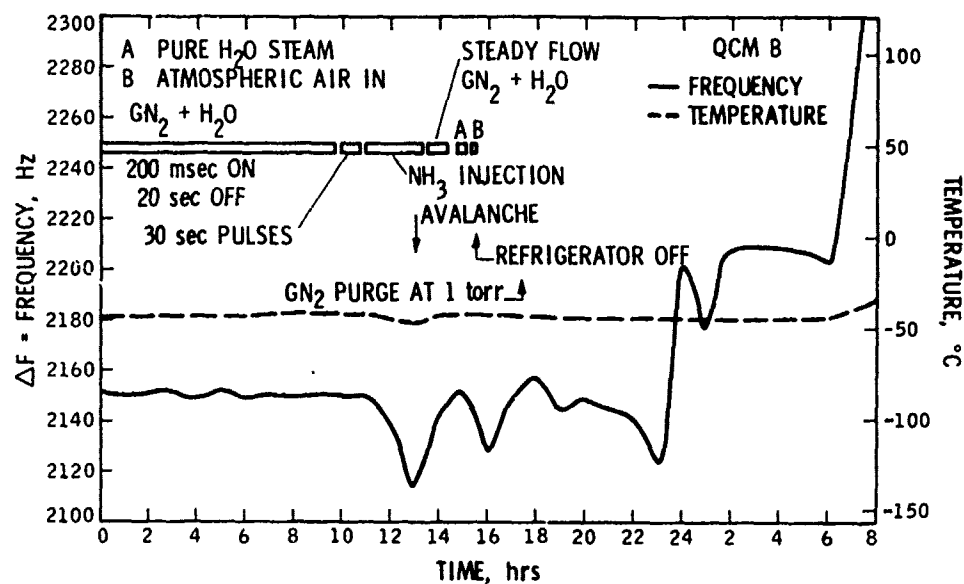


Figure 33b. Frequency and Temperature Readings for Crystal B, May 24, 1974

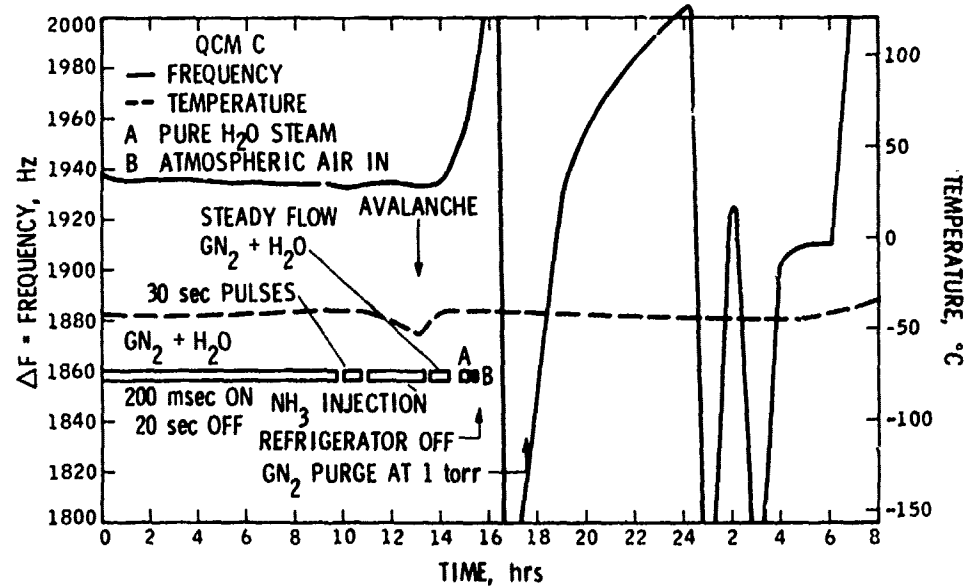


Figure 33c. Frequency and Temperature Readings for Crystal C, May 24, 1974

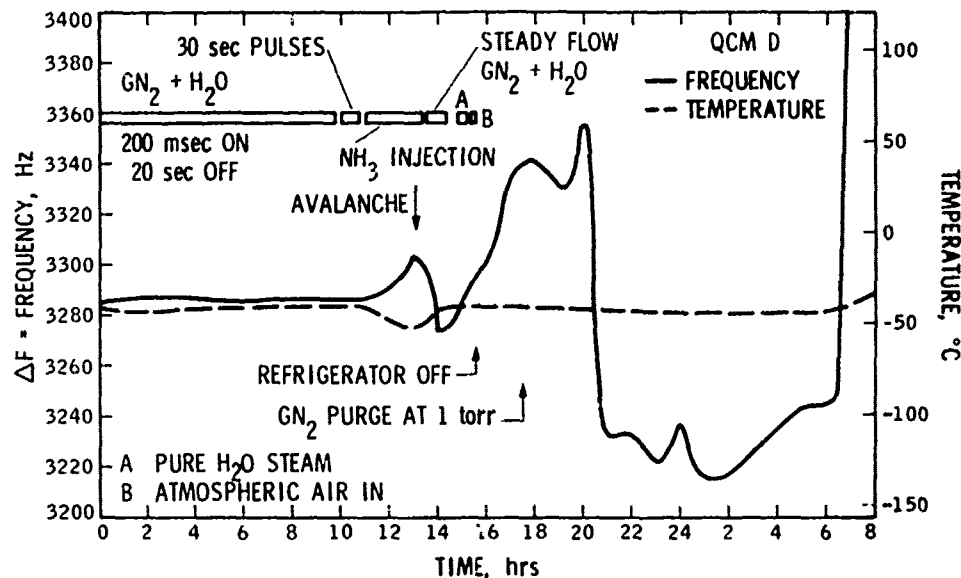


Figure 33d. Frequency and Temperature Readings for Crystal D, May 24, 1974

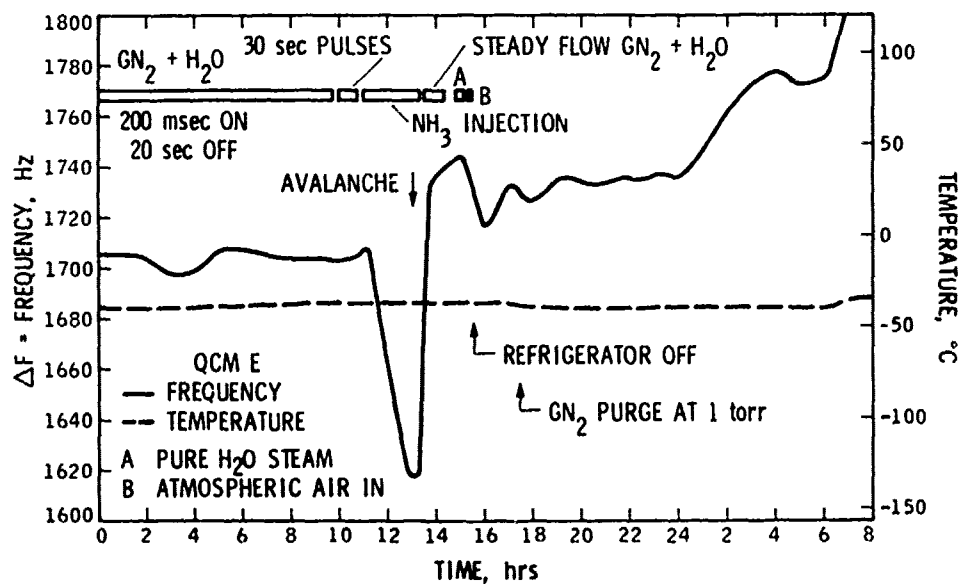


Figure 33e. Frequency and Temperature Readings for Crystal E, May 24, 1974

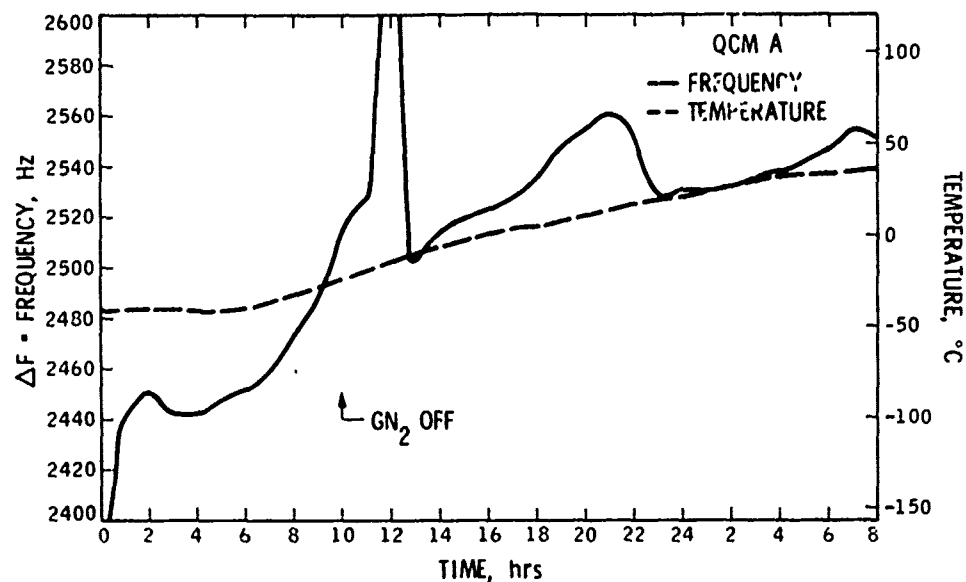


Figure 34a. Frequency and Temperature Readings for Crystal A, May 25, 1974

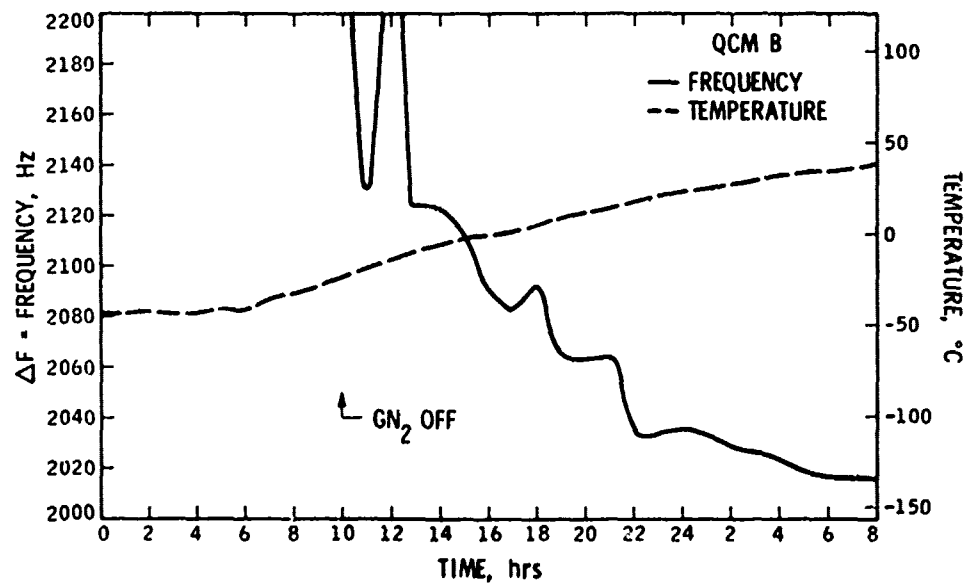


Figure 34b. Frequency and Temperature Readings for Crystal B, May 25, 1974

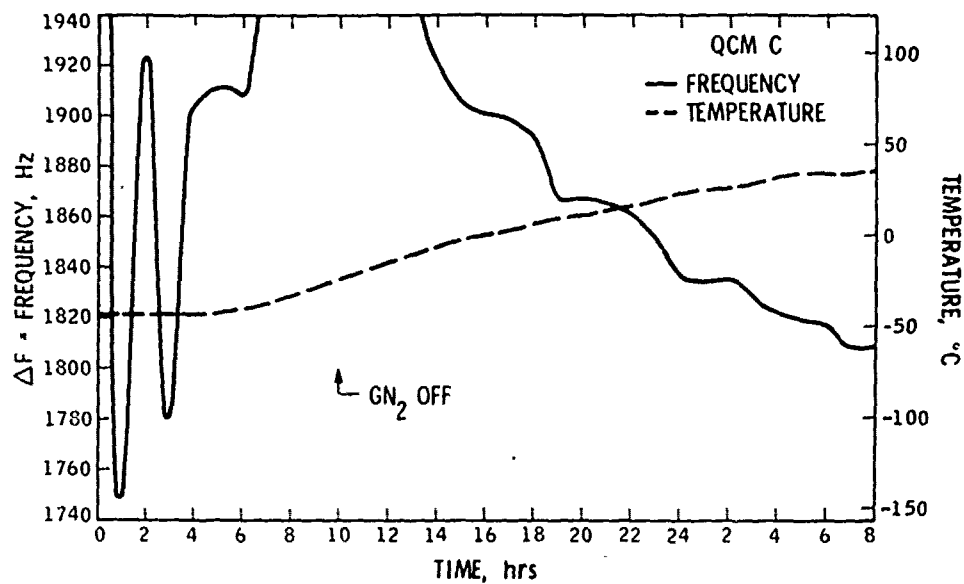


Figure 34c. Frequency and Temperature Readings for Crystal C, May 25, 1974

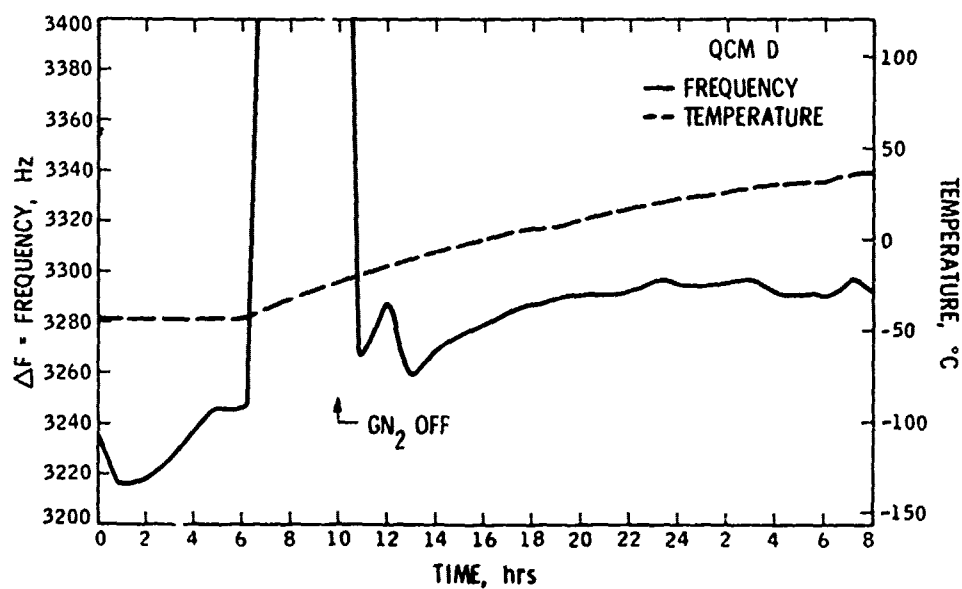


Figure 34d. Frequency and Temperature Readings for Crystal D, May 25, 1974

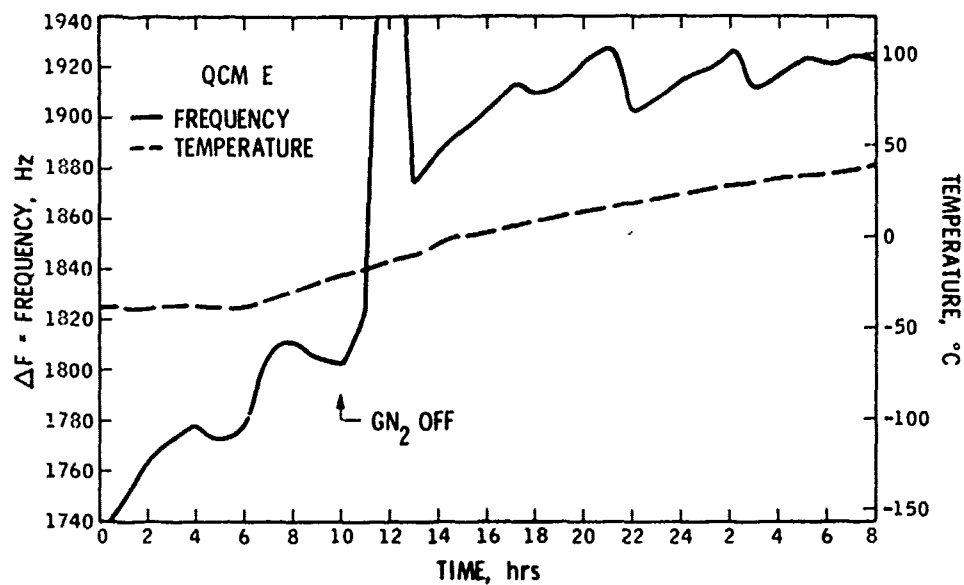


Figure 34e. Frequency and Temperature Readings for Crystal E, May 25, 1974

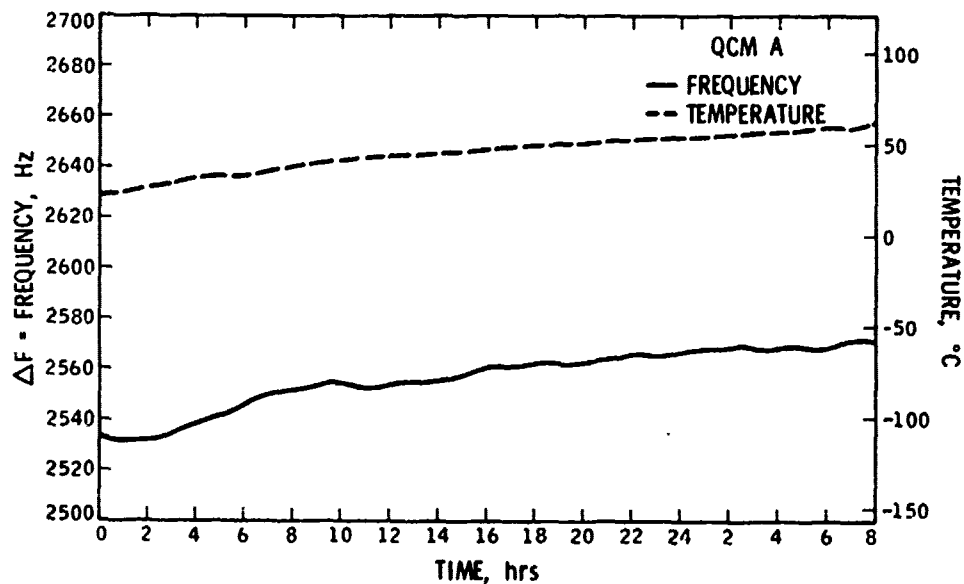


Figure 35a. Frequency and Temperature Readings for Crystal A, May 26, 1974

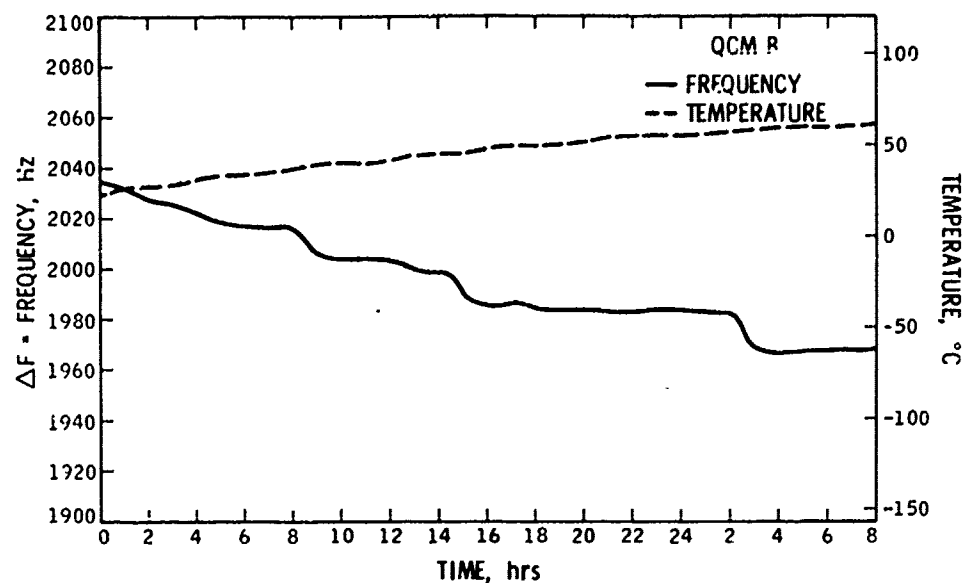


Figure 35b. Frequency and Temperature Readings for Crystal B, May 26, 1974

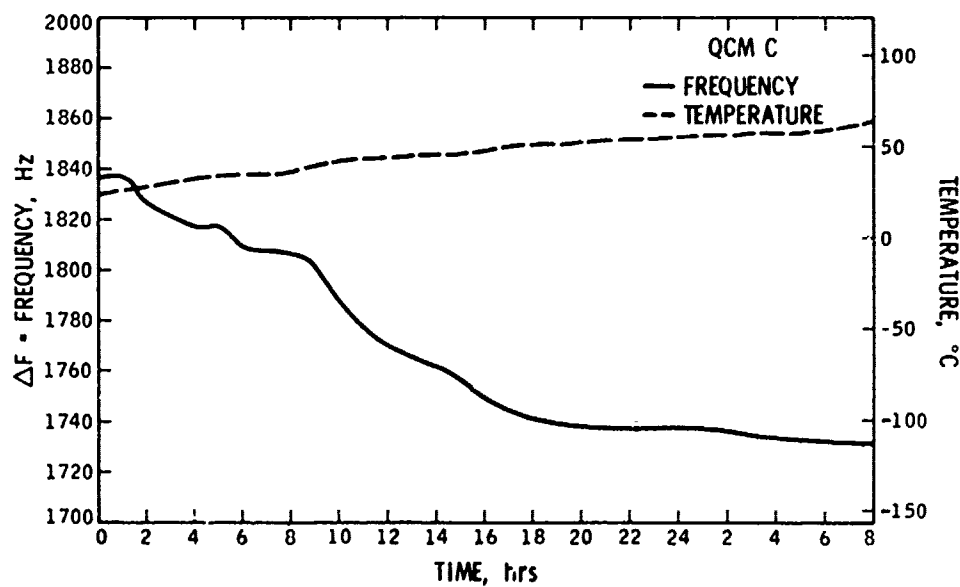


Figure 35c. Frequency and Temperature Readings for Crystal C, May 26, 1974

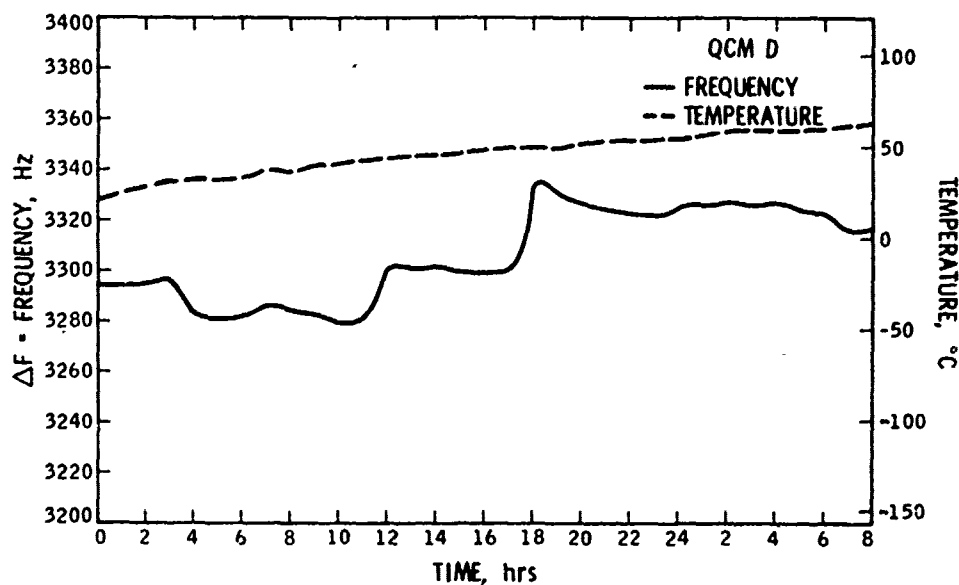


Figure 35d. Frequency and Temperature Readings for Crystal D, May 26, 1974

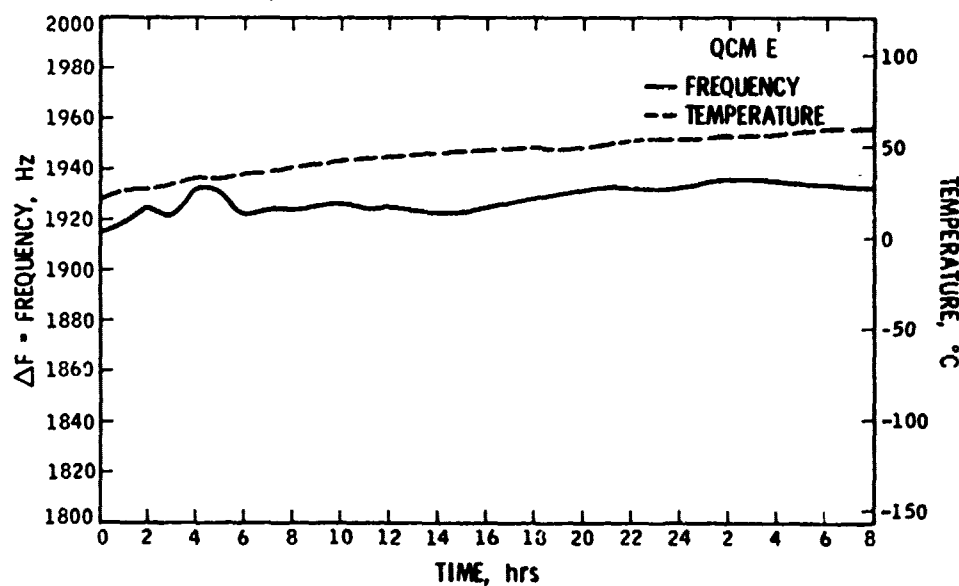


Figure 35e. Frequency and Temperature Readings for Crystal E, May 26, 1974

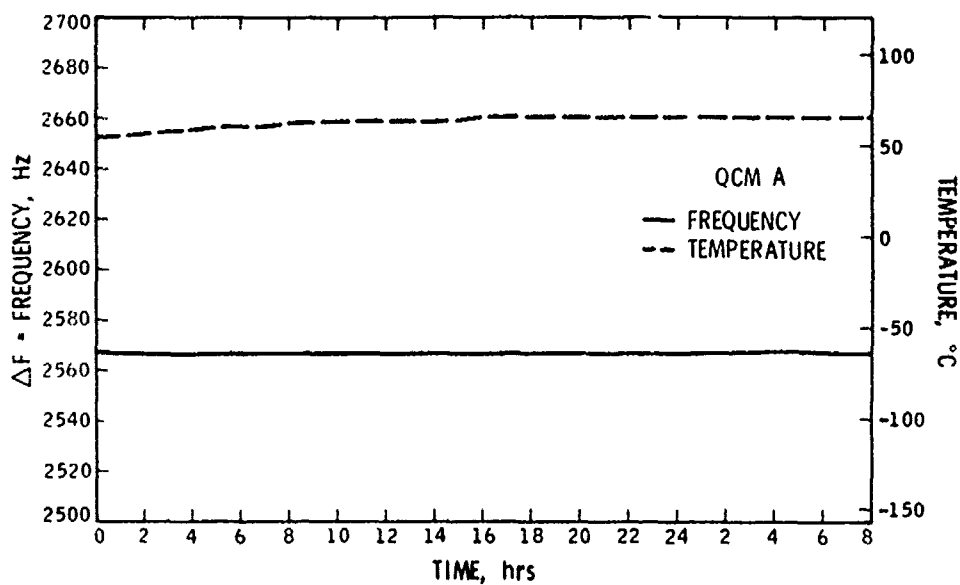


Figure 36a. Frequency and Temperature Readings for Crystal A, May 27, 1974

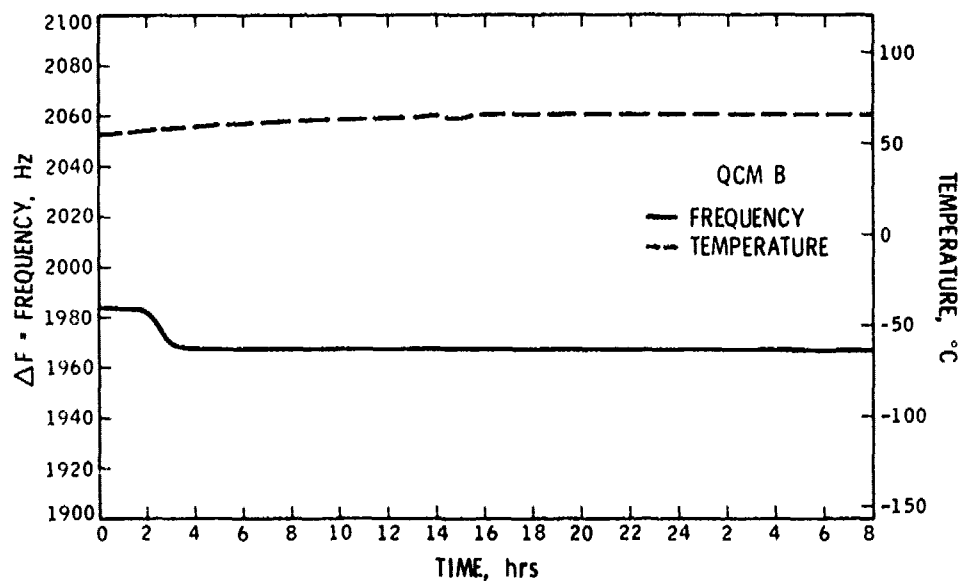


Figure 36b. Frequency and Temperature Readings for Crystal B, May 27, 1974

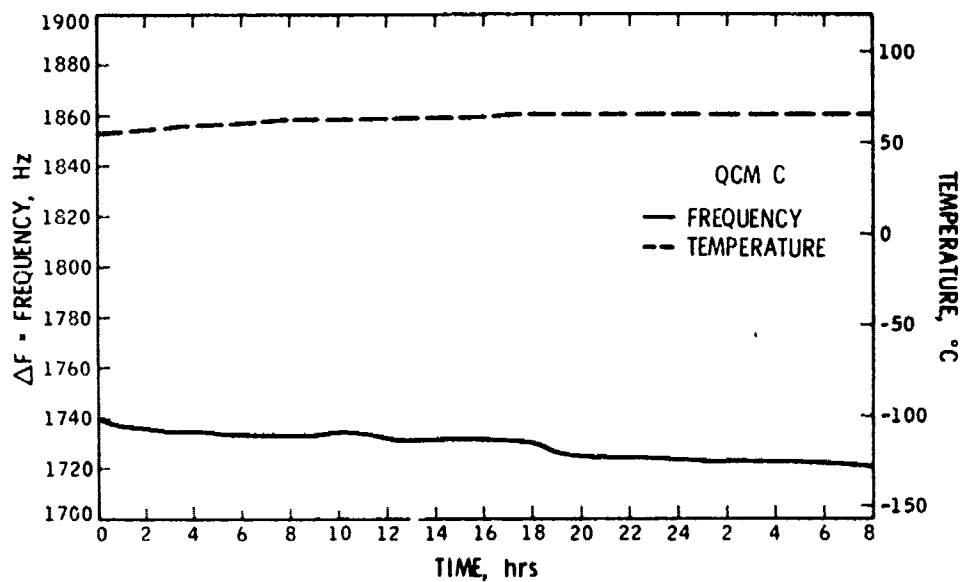


Figure 36c. Frequency and Temperature Readings for Crystal C, May 27, 1974

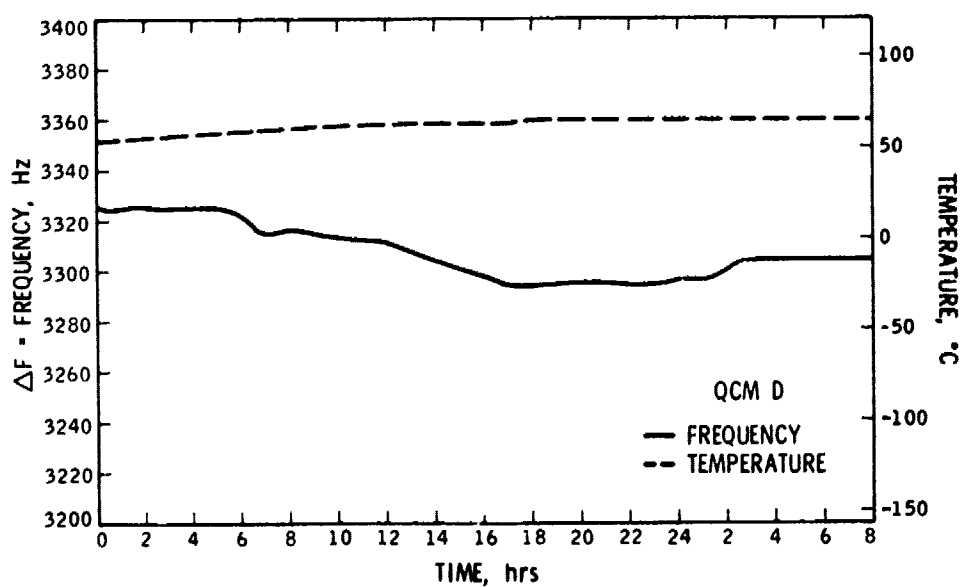


Figure 36d. Frequency and Temperature Readings for Crystal D, May 27, 1974

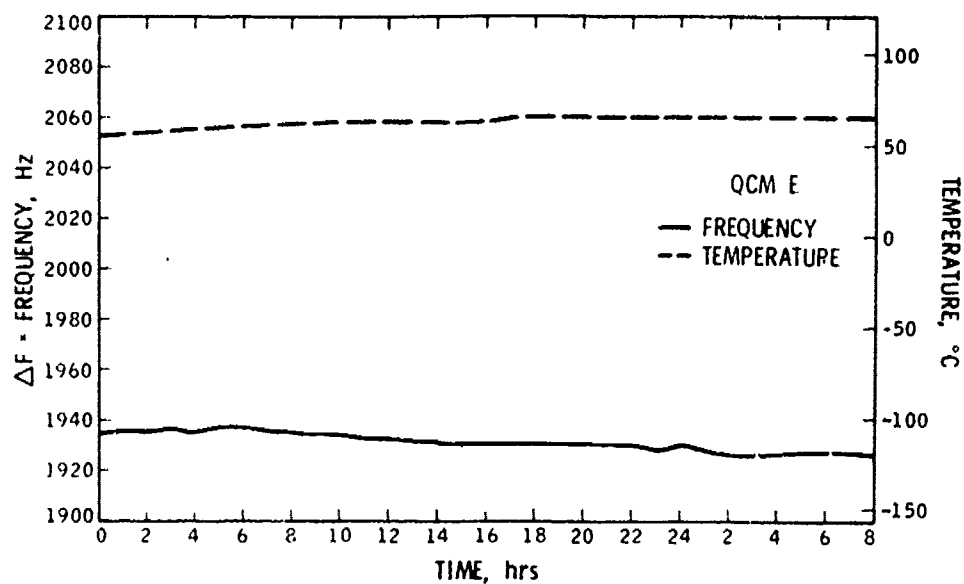


Figure 36e. Frequency and Temperature Readings for Crystal E, May 27, 1974

REFERENCES

1. Stephens, J. B., "Spacecraft Mechanism Testing in the Molsink Facility," in Proceedings of the 4th Aerospace Mechanisms Symposium, Technical Memorandum 33-425, edited by G. G. Herzl and M. J. Buehler, Jet Propulsion Laboratory, Pasadena, California, January 15, 1970.
2. Stephens, J. B., "Molecular Sink," Research/Development, July 1967.
3. Stephens, J. B., "Space Molecular Sink Simulator Facility Design," Journal of Spacecraft and Rockets, June 1966.
4. J. Bassichis et al "FLTSATCOM, Reaction Control Subsystem Design Audit #2 Package". TRW Document No. 24200-450-002-01, January 25 1974.
5. Chirivella, J. E., "ATS-F Radiant Cooler Contamination Test in a Hydrazine Thruster Exhaust." Technical Memorandum 33-592 Jet Propulsion Laboratory, California Institute of Technology, Pasadena, California, April 15, 1973.
6. Warner, A. W., "Micro Weighing with the Quartz Crystal Oscillator Theory and Design," in Ultra Micro Weight Determination in Controlled Environments, edited by S. P. Wolsky and E. J. Zdanuk, Interscience Publishers, 1969.
7. Saurbrey, G. Z., Zeitschrift fur Physik, Vol. 155, p. 206, 1959.
8. Stockbridge, C. D., Vacuum Microbalance Techniques, Vol. 5, pp. 193-205, 1965.
9. Eschbach, H. L., and Kruidhof, E. W., Vacuum Microbalance Techniques, Vol. 5, pp. 207-216, 1966.
10. Niedermayer, R., et al, Vacuum Microbalance Techniques, Vol. 5, pp. 217-229, 1966.
11. King, W. H., and Varga, G. M., Contract RC 9-439088 Final Report, Exxon Research Center, Linden, N. J., December 1969.
12. Crawford, H. M., et al, "The Design and Performance of the Piezo-electric Sorption Hydrometer," in Analysis and Instrumentation, Plenum Press, 1964.
13. Bartera, R. E., Quartz Crystal Oscillator Apparatus for Measuring Mass Accretion and Temperature Independently of Each Other, JPL Patent Case 11279, Jet Propulsion Laboratory, Pasadena, California.

REFERENCES (contd)

14. Chirivella, J. E., "Molecular Flux Measurements in the Back Flow Region of a Nozzle Plume" Technical Memorandum 33-620, Jet Propulsion Laboratory, California Institute of Technology, Pasadena, California, July 15, 1973.
15. Hill, J. A. F., and Draper, J. S., "Analytical Approximation for the Flow From a Nozzle into a Vacuum", J. Spacecraft and Rockets, Vol. 3, No. 10, pp. 1552-1559, October 1966.

GLOSSARY

C_F = thrust coefficient

$C_M = \left. \frac{\partial f}{\partial M} \right)_T$, Hz-cm²/gm

$C_T = \left. \frac{\partial f}{\partial T} \right)_M$, Hz/°K

$\frac{dm}{d\Omega}$ = mass flow rate per unit solid angle

Δe = expansion ratio

Δf = change in crystal frequency, Hz

ΔF = change in beat frequency between two crystals, Hz

ΔM = mass deposits, gm/cm²

ΔT = temperature variation, °K

F_c = resonant frequency, MHz

γ = specific heat ratio

\dot{m}_w = nozzle total mass flow

P_e = exit pressure

P_0 = plenum pressure

ϕ = QCM surface orientation angle

r = radial distance to nozzle exit center

θ = turning angle

APPENDIX A

The derivation of Equation 2 in the report follows quite easily from the relationship of the natural frequency of a quartz crystal excited in the thickness shear mode to its thickness. This relationship is given by

$$f = \frac{V_{tr}}{2t} = \frac{N}{t} \quad (A1)$$

where V_{tr} is the velocity of the elastic transverse wave in thickness direction and t is the crystal thickness. For crystals having AT-cuts, the constant N is 1.670×10^6 Hz-mm. Differentiating Equation (A1) gives the change of frequency df caused by a variation of the thickness dt :

$$df = -\frac{N}{t^2} dt \quad (A2)$$

The thickness is given by the expression

$$t = \frac{m}{\rho A} \quad (A3)$$

where m , ρ and A are the mass, density and area of the crystal plate respectively. Differentiating Equation (A3), with ρ and A constant, yields

$$dt = \frac{dm}{\rho A} = \frac{dM}{\rho} \quad (A4)$$

where dM is the change of mass per unit area. Inserting Equations (A1) and (A4) into Equation (A2) gives

$$df = -\frac{f^2}{N\rho} dM$$

or rearranging

$$dM = - \frac{NP}{f^2} df \quad (A5)$$

When the resonant frequency f (Hz) is converted to F_c (MHz) and the density, $\rho = 2.280 \text{ gm/cm}^3$, is introduced into Equation (A5) the following expression results for the mass change per unit area:

$$\Delta M = - \frac{3.81 \times 10^{-7}}{F_c^2} \Delta f \quad (A6)$$

This is the desired equation where ΔM is in gm/cm^2 , F_c is in MHz and Δf is in Hz. The negative sign in Equation (A6) is arbitrary in that it can be changed in the electronics. The difference in constant, 3.81 as compared to 4.30, is due to a new calculation of the density. The data was reduced using 4.30 which results in an error that is 12.8% high. Since this is within the error band of the data it has been decided not to redo the data reduction.

APPENDIX B

LOGGING OF OPERATIONS

May 15, 1974. The temperature of the crystals was kept constant 303°K (30°C) until 9:00. At 9:00 the controls were set at 283°K (10°C) and the QCM's reached this temperature around 11:00. In spite of the precautions taken for the stability of QCM frequencies, some malfunction of the selective amplifier introduced noise of the order of 5Hz, which plagued the instrumentation for several hours. At 11:21 engine priming was initiated. The fuel tank pressure was set at $27.17 \times 10^4 \text{ N/m}^2$ (25 psig) and the engine was fired. The pulse width was set at 200 msec and 40 pulses were fired to obtain evidence of repeatability in the pressure pulse. At 11:40 the tank pressure was set at $95.60 \times 10^4 \text{ N/m}^2$ (125 psig) and the pulse width to 200 msecs. A total of 16 pulses were fired at these conditions. After obtaining evidence of the reliability of the propulsion systems, the reference duty cycle supplied by TRW to check the performance of the thruster by observing the temperature rise in the throat and chamber of the thruster-nozzle wall was repeated. This duty cycle consisted of 20 msec on-time and 5 secs off-time with the tank pressure at $102.45 \times 10^4 \text{ N/m}^2$ (135 psig). During the TRW checkout tests, this duty cycle required 150 pulses before the temperature was stabilized at 601°K (650°F). In the MOLSINK environment, however, the temperature rose only to 575°K (600°F) after 150 pulses. The test was repeated again with the tank pressure at $95.60 \times 10^4 \text{ N/m}^2$ (125 psig) (which corresponds to 0.1 lbf thrust) and after 251 pulses the temperature stabilized at 562°K (580°F). The lower engine temperature results from the higher radiation cooling rates within the MOLSINK environment. This test was followed by 17 pulses of 20 msec on-time and 60 secs off-time. At 15:28 the propulsion systems shut off. At 17:10 the QCM's data recording systems were adjusted, as well as their polarization voltage, in order to stabilize the frequency. At the same time, their temperature was also set at 255.23°K (0°F), a value which was reached at 17:00. A total of 474 pulses were fired during this day. Figures 24a, 24b, 24c, 24d, and 24e show the QCM's frequency and temperature readings during this day.

May 18, 1974. The hydrazine tank pressure was set to operate the thruster at the 0.44 N (0.1 lbf) thrust level. At 8:49 the thruster began pulsing at a duty cycle of 300 pulses of 150 msec on and 20 sec off. The duty cycle was completed at 10:29. A second duty cycle was then initiated at 10:43 with 200 msec on, 20 sec off, and ended at 12:23 after 300 pulses. The accumulation of hydrogen in the chamber exceeded the critical level and an avalanche was triggered. During an avalanche, the refrigerator is turned off, and the MOLSINK wall temperature is allowed to raise slowly, desorbing the hydrogen, which is pumped out by the diffusion and mechanical pumps. In this manner, although the pressure in the MOLSINK chamber is allowed to raise up to 0.1 N/m^2 ($\approx 10^{-3}$ torr), the rest of the systems in the chamber are maintained at the same temperature as before the avalanche, since only the wall temperature is allowed to rise a few degrees. Therefore, all the trapped gases remain condensed except hydrogen, which is pumped out. When the amount of hydrogen in the chamber is reduced to a desirable level, the pumping is stopped and the refrigerator restarted, thus restoring the high vacuum in the chamber. The whole operation takes less than 15 minutes. At 15:28 a series of 1000 pulses of 10 msec on and 100 msec off was initiated. The 1000 pulses were given in trains of approximately 50 pulses. This operation was finished at 16:22 and the activities at the MOLSINK were terminated for the day. A malfunction in the refrigerator at 24:00 caused an avalanche which was brought under control when alarm systems sounded at 1:00 of the following day. The temperatures of the QCMs were maintained at 255.23°K (0°F) during the day. The temperature and frequency readings are presented in Figures 27a, 27b, 27c, 27d, and 27e. Some increase in mass deposit was registered during this day, mostly in QCMs A, C, while QCM D reacted slightly in the opposite direction. The number of pulses during this day ascended to 1600 and the cumulative total pulses reached 3984 pulses.

May 19, 1974. With the propulsion systems set to operate the thruster at a 0.44 N (0.1 lbf) thrust level and initial temperature at 477°K (400°F), a duty cycle of 20 msec on-time and 100 msec off-time was prepared. The total number of pulses was 1000 and the duty cycle was started at 9:00. The duty cycle was conducted in the form of 50 pulse trains. The 1000 cycles

May 18, 1974. The hydrazine tank pressure was set to operate the thruster at the 0.44 N (0.1 lbf) thrust level. At 8:49 the thruster began pulsing at a duty cycle of 300 pulses of 150 msec on and 20 sec off. The duty cycle was completed at 10:29. A second duty cycle was then initiated at 10:43 with 200 msec on, 20 sec off, and ended at 12:23 after 300 pulses. The accumulation of hydrogen in the chamber exceeded the critical level and an avalanche was triggered. During an avalanche, the refrigerator is turned off, and the MOLSINK wall temperature is allowed to raise slowly, desorbing the hydrogen, which is pumped out by the diffusion and mechanical pumps. In this manner, although the pressure in the MOLSINK chamber is allowed to raise up to 0.1 N/m^2 ($\approx 10^{-3}$ torr), the rest of the systems in the chamber are maintained at the same temperature as before the avalanche, since only the wall temperature is allowed to rise a few degrees. Therefore, all the trapped gases remain condensed except hydrogen, which is pumped out. When the amount of hydrogen in the chamber is reduced to a desirable level, the pumping is stopped and the refrigerator restarted, thus restoring the high vacuum in the chamber. The whole operation takes less than 15 minutes. At 15:28 a series of 1000 pulses of 10 msec on and 100 msec off was initiated. The 1000 pulses were given in trains of approximately 50 pulses. This operation was finished at 16:22 and the activities at the MOLSINK were terminated for the day. A malfunction in the refrigerator at 24:00 caused an avalanche which was brought under control when alarm systems sounded at 1:00 of the following day. The temperatures of the QCMs were maintained at 255.23°K (0°F) during the day. The temperature and frequency readings are presented in Figures 27a, 27b, 27c, 27d, and 27e. Some increase in mass deposit was registered during this day, mostly in QCMs A, C, while QCM D reacted slightly in the opposite direction. The number of pulses during this day ascended to 1600 and the cumulative total pulses reached 3984 pulses.

May 19, 1974. With the propulsion systems set to operate the thruster at a 0.44 N (0.1 lbf) thrust level and initial temperature at 477°K (400°F), a duty cycle of 20 msec on-time and 100 msec off-time was prepared. The total number of pulses was 1000 and the duty cycle was started at 9:00. The duty cycle was conducted in the form of 50 pulse trains. The 1000 cycles

were completed at 11:38. QCM E had a malfunction in the control thermocouple and warmed up to 429° K (320° F). Operations were then stopped to let the temperature decrease. In view of the unsuccessful collection of contaminant mass on the crystals, when operating them at 255.23° K (0° F), a decision was made to lower their temperature to about 233° K (-40° F). Figures 28a, 28b, 28c, 28d, and 28e show the QCM temperatures and frequency readings during this day. Even though a temperature control device was in each QCM package, changes in frequency associated with temperature variation can be detected. The refrigerator presented another anomaly in its function at 4:00 of 5/20/74 with no serious consequences. The small variations of frequency observed in the figures for some QCMs are probably due to migration induced by the QCM's temperature variations. During this day 1000 pulses were fired, which brought the total number of pulses during the test to 4984 pulses.

May 20, 1974. After several hours, the QCMs stabilized and preparations to operate the thruster were initiated. The thruster was set once again to operate at 577° K (400° F) and 0.44N (0.1 lbf). The valve timer was set for 100 msec on, 400 msec off. At 8:50 a duty cycle of 388 pulses was started and was completed at 11:06. At this time the refrigerator was stopped and the excess hydrogen in the MOLSINK chamber was pumped out. At 11:20 the thruster was activated again for 1000 pulses which took until 12:10 to complete. The propellant lines developed a plugging problem at the end of the thrusting and, therefore, no thrusting operations were conducted during the rest of the day. Most of the effort after 12:00 was directed toward obtaining a clean steady flow of gaseous pure nitrogen through the thruster and verification of repeatability in the MOLSINK chamber pressure pulse was established. The QCM's temperature and frequency readings are given in Figures 29a, 29b, 29c, 29d, and 29e. The readings show a close correlation between thruster operation and mass deposit, particularly in QCMs B, C, and E. QCM A shows the same trend in frequency increase as QCM B, C and E while QCM D seems to react in the opposite way. Since 20 cycles of mass were accumulated on some of the QCMs, their temperatures were increased and later were kept at 296° K (73° F) to observe the vaporization

At 14:11 the thruster was pulsed 15 times with the duty cycle of 10 msec on, 60 sec off. At 14:30 the thruster was activated for 300 pulses of 10 msec on, 20 msec off, which concluded with an avalanche of the chamber. At 15:28, 15 pulses were given of 20 msec on, 60 sec off. The QCMs were maintained at approximately 233° K (-40° F) and their temperatures and frequencies are presented in Figures 31a, 31b, 31c, 31d, and 31e. One can see that only the first set of firings at 8:53 resulted in any frequency variation. For the rest of the day, the frequencies did not vary appreciably, except during the avalanches. This is possibly due to the short number of pulses given at the later times. The thruster was fired 1330 times this day, bringing the cumulative total to 7914 pulses.

May 23, 1974. The initial temperature of the thruster was set at 477° K (400° F) and the module operated at the 0.88N (0.2 lbf) level. The first duty cycle was started at 8:50 and consisted of 15 pulses of 50 msec on and 60 sec off. It was completed at 9:04. A second duty cycle of 15 pulses of 100 msec on and 60 sec off was conducted at 9:32. A third duty cycle, initiated at 9:51, was made consisting of 200 pulses of 20 msec on, 50 msec off. This duty cycle was completed at 11:18, after an interruption at 10:14 to dump the chamber hydrogen. A fourth duty cycle was initiated at 11:36 having 50 msec on and 200 msec off. One hundred and thirty-eight (138) pulses were made before an avalanche occurred at 12:14, after which 200 pulses were made and completed at 13:25. Finally, the time controls were adjusted to 100 msec on-time, 500 msec off-time, and a total of 106 pulses were fired until 14:24. The operation was terminated because of the failure to detect a substantial amount of contaminants, and also some trouble developed at the valve with new plugging. The lines were then cleaned, and a mixture of gaseous nitrogen and traces of water were run through the thruster during the night at a given pulse rate. QCMs B and C seemed to show some sensitivity to thruster operations. The characteristic increase of frequency during the night should be noted for these QCMs, even though some slight variations can be observed in the other QCMs. Five hundred and thirty (530) pulses were fired this day, which brought the total to 8444 pulses.

May 24, 1974. A mixture of gaseous nitrogen and water vapor was passed through the thruster by pulsing once every 20 seconds with a 200 msec pulse width. At 9:40, the pulsing was stopped and a series of long 30 second pulses were conducted for about one hour. Another series of bursts of NH_3 were made through an additional nozzle from 11:00 to 13:30 followed by a steady state flow of gaseous nitrogen and water vapor from 13:40 to 14:13. At 15:00 pure water vapor was introduced in the chamber, and at 15:30 atmospheric air was introduced by the additional nozzle for a few seconds. At this time the test was terminated and the refrigerator was shut off. At 17:30 the chamber was warm enough (about 30°K) to purge it with gaseous nitrogen at a pressure of (1 torr). The temperature of the QCMs was kept at about 233°K (-40°F), and except for QCM E, which showed a fluctuation of about 1 Hz, the rest of the QCMs did not experience any variation until 11:00. At this time, there were several bursts of NH_3 which triggered overpressures in the chamber, and together with a temporary power loss in the QCM heaters, caused the QCM temperatures to drop a few degrees. The original temperature was recovered and a steady flow of the wet nitrogen mixture was allowed to flow until 14:14, with the corresponding increase in mass deposit shown by all crystals. At the moment of the steam injection, one can observe QCMs B, C and E accepting mass, while QCMs A and D desorb mass at practically the same rate as if no water injection had taken place. Atmospheric air injection did not seem to affect the crystal readings, while chamber back filling operations affected the QCM readings drastically (see Figure 33a, b, c, d, e).

May 25, 1974. The temperature and frequency readings were recorded and are shown in Figure 34a, b, c, d, e. At 10:00 the gaseous nitrogen purge was turned off, the liquid nitrogen in the inner liner shut off, and the chamber was allowed to come slowly to thermal equilibrium with ambient temperature, although it was kept under vacuum.

May 26, 27, 1974. Figures 35a, b, c, d, e and 36a, b, c, d, e show the QCM temperature and frequency readings as the chamber temperature and pressure were brought up to 287.2°K (58°F), and about one atmosphere,

respectively. The reason for the warmer than room QCM temperature is due to purging the chamber with warm, dry gaseous nitrogen on the last day of operation.